Ore Geology Reviews 48 (2012) 278–305

Contents lists available at SciVerse ScienceDirect

Ore Geology Reviews

journal homepage: www.elsevier.com/locate/oregeorev

Review of platinum-group element distribution and mineralogy in chromitite ores from southern Iran

Mohammad Reza Jannessary [a], Frank Melcher [b,*], Jerzy Lodziak [b], Thomas C. Meisel [c]

[a] Geological Survey of Iran (GSI), Box 13185-1494, Tehran, Iran
[b] Federal Institute for Geosciences and Natural Resources (BGR), Stilleweg 2, 30655 Hannover, Germany
[c] General and Analytical Chemistry, Montanuniversität, Franz-Josefstr. 18, 8700 Leoben, Austria

ARTICLE INFO

Article history:
Received 9 November 2010
Received in revised form 30 April 2012
Accepted 1 May 2012
Available online 12 May 2012

Keywords:
Chromite
Chromitite
Platinum-group elements
Platinum-group minerals
Ophiolite
Iran

ABSTRACT

The platinum-group element (PGE) potential of four chromite mining districts in southern and south-eastern Iran was investigated using geochemical and mineralogical methods. A total of 20 mines and prospects were sampled in the Neyriz ophiolite, the Abdasht and Sikhuran complexes in the Esfandagheh district, and the Faryab district. Chromitite and dunite were analysed for major, trace element and PGE geochemistry, and the platinum-group element mineralogy (PGM). In all mining districts, chromites analysed from mantle tectonite, probable transition zone and cumulate zone chromitites are refractory, low in TiO_2 (<0.3 wt.%) as well as Cr- and Mg-rich, with Cr# [100∗Cr/(Cr + Al)] ranging from 70 to 81 and Mg# [100∗Mg/(Mg + Fe^{2+})] ranging from 40 to 83. Associated olivine is highly magnesian (Mg# 89–98) and Ni-rich (0.1–1.0 wt.% NiO).

PGE concentrations range from <100 to >5000 ppb, with median values around 200 ppb in all complexes investigated. The $^{187}Os/^{188}Os$ isotope ratios of chromitite indicate chondritic to slightly suprachondritic initial Os. Mantle-normalised Pt/Ir ratios are generally low (<0.2), but are up to 0.5 in small chromite pods in the harzburgitic mantle section of the Neyriz ophiolite. PGM, mainly laurite–erlichmanite, mostly occur as small (<1 to 30 μm) inclusions in chromite. They are associated with hydrous silicates (calcic amphibole), base metal sulphides (Ni- and Cu-sulphides) and other PGM, such as cuproiridsite, Ni–Ir sulphides, and Os–Ir alloys. PGMs interstitial to chromite are represented by irarsite, hollingworthite, Ru–Os–Ir alloys, tolovkite, RhNiAs, Pt–Fe alloy, probable Ru-rich oxides, and others.

In the Sikhuran complex, pods of sulphide-bearing chromitite (0.2–1.2% sulphides) occur in a dunite zone interpreted as an ultramafic cumulate zone. Chromites in chromitite are characterised by high Cr# (75–81) and intermediate Mg# numbers (45–65); in associated dunite, chromites (Cr#, 74–80) are more Fe-rich (Mg#, 29–50). Chromitite and dunite carry up to 5.2 ppm total PGE and are characterised by high normalised Pt/Ir (up to 5), Pt/Pd<1, and radiogenic Os (moderately suprachondritic initial Os). The interstitial sulphides are dominated by pentlandite that carries on average 0.45% Co, 25 ppm Os, 11 ppm Ir and 8 ppm Rh. Palladium and Pt concentrations in pentlandite are below the detection limit of the Laser Ablation–ICP-MS technique. Pentlandite is associated with rare grains of Pd- and Pt-minerals such as stibiopalladinite and Pt–oxide, and with Cu-rich phases.

Large degrees of partial melting in a supra-subduction zone geotectonic setting, probably in a two-stage melting process, produced boninitic melts that crystallised refractory, Cr–Mg rich and Ti-poor chromite. In some cases, sulphide saturation was achieved during and after chromite formation. Saturation during chromite crystallisation is evidenced by Ni–Cu-rich sulphide droplets preserved in some chromitites. Sulphur saturation after chromite crystallisation governed the formation of Ni-rich sulphide liquids that exsolved monosulphide solid solution, which later crystallised to form PGE-bearing pentlandite. Platinum and Pd did not partition into pentlandite but crystallised as Pt- and Pd-rich PGM associated with the pentlandite.

1. Introduction

Stratiform chromitites in layered ultramafic–mafic complexes such as the UG2 chromitite of the Bushveld complex, South Africa, may constitute economic reserves of the platinum-group elements (PGEs) (e.g., Cawthorn et al., 2005; Naldrett and von Gruenewaldt, 1989). In contrast, podiform and stratiform chromitites in ophiolite complexes commonly host subeconomic concentrations of the PGE only and usually, the IPGE (Ir-subgroup PGE; Os, Ir, Ru) predominate over the PPGE (Pt-subgroup PGE; Rh, Pt and Pd). In a few ophiolite complexes, however, the PGE are enriched to values of 2–20 ppm, e.g. in chromitites of the "transition zone" from the oceanic crust to

* Corresponding author. Tel.: +49 511 643 2562.
E-mail address: F.Melcher@bgr.de (F. Melcher).

0169-1368/$ – see front matter © 2012 Elsevier B.V. All rights reserved.
doi:10.1016/j.oregeorev.2012.05.001

the oceanic mantle, and in the lowermost cumulate sequences. Examples of ophiolithic chromitites where enrichment of the PGE has been documented are from the Shetland islands, Great Britain (Prichard and Tarkian, 1988; Prichard et al., 1986, 1994), Leka, Norway (Pedersen et al., 1993), Albania (Ohnenstetter et al., 1991), NW Spain (Moreno et al., 1999), the Pindos ophiolite, Greece (e.g. Economou-Eliopoulos, 1996; Prichard et al., 2008b), the Al'Ays massif in Saudi Arabia (Prichard et al., 2008a), and others.

Chromitites in the lower mantle sections commonly have 100 to 300 ppb PGE contents dominated by the IPGE, but may also carry more than 1 ppm Ru, Os and Ir (e.g. Oman: Ahmed and Arai, 2002, 2003; Saudi Arabia: Prichard et al., 2008b). Higher concentrations of Pd (several ppm) are only reported in sulphide-bearing dunites of the mantle–crust transition zone ("high-level dunites", "transition-zone dunites") in some ophiolites (e.g. Bulqiza and Krasta, Albania; Burgath et al., 2002; Ohnenstetter et al., 1991), and in the cumulate sequence (e.g. Acoje, Philippines; Orberger et al., 1988). Small sizes, low tonnages and highly variable PGE grades do not permit economic extraction of the PGE at present. However, chromitite and sulphide-bearing dunite are potentially valuable for PGE exploration in ophiolites.

With an annual production of 185,760 tonnes of chromite concentrate from 42 active mines in 2007, Iran is on rank 13 of the World's chromite producers (Mobbs, 2010). From 1992, production was gradually rising, culminating to 512,640 tonnes in 2002. Reserves are considered significant: Industrial Minerals indicate proven reserves of 16,371 million tonnes (Papp, 2004), which is 2% of the world reserves. According to Yaghubpur (2005), more than 70 chromite deposits and prospects have been discovered in Iran, with 18 of them currently in production and four in different stages of exploration.

Chromite is mined in different regions of Iran, and the geology of the chromite deposits and the economic significance of the chromite-producing regions of Iran have been discussed in several publications (Hillebrand, 1983; Schmidt, 1974; Schürenberg, 1959; Weber-Diefenbach and Davouadzadeh, 1998; Yaghubpur and Hassannejad, 2006). The four important chromite mining areas are: northeast Iran (Sabzevar), south Iran (Hormozgan with important mining areas at Faryab and Esfandagheh), southwest Iran (Neyriz, Fars) and southeast Iran

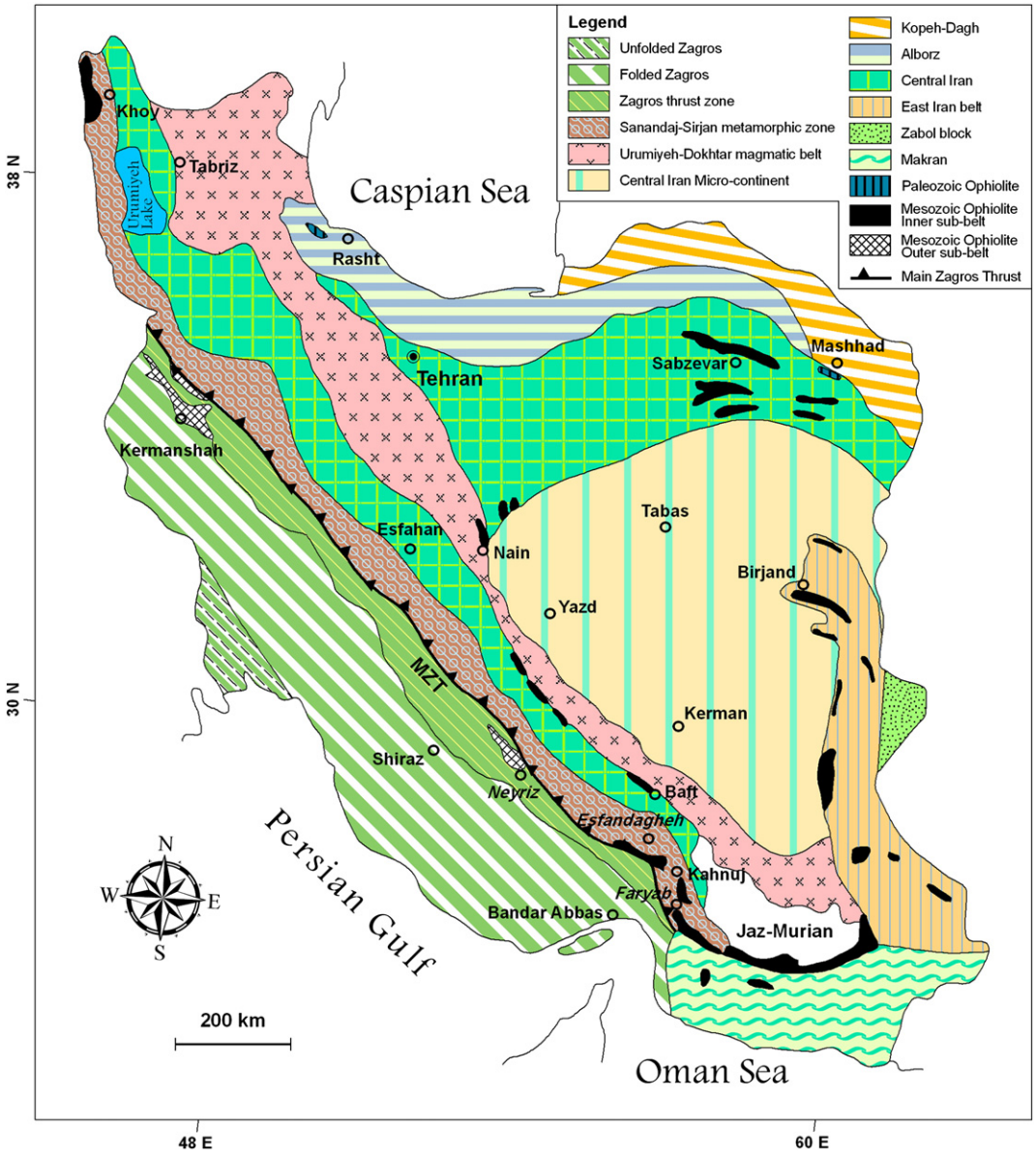

Fig. 1. Schematic map of the major structural units of Iran and pointing out the position of Paleozoic and Mesozoic ophiolites.

(Makran, Baluchestan). Smaller deposits and occurrences are distributed all over the country, from the Turkish and Armenian borders to Afghanistan (Lotfi et al., 1993) (Fig. 1). Chromitite is exclusively associated with ultramafic rocks of the upper mantle and the lower cumulate sequences of ophiolite complexes. Some ophiolites, e.g. Neyriz and Kermanshah, are Cretaceous in age (100 Ma), whereas others, e.g. those of Esfandagheh and Faryab are considered by some authors as Paleozoic or even Upper Precambrian to Lower Paleozoic in age.

The knowledge on the distribution of PGE and PGM in ophiolite complexes of Iran and the PGE potential of Iranian chromitites is poor. Just 38 analyses of the PGE were found in the literature from 1979 to 2008 (Alinia and Facherabadi, 2005; Najafzadeh et al., 2008; Page et al., 1979; Rajabzadeh, 1998; Weber-Diefenbach and Davouadzadeh, 1998). The highest concentrations were reported from Sikhuran (435 ppb Pt and 277 ppb Pd; Alinia and Facherabadi, 2005). Most chromitite samples from Neyriz and Faryab are enriched in the IPGE with respect to the PPGE; only one exception was reported from Faryab with Pd/Ir = 2.1 (Najafzadeh et al., 2008).

Moore and Rajabzadeh (1993) and Rajabzadeh (1998) identified inclusions of platinum-group minerals (PGMs) in chromite ores from the Neyriz and Faryab ophiolite complexes. Similar to many ophiolitic chromitites, minerals of the laurite–erlichmanite series (RuS_2–OsS_2) dominate. Rare phases include alloys of Os, Ir, Ru and Pd, sulpharsenides of Rh and Ir, cuproiridsite–malanite ($CuIr_2S_4$–$CuPt_2S_4$), as well as unnamed Ni–Ir sulphides.

It is the purpose of this study to improve the data base on PGE concentrations and mineralogy in Iranian ophiolites (chromitites and sulphide-bearing dunite), and to develop a concept that could assist in regional PGE exploration.

2. Geological background

2.1. Iranian ophiolites

The Iranian ophiolites are divided into two age groups: Paleozoic and Mesozoic (Fig. 1). The less abundant Paleozoic ophiolites are considered to be remnants of the Paleo-Tethys ocean situated between the Eurasian plate in the north and the Gondwanian plate in the south. They crop out in the north and northeast of Iran as the Asalem–Shanderman and Mashhad ophiolites (Sengör, 1979; Stöcklin, 1977; Wensink and Varekamp, 1980). The more abundant Mesozoic ophiolites are considered to be remnants of the Neo-Tethys ocean situated between the Iranian plate in the north and the Arabian plate in the south, and have been divided by Lensch and Davoudzadeh (1982) and Stöcklin (1977) into an outer and an inner sub-belt. The outer or southern sub-belt (Zagros type), located immediately to the southwest of the Main Zagros Thrust Zone (MZT), includes the Kermanshah and Neyriz ophiolites that extend into the Oman ophiolite (Arvin, 1987; Babaie et al., 2001, 2006; Braud, 1970; Jannessary, 2003; Ricou, 1971b; Sarkarinejad, 2003). The outer sub-belt is interpreted as a remnant of the Neo-Tethys ocean that was obducted along the main Zagros Thrust bounding the southern margin of the Sanandaj–Sirjan Zone. The inner or northern sub-belt (Central Iran type), represented by extensive Coloured Mélange zones, is located around the Central Iranian micro-continent and includes the Sabzevar, Nain-Baft, Esfandagheh, Makran and Birjand ophiolites (Ahmadipour et al., 2003; Alavi-Tehrani, 1977; Arvin and Robinson, 1994; Davoudzadeh, 1972; Delaloye and Desmons, 1980; Desmons and Beccaluva, 1983; Gansser, 1960; Ghasemi et al., 2002; Kananian et al., 2001; Lensch et al., 1977; McCall, 1997). One part of this belt is a remnant of the Nain-Baft paleo-ocean along the northern margin of the south Sanandaj–Sirjan Zone (Ghasemi and Talbot, 2006).

In the following we will briefly discuss the geology of the ultramafic complexes and the chromite ores investigated during this study using the available literature and field data. Table 1 summarises the field information on the chromitites.

2.2. Neyriz ophiolite

The Neyriz ophiolite is situated in the south-eastern part of the Zagros Range about 200 km east of the city of Shiraz and extends for more than 120 km in a NW–SE direction along the salt lakes of Bakhtegan and Tashk (Fig. 2). Along with a series of sedimentary sequences, Triassic to Coniacian in age, and a Coloured Mélange zone, the ophiolite was obducted onto the Arabian platform in Senonian times (Babaie et al., 2005; Ricou, 1971b, 1976; Stöcklin, 1977). The association of mantle harzburgite and high-grade metamorphic lenses of marble makes the Neyriz ophiolite unusual. The marbles are probably derived from Upper Triassic marine carbonates by contact metamorphism caused by the peridotites (Hall, 1980; Ricou, 1971a). The contacts are characterised by discontinuous hydrogrossular-bearing reaction zones which are restricted to areas where gabbro dikes cut the peridotites (Jannessary, 2003). The Neyriz ophiolite is composed of foliated highly depleted upper mantle harzburgite cross cut by thick residual dunite (up to 150 m), overlain by a sequence of mainly isotropic gabbros. In contrast to the Oman ophiolite, basaltic lava directly rests on gabbro, without development of a sheeted dyke complex. Locally, there are abundant dunite–websterite levels constituting reaction zones of percolating mantle melts with peridotite (Jannessary, 2003). The Neyriz ophiolite represents the western portion of Cretaceous N–S orientated accretion cells separated by a dextral N110°–130°E transform fault in a slow-spreading environment (Jannessary, 2003).

The discordant to concordant chromitite bodies of the Neyriz ophiolite were generated in the mantle section. The concordant bodies resulted from plastic deformation in the mantle and tectonic reorientation towards the foliation during upwelling of the mantle diapir and mantle flow below the spreading centre (Cassard et al., 1981).

2.3. Esfandagheh district

Thirty-one ultramafic complexes, including the Abdasht and Sikhuran complexes, are known in an E–W trending belt of 60 km length and 5–10 km width in the Esfandagheh district of the Kerman province, constituting Iran's second largest chromite producer after the Faryab area. According to Hillebrand (1983), this “northern Belt” forms part of the “Coloured Mélange”, a late-Alpine orogenic zone that is embedded into pre-Triassic metamorphic rocks of the Sanandaj–Sirjan zone. The Coloured Mélange consists of an Upper Cretaceous assemblage of radiolarite, carbonate and schist associated with exotic blocks, e.g. mantle fragments and ophiolites. Weber-Diefenbach et al. (1986) attributed the ultramafic complexes to the Paleozoic metamorphic complexes, and not to the Mesozoic Coloured Mélange. In the Esfandagheh district, a clear separation between the two sub-belts as proposed by Stöcklin (1977) is difficult. Sabzehei (1974, 1998) proposed that these complexes are polygenetic and resulted from differentiation of a komatiitic magma, intruding Paleozoic metamorphic rocks in the late Triassic in a rift-like intra-cratonic trough. The Soghan complex, located between the Abdasht and Sikhuran complexes, was recently interpreted as a Paleozoic mantle diapir (Ahmadipour et al., 2003).

The ultramafic complex of Abdasht extends for 5 × 7 km in E–W and N–S directions, respectively (Fig. 2). It is mainly composed of variably serpentinized dunite, harzburgite, websterite and minor wehrlite and lherzolite. The Soghan complex east of Abdasht has a similar petrographic and geochemical signature and consists of a lower part composed of dunite, harzburgite and chromitite, and a transition zone with lherzolite, dunite, pyroxenite and wehrlite that transitionally changes into gabbro (Ahmadipour et al., 2003). The ultramafic–mafic body of Sikhuran east of Soghan covers 300 km^2 (Fig. 2). Ghasemi et al. (2002) distinguished the following units: (1) foliated harzburgite and dunite overlain by (2) cumulates, that are subdivided into a lower ultramafic unit (2a), 1 km thick (dunite, wehrlite, olivine websterite, websterite, clinopyroxenite) and an upper gabbroic unit (2b), 2 km

Table 1
Sample localities of chromitites from southern Iran.

No.	Massif	Mine/ prospect	North	East	Sample number (IR05-)	Host rock	Size, number, elongation	Morphostructural type	Chromite type
1	Neyriz	Tange Hana	2922745	5410411	2–4	Altered harzburgite	Small lenses	Podiform	Massive to dense chromitite with dunite halos
2	Neyriz	Tange Hana	2922863	5508986	5–6	Clinopyroxene-impregnated dunite, clinopyroxenite		Orbicular/ disseminated	Massive, disseminated and orbicular chromite
3	Neyriz	Khajeh Jamali	2348349	5351651	14–20 (21–24)	Harzburgite and dunite	Small and medium-sized	Schlieren	Folded schlieren, disseminated
4	Neyriz	Cheshmeh Bid	2952552	5345730	26–32	Harzburgite and dunite	Several 100 m along strike and >400 m in depth, about 3 m thick	Tabular	Massive, disseminated
5	Abdasht	Level 1 chromite, Abdasht	2821141	5646571	37–39	Dunite	Mineralized zone 1000 m long; chromitite lenses 10–25 m long, 0.5–3 m thick	Tabular to schlieren	Nodular to massive, defomred and altered, folded schlieren
6	Abdasht	Level 1 chromite, Mine No. 7	2821569	5644563	49–50	Dunite		Tabular or layered	Nodular ore, sometimes undeformed, forming round massive aggregates in finely disseminated chromite
7	Abdasht	Level 2 chromite, Shabahang	2822858	5646231	44–48	Granoblastic, coarse grained, recrystallised dunite	More than 5 m thickness	Schlieren	Steeply inclined folded schlieren and layers
8	Abdasht	Level 3 chromite, Mine No. 6	2823231	5646866	40–43	Dunite	Boudins of 0.5 to 3 m thickness	Tabular?	Transitions from massive, tectonized, to nodular and disseminated types
9	Sikhuran	Razouki	2828252	5700615	52–55	Light green coarse-grained porphyroclastic dunite	2–3 m thick zone exposed >50 m along strike	Schlieren	Disseminated, partly massive, occasionally banded chromite
10	Sikhuran	Sorkh Jallab	2827102	5658159	58–60	Dunite	5 m thick, N–S trending lens	Schlieren	Disseminated, folded schlieren, with some massive and nodular ore
11	Sikhuran	Sobhan	2824769	5657390	61–63	Transition zone dunite	2 m thick, trending E–W, 30 m along strike	Tabular	Banded chromite
12	Sikhuran	Sikhuran	2825145	5700292	64–81	Cumulate dunite	Interlayered dunite–chromitie over 20 m thickness	Layered	Banded chromitite, partly wavy, massive and nodular types; cumulate texture
13	Sikhuran	Sikhuran	2825189	5700550	82–88	Cumulate dunite		Layered	Sulphide-bearing chromitite, nodular and disseminated ores
14	Faryab	Doveis	2724322	5722705	96–103	Banded dunite	Nine to eleven subvertical to 10° NE dipping chromite horizons, 0.5–3 m thick,	Layered	Disseminated to banded ore, open folds
15	Faryab	Sohrab–Kamali	2723314	5722742	104–106	Dunite, clinopyroxenite	1 and 0.5 m thick	Layered	Banded and disseminated chromitite
16	Faryab	Shahin	2722851	5723027	107	Dunite, clinopyroxenite		Layered	Disseminated chromite
17	Faryab	Fètr Tunnel 6	2723956	5724581	108–114, 124	Dunite, clinopyroxenite		Layered	Disseminated, but usually massive and cataclastic
18	Faryab	Amir	2723412	5724604	115–117	Dunite, clinopyroxenite	Lower ore (5 m thick and extending for 135×35m), upper ore (12 m thick and extending for 170×60 m)	Layered	Banded ore , upper disseminated, partly schlieren-type ore
19	Faryab	Nemat	2723186	5724435	118	Dunite, clinopyroxenite		Layered	Densely disseminated to massive-cataclastic ore
20	Faryab	Shahriar	2723170	5724103	120–123	Massive pyroxenite, wehrlite, olivine websterite	24 m thick	Layered	Single chromite layers are isoclinally folded and display shallowly dipping fold axes
21	Faryab	Reza	2722175	5725199	126–127	Serpentinized dunite	Eight steeply dipping ore bodies, each extending for >100 m and several m thick	Podiform	Disseminated and nodular ores

thick, comprising feldspathic pyroxenite and lherzolite, layered gabbro, troctolite, olivine gabbro, clinopyroxenite, gabbronorite and ferrogabbro. In addition, an intrusive unit (3) is present which is composed of hornblende-bearing, occasionally pegmatoidal gabbros. K–Ar ages indicate a complex polygenetic history. Pegmatoidal gabbro intruded into the ultramafic–mafic sequence about 250 Ma ago. Diabase dykes are 165 Ma old (Middle Jurassic; Ghasemi et al., 2002). Both the lower ultramafic and the upper ultramafic–mafic cumulate units carry chromite. In dunite horizons of the mantle unit, disseminated and massive chromitites show evidence of plastic mantle deformation. More stratiform, concordant chromitites and lenses carrying disseminated sulphides are exposed in the cumulate sequence (Ghasemi et al., 2002).

2.4. Faryab district

The Coloured Mélange Complex to the south of the Sanandaj–Sirjan/Bajgan–Durkan block contains two intact ophiolite complexes, each several kilometres in length, the Sorkhband and Rudan complexes (McCall, 1997). The ultramafic complex at Kuh-e Sorkhband measures 18 km in NW–SE and 6 km in SW–NE direction (Fig. 2). It

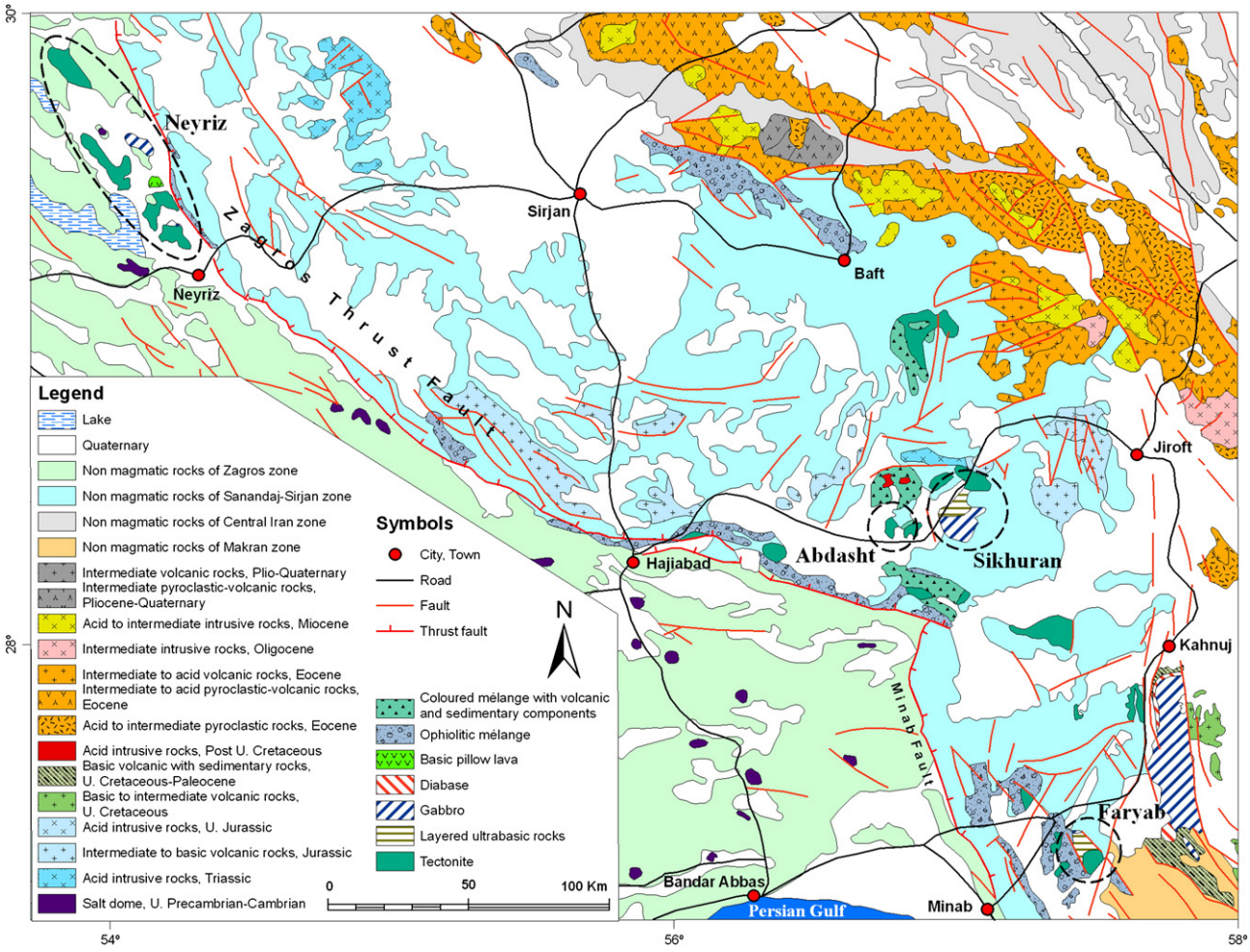

Fig. 2. General geological map of the studied areas, based on the map "Magmatic rocks of Iran", compiled by A. Aghanabati, Scale: 1:2.500.000, Geological Survey of Iran, 1990.

is the largest chromite mining district in Iran and usually named "Faryab district" based on the mining company Faryab Mining Co. Rajabzadeh (1998) used the term "Assemion" complex. Towards the west, the ultramafic complex is bound by the Dastgerd fault against the Mesozoic Coloured Mélange Complex. Towards the east, it is separated from the pre-Mesozoic, metamorphic Bajgan complex by the Rudan fault. The Sorkhband complex has been subdivided into a northern unit composed of rhythmically banded dunite (70%) and pyroxenite with little harzburgite, websterite and wehrlite, and into a southern unit of non-banded, massive, monotonous ultramafic rocks (mainly dunite and harzburgite, less clinopyroxenite). Numerous chromite deposits occur in the northern part (Najafzadeh et al., 2008); in the southern unit, deposits are present only along the northern margin (deposits of Reza and Ismail). Cumulate textures have only been described from the chromitites in the northern unit. A small gabbro body that is possibly genetically related to the complex is exposed along the northern margin of the Faryab complex. Radiometric dating of pyroxene from an olivine clinopyroxenite by the K–Ar method has yielded an age of 476 ± 35 Ma (McCall, 1985); this is interpreted as a recrystallisation age of the gabbro, and might have been affected by excess argon. The obduction or tectonic emplacement of the complex took place during the Alpine orogenic events. All rocks are strongly recrystallised and foliated parallel to initial layering (Fig. 3A). The banded texture results from recrystallisation of ortho- and clinopyroxene during solid-state deformation in the upper mantle, and thus is not a product of cumulus layering.

3. Methods of investigation

Chromite- and sulphide bearing samples were taken from surface outcrops, in underground adits and on dumps. Polished sections were prepared to study the mineralogy and textures. In order to receive comparable geochemical results, chromite was concentrated from disseminated and nodular ores on a shaking table. For major and trace element analyses by X-ray fluorescence at the BGR, glass discs were prepared using 0.1 g sample powder and 4.915 g mixed Li metaborate/tetraborate flux for Cr-rich samples, and 1 g sample and 5 g Li metaborate flux for silicate-rich samples (Appendix 1).

In 41 chromitite and whole-rock samples, the concentrations of the PGE, Re and the $^{187}Os/^{188}Os$ isotopic ratios were measured using isotope dilution (ID)-ICP-MS at the Montanuniversität Leoben (Austria) following methods described by Meisel and Moser (2004), Meisel et al. (2001b, 2003a,b), Kocks et al. (2007), and Paliulionyte et al. (2006). In addition, PGE, Au and Re concentrations of 17 samples (5–20 g) were determined using the Ni fire assay preconcentration method with INAA finish (Activation Laboratories, Ontario, Canada). Results of the PGE determinations are presented in Table 2.

Three samples (IR005-2, -29, -86) were analysed by both methods in order to check sample homogeneity and comparability. Considerable deviations are regarded to reflect sample inhomogeneity (nugget effect) due to different sample weights, and probably incomplete dissolution for the second method (HPA versus conventional dissolution; Meisel et al., 2003b). However, normalised PGE distribution

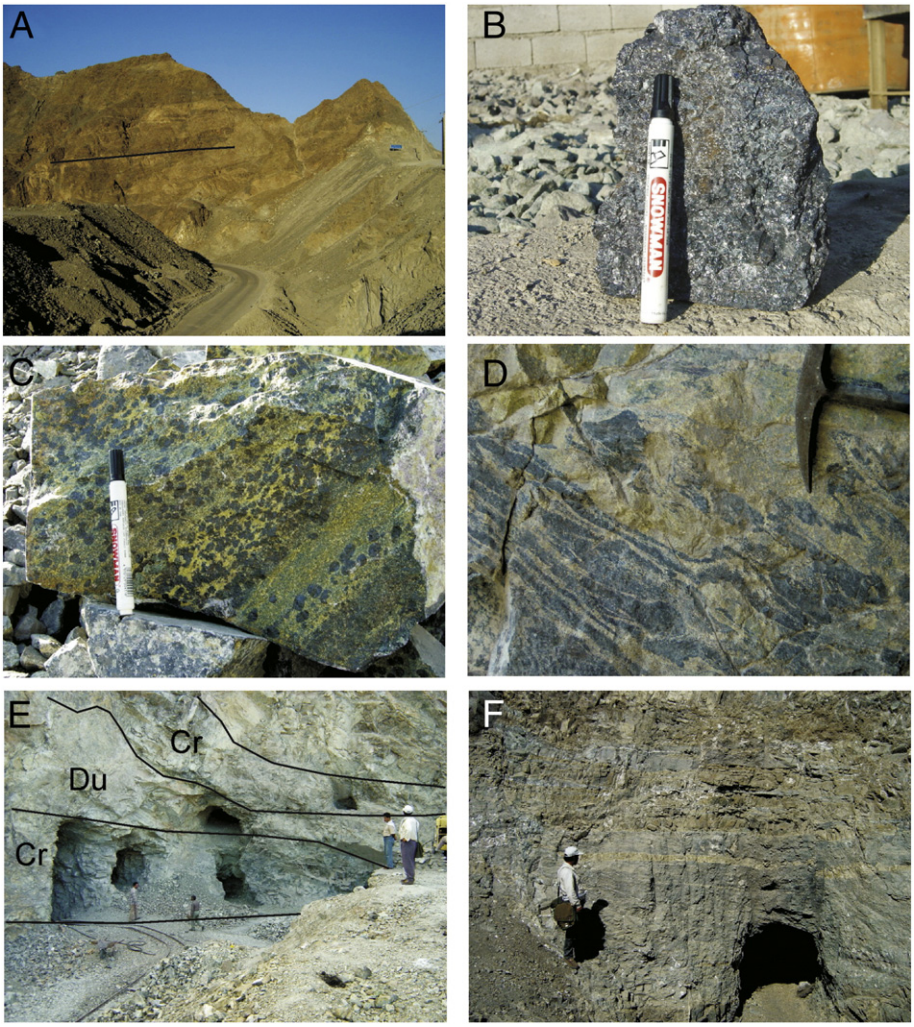

Fig. 3. Chromitite textures in southern Iran. A) folded and banded dunite–pyroxenite sequence, Faryab mining area; B) massive chromitite, tunnel No. 8, Cheshmeh Bid, Neyriz ophiolite; C) nodular chromitite, Abdasht mining area, Esfandagheh district; D) folded schlieren-type chromitite, level 2, Abdasht mining area, Esfandagheh district; E) interlayered chromitite (Cr) and dunite (Du) in cumulate zone, Sikhuran mine, Esfandagheh district; F) banded chromitite (dark) in dunite–pyroxenite sequence, Shahriar mine, Faryab ophiolite.

patterns are rather similar, except for constantly lower Os concentrations reported in the Activation Laboratories data set.

Eighty-six polished sections were studied using reflected light microscopy (LEICA DMRP) and electron microscopy (FEI Quanta 600 FEG). In 67 samples, chromite, silicates (mainly olivine), base metal sulphides and platinum-group minerals were analysed at the BGR by wavelength-dispersive electron microprobe techniques (CAMECA SX 100). Chromite and silicates were analysed using acceleration voltages and beam currents on brass of 20 kV/30 nA (chromite), and 15 kV/20 nA (silicates), respectively. A total of 959 microprobe analyses from chromite cores, and 505 analyses of olivine and other silicates were carried out. Two-hundred-sixty-six analyses of PGM and base metal phases were performed at 20 kV and 20 nA using pure metals, synthetic phases and some natural minerals as standards. Oxygen was measured in a few grains of probable PGE oxides using the Kα line on a multilayer crystal at 10 kV and 20 nA, and oxygen was calibrated against hematite. Pentlandite (n = 130) was analysed at 20 kV, 80 nA and longer counting times (400 s on peak) to achieve lower detection limits for Rh (120 ppm), Pt (230 ppm) and Pd (50 ppm).

For analysis of low levels of PGE in pentlandite and chromite, two samples of PGE- and sulphide-bearing chromitite (samples AS7541, AS7543) from Sikhuran were analysed by Laser Ablation–ICP-MS techniques at the University of Erlangen-Nürnberg, Germany. The Agilent 7500i quadrupole mass spectrometer is equipped with a UP193FX laser, New Wave Research. Single spot measurements were carried out at 20 Hz repetition rates producing craters of 25 μm in diameter at a laser energy of 0.65 GW/cm^2 and an energy density of 3.22 J/cm^2. The following isotopes were monitored: ^{29}Si, ^{59}Co (5 ms each measurement time at maximum peak), ^{33}S, ^{34}S, ^{53}Cr, ^{57}Fe, ^{60}Ni, ^{63}Cu, ^{208}Pb (10 ms), ^{101}Ru, ^{103}Rh, ^{105}Pd, ^{185}Re, ^{189}Os, ^{193}Ir, ^{195}Pt (30 ms) and ^{197}Au (40 ms). PGE and Au in sulphides were calibrated using the Po 724 B2 SRM (Memorial University Newfoundland), and Ni and Re were calibrated using the $(Fe,Ni)_{1-x}S$ sulphide standard provided by the University of Münster (Wohlgemuth-Ueberwasser et al., 2007). Concentrations were calculated from raw data using the GLITTER 3.0 software (On-line Interactive Data Reduction for the LA–ICP-MS, Macquarie Research Ltd., 2000). The following interferences could not be resolved: ^{61}Ni^{40}Ar, ^{65}Cu^{36}Ar and ^{202}Hg^{++} interfere with ^{101}Ru; ^{63}Cu^{40}Ar and ^{206}Pb^{++} interfere with ^{103}Rh; ^{65}Cu^{40}Ar interferes with ^{105}Pd.

4. Geology of the chromite ores

Chromite is an abundant accessory phase in the ultramafic complexes studied, and locally enriched to form chromitite ore bodies of different size and texture. Table 1 and Fig. 4 summarise the field evidence and literature data in synthetic logs of the four complexes studied. The morphostructural scheme used by Burgath et al. (2002) is

Table 2
Concentrations of PGE, Au and Re, and $^{187}Os/^{188}Os$ isotope ratios in chromite concentrates separated on a shaking table from chromitite, and in some host rocks (bulk rock values).

Sample No	Rock, type	Locality, complex	Method	Os	Ir	Ru	Rh	Pt	Pd	Au	Re	Total	Pt_n/Ir_n	$^{187}Os/^{188}Os$
				ppb	ppb	ppb	ppb	ppb	ppb	ppb	ppb	ppb		
IR05-002	Chr, e	Tange Hana, Neyriz	1	435	321	748	122	367	24.5	n.a.	0.199	2018	0.55	0.1273
IR05-002	Chr, e	Tange Hana, Neyriz	2	230	315	564	124	294	7	7.1	<5	1534	0.45	
IR05-004	Chr, e	Tange Hana. Neyriz	2	230	289	402	63.1	143	34	8.6	<5	1161	0.24	
IR05-005	Chr, f	Tange Hana, Neyriz	1	10.3	7.54	55.1	5.12	2.63	1.1	n.a.	0.178	82	0.17	0.1283
IR05-014	Chr, c	Khajeh-Jamali, Neyriz	2	40	16.2	120	18.7	<5	13	9.9	<5	208		
IR05-018	Chr, c	Khajeh-Jamali, Neyriz	2	6	6.9	37	5	<5	2	2.3	<5	57		
IR05-020	Chr, c	Khajeh-Jamali, Neyriz	1	15.4	11.3	48.3	7.13	3.92	1.35	n.a.	0.272	87	0.17	
IR05-021	Chr	Ore plant, Neyriz	1	44.6	22.9	82.8	6.83	2.53	2.69	n.a.	0.178	162	0.05	0.13
IR05-022	Chr	Ore plant, Neyriz	1	64.8	35.2	123	10.48	1.33	1.17	n.a.	0.212	236	0.02	0.1291
IR05-023	Chr	Ore plant, Neyriz	1	84.8	41.1	156	11.33	9.01	1.43	n.a.	0.235	304	0.11	0.1245
IR05-024	Chr	Ore plant, Neyriz	1	56.8	31.6	114	10.53	2.5	2.6	n.a.	0.206	218	0.04	0.1286
IR05-027	Chr, b	Chesh. Bid T8, Neyriz	1	52.6	35.4	99.1	8.86	6.7	1.8	n.a.	0.288	205	0.09	0.129
IR05-028	Chr, b	Chesh. Bid T8, Neyriz	1	58.3	37.7	100	8.55	0.5	0.9	n.a.	0.269	206	0.01	0.1278
IR05-029	Chr, b	Chesh. Bid T8, Neyriz	1	65.7	n.a.	128	13.04	3.8	1.7	n.a.	0.35			0.128
IR05-029	Chr, b	Chesh. Bid T8, Neyriz	2	69	51	107	10.7	<5	8	10.5	<5	246		
IR05-030	Chr, b	Chesh. Bid T8, Neyriz	1	82.3	31.2	129	8.85	2.6	4	n.a.	0.254	258	0.04	0.1292
IR05-031	Chr, b	Chesh. Bid T7, Neyriz	1	45	21.9	79.4	6.14	4.5	2.8	n.a.	0.115	160	0.1	0.1271
IR05-032	Chr, b	Chesh. Bid T1, Neyriz	1	47.2	n.a.	87.2	10.04	32.8	31.5	n.a.	0.276	209		0.1294
IR05-038	Chr, c	Level1, Abdasht	1	42.2	50.3	140	14.13	1.1	1.1	n.a.	0.155	249	0.01	0.1252
IR05-041	Chr, a	Level3, Abdasht	1	20.9	29.2	107	11.18	1.5	2.5	n.a.	0.164	172	0.03	0.1253
IR05-042	Du	Level3, Abdasht	1	5.5	4.2	7.3	2.19	9.7	6.7	n.a.	0.073	36	1.13	0.1275
IR05-043	Chr, a	Level2, Abdasht	1	22.2	17.1	59.1	5.21	1.6	2.2	n.a.	0.073	107	0.04	0.1267
IR05-050	Chr, c	Level1, Abdasht	1	12.8	21.3	39.3	6.96	0.4	0.7	n.a.	0.071	81	0.01	0.1254
IR05-051	Chr, c	Ore plant, Abdasht	1	47.8	32.1	71.5	11.19	14.5	2	n.a.	0.051	179	0.22	0.1261
IR05-052	Chr, c	Razouki, Sikhuran	1	27.3	24.7	130	17.94	265	116	n.a.	0.104	581	5.21	0.129
IR05-054	Chr, c	Razouki, Sikhuran	2	32	45.9	66	8.5	6	<2	29.2	<5	158	0.06	
IR05-058	Chr, c	Sorkh Jallab, Sikhuran	1	31.9	24.3	67.2	6.17	1.6	2.8	n.a.	0.154	134	0.03	0.1261
IR05-061	Chr, b	Sobhan, Sikhuran	2	18	24.7	48	6.3	<5	<2	1.8	<5	97		
IR05-064	Chr, a	New mine, Sikhuran	1	17.8	22.9	75	7.69	2.8	0.8	n.a.	0.113	127	0.06	0.1278
IR05-065	Chr, a	New mine, Sikhuran	1	48.2	26.7	80.7	3.86	7.9	1.7	n.a.	0.228	169	0.14	
IR05-068	Chr, a	Old mine, Sikhuran	2	15	27.2	58	9.8	<5	<2	1.5	<5	110		
IR05-069	Chr, a	Old mine, Sikhuran	1	44.2	47.2	120	14.87	23.3	12.7	n.a.	0.234	262	0.24	0.1278
IR05-070	Chr, a	Old mine, Sikhuran	1	53.4	49	134	16.61	40.8	12.3	n.a.	0.1	307	0.4	0.125
IR05-074	Chr, a	New mine, Sikhuran	1	n.a.	22.8	76.4	4.52	2.9	2.9	n.a.	0.061		0.06	
IR05-076	Du-chr	New mine, Sikhuran	2	20	52.7	84	14	61	44	4.6	<5	276	0.56	
IR05-077	Du-sul	New mine, Sikhuran	2	119	81.6	100	65.8	221	828	20.3	<5	1415	1.31	
IR05-080	Chr, a	New mine, Sikhuran	2	16	21.3	72	18.1	<5	31	2.5	<5	158		
IR05-082	Du-sul	Ore dump, Sikhuran	2	44	30.6	36	20	283	448	83.8	<5	862	4.48	
IR05-083	Chr, a	Ore dump, Sikhuran	1	70.9	55.1	124	17.57	144	293	n.a.	0.36	704	1.26	0.1302
IR05-084	Chr-sul	Ore dump, Sikhuran	1	164	93.6	168	38.36	384	617	n.a.	2.198	1465	1.99	0.1315
IR05-086	Chr-sul	Ore dump, Sikhuran	1	250	153	294	103	1524	2859	n.a.	3.527	5183	4.82	0.1337
IR05-086	Chr-sul	Ore dump, Sikhuran	2	60	64.6	88	96.8	612	715	533	<5	1636	4.59	
IR05-087	Chr-sul	Ore dump, Sikhuran	2	145	128	176	104	751	971	229	<5	2275	2.84	
IR05-096	Chr, a	Doveis, Faryab	1	18	13.2	56.3	4.71	1.3	0.6	n.a.	0.033	94	0.05	0.1287
IR05-099	Chr, a	Doveis, Faryab	2	51	93.5	109	15.1	17	12	14	<5	298	0.09	
IR05-100	Chr, a	Doveis, Faryab	1	50.3	34.7	66.9	8.94	54.9	39.8	n.a.	1.028	255	0.77	0.1269
IR05-101	Du-sul	Doveis, Faryab	2	10	3.8	< 5	6.2	7	58	38.1	<5	85	0.89	
IR05-102	Du-sul	Doveis, Faryab	1	1.5	1.8	1.9	2.2	33	42.3	n.a.	2.468	83	8.94	0.166
IR05-103	Chr, a	Doveis, Faryab	1	33.7	31.2	63.8	7.36	14.3	17.4	n.a.	1.436	168	0.22	0.129
IR05-105	Chr, a	Sohrab-Kamali, Faryab	1	233	123	59.5	14.28	13.6	8.1	n.a.	0.129	452	0.05	0.128
IR05-107	Chr, a	Shahin, Faryab	1	86.3	47.7	91.8	5.84	1.6	1.7	n.a.	0.211	235	0.02	0.1259
IR05-108	Chr, a	Fètr Tunnel 6, Faryab	1	127	109	67.5	15.68	4.4	2	n.a.	0.161	326	0.02	0.1267
IR05-111	Chr, a	Fètr Tunnel 6, Faryab	2	30	43.4	29	2.7	<5	<2	21.6	<5	105		
IR05-113	Chr, a	Fètr Tunnel 6, Faryab	1	93	70	69.1	9.29	2.4	2.6	n.a.	0.209	246	0.02	0.1342
IR05-115	Chr, a	Amir, Faryab	1	44	21	77.9	5.58	2.7	1.1	n.a.	0.193	152	0.06	0.1282
IR05-121	Du-chr	Shahriar, Faryab	1	59	30	48.5	4.68	1.9	2.2	n.a.	0.159	146	0.03	0.1401
IR05-124	Pyr-sul	Fètr Tunnel 6, Faryab	1	5	1	0.6	1.03	26.6	28.6	n.a.	3.103	62	17.46	0.2130
IR05-126	Chr, e	Reza, Faryab	1	27	17	54.8	4.86	2.5	1.8	n.a.	0.154	108	0.07	0.1261

Rock: Chr, chromitite; Du, dunite; sul, sulphide-bearing; Pyr, pyroxenite.
Type: (a) layered/massive to disseminated, (b) tabular/disseminated to massive, (c) schlieren (-folded)/disseminated, (e) podiform s.str./massive, and (f) orbicular/disseminated chromitite.
Method (1): ID-ICP-MS, MUL; (2): Ni-FAA, ActLabs, Canada; n.a., not analysed.

followed to attribute the chromitites to one out of six classes: (a) layered/massive to disseminated, (b) tabular/disseminated to massive, (c) schlieren (-folded)/disseminated, (d) pencil-shaped/disseminated to massive, and (e) podiform s.str./massive. Chromitite conformable to class (d) was not observed in the investigated area. However, class (f), orbicular/disseminated chromitite was added to describe textures associated with clinopyroxenite. This classification also allows for a positioning of the ore bodies into an ophiolite stratigraphy; however, it must be kept in mind that geochemical and petrological information is almost non-existing in most of the complexes.

4.1. Neyriz ophiolite

In the Neyriz ophiolite, several types of chromitite were observed, including schlieren-type and tabular ore bodies, and smaller podiform massive, as well as rare orbicular and disseminated ores. Most chromitites are

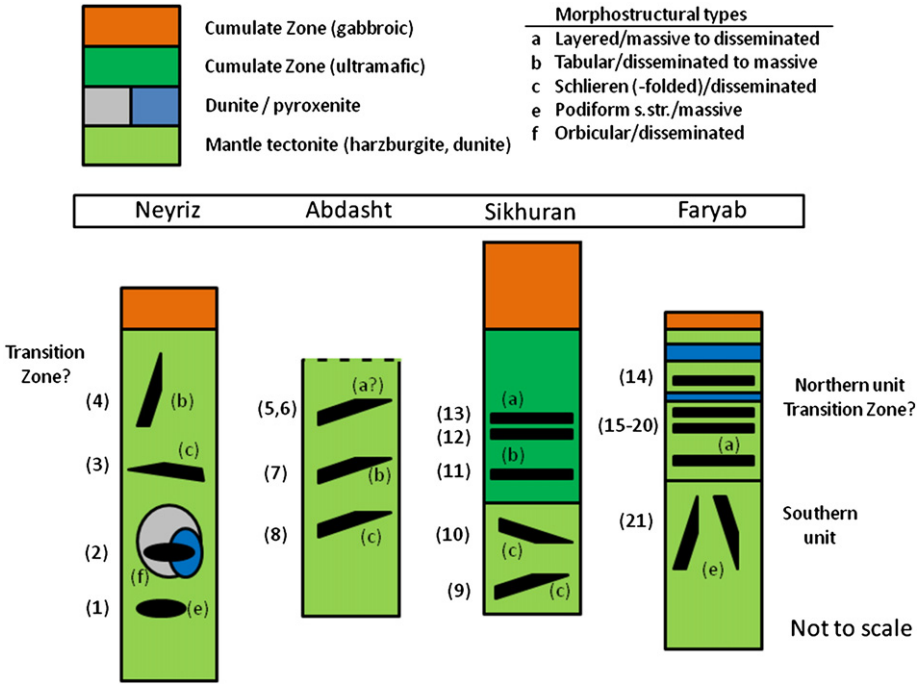

Fig. 4. Schematic stratigraphic columns of the ultramafic–mafic complexes showing approximate position of the chromite ores investigated and their prevailing textural types. Classification of chromitite modified from Burgath et al. (2002).

located within the mantle tectonite zone, with no indications supporting a transition zone setting. With the Khajeh Jamali and Cheshmeh Bid chromite mines, two small production sites are in operation. In the Khajeh Jamali chromite mine (see No. 3 in Table 1 for details of location and petrography) chromite lenses of the folded schlieren-type occur in harzburgite and dunite, with a chromite potential of approximately 0.12 million tonnes (Rajabzadeh, 1998). The Cheshmeh Bid chromite mine (Table 1, No. 4) exposes a steeply dipping, probably continuous platy chromitite. The main ore type is medium- to coarse-grained, cataclastic massive ore (Fig. 3B) besides disseminated and schlieren-type ore. Dunite halos and discordant veinlets of clinopyroxenite were identified. The ore body was attributed to the upper transition zone by Rajabzadeh (1998), with minor portions in the basal crustal cumulates.

Small lenses of podiform massive to dense chromitite with dunite halos in serpentinized harzburgite occur close to Tange Hana (No. 1, Table 1); these chromitites are unusually enriched in PGE (see following paragraphs). Close to this location, chromitite with abundant orbicular textures is hosted by clinopyroxene-impregnated dunite containing clinopyroxene oikocrysts, and also by clinopyroxenite; the chromitite body of 10 m length is transected by gabbroic dykes up to 10 cm wide, and troctolite, pyroxenite, wehrlite and gabbro occur close by indicating crystallisation of mafic melts in portions of the upper mantle.

4.2. Abdasht complex

The ultramafic mantle section contains several chromitite ore bodies that follow three distinct pseudostratigraphic levels. Ore bodies are up to 3 km long and some are actively mined. In 1969, reserves of 0.5–1 million tonnes were indicated (Schmidt, 1974). At that time, about 130 tonnes per day of ore (grading 52% Cr_2O_3) was mined at three levels connected by a shaft inclined at 48°. According to Hillebrand (1983), the main ore body extends for 1000 m along strike and dips 40 to 60° north. Some massive chromitite lenses are 10 to 25 m long and 0.5–3 m thick. In 2005, production took place in ore body 1 on level 8 at 220 m depth. This level 1 ore body at Abdasht Mine (Loc. 5, Table 1) consists of strongly deformed ore with ore boudins reaching 3 m in thickness. Level 1 chromitite with abundant, undeformed nodular ore (Fig. 3C) is also exposed along the south-western border of the complex (Loc. 6, Table 1). A small active mine in the centre of the Abdasht complex exploits a steeply inclined folded schlieren-type chromitite attributed to level 2 chromitite (Loc. 7, Table 1; Fig. 3D). The level 3 chromitite (Loc. 8, Table 1) exposes the stratigraphic footwall in the area along the eastern border of the complex, with boudin-shaped lenses of 0.5 to 3 m thickness that can be traced for 3 km along strike. The succession from schlieren-type ore to tabular and layered massive ore types points to a position high up in the mantle tectonite zone, probably close to the transition zone towards the base of the cumulates.

4.3. Sikhuran complex

Chromitite in the dunite zone along the northern margin of the Sikhuran massif consists of disseminated, occasionally banded ore of the schlieren-folded type (Loc. 9 and 10, Table 1), with some massive and nodular ore. In the transition zone 200 m below the basal cumulates (Sobhan, Loc. 11, Table 1) lenses of banded and net-textured chromitite are crosscut by veinlets of websterite and gabbro.

The Sikhuran mine (Loc. 12, Table 1, Fig. 3E) is an active small-scale mining operation comprising an open pit and a system of adits in “cumulate dunite” according to Ghasemi et al. (2002). The banded chromitite is composed of alternating chromite- and olivine-rich layers, and occurs in a package totalling to 20 m in thickness. Single chromite-rich layers are 1–2 m thick and laterally extensive, showing complex internal textures. Chromitite is composed of finely banded, partly wavy, massive and nodular types. Cumulate textures are locally developed. Some layers show textures of magmatic breccia, e.g. consisting of angular olivine fragments embedded in fine grained chromite. Some fairly thin (<0.5 m) layers of olivine that are intercalated between chromite carry disseminated sulphides (pentlandite, chalcopyrite, pyrrhotite). In the vicinity of the Sikhuran Mine (Loc. 13, Table 1), hard lumpy ore was sampled from an ore pile next to a prospect of sulphide-bearing chromitite. Such nodular and disseminated ores contain visible, up to 1.2% intergranular sulphides that mainly consist of pentlandite.

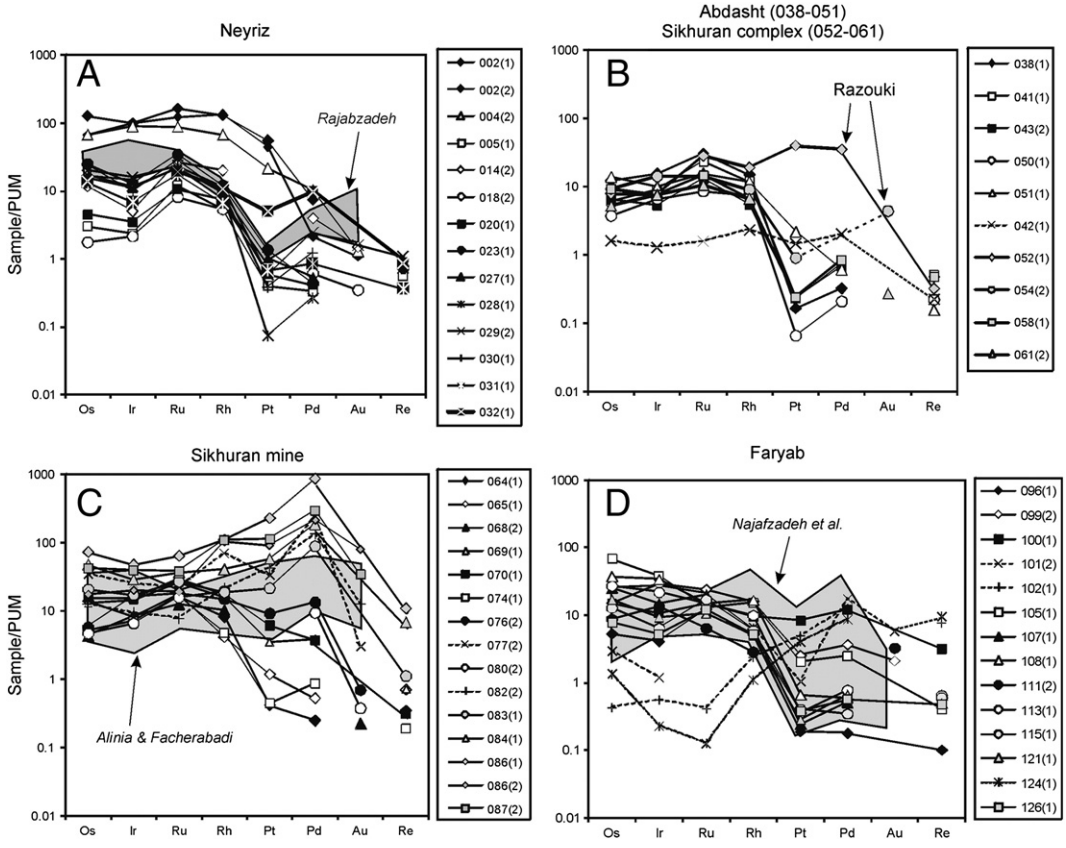

Fig. 5. Distributions of PGE, Au and Re concentrations normalised to primitive upper mantle (PUM; Becker et al., 2006) in chromitites, dunites and pyroxenites (stippled lines). A) Neyriz ophiolite; grey field indicates range of three PGE patterns published by Rajabzadeh (1998); B) Abdasht complex (samples 038 to 051) and lower unit of Sikhuran complex (samples 052 to 061); C) Sikhuran mine area; grey field for 5 analyses from Alinia and Facherabadi (2005); D) Faryab complex; grey field gives range of 10 analyses from Najafzadeh et al. (2008) and of 5 analyses from Rajabzadeh (1998). Sample numbers refer to Table 2; number in brackets refers to the analytical method used (1: ID-ICP-MS on chromite concentrates prepared on a Wilfley table; 2: Ni sulphide fire assay on whole-rock samples).

4.4. Faryab complex

Reserves plus past production of chromite are estimated to 5–10 million tonnes. In the northern unit (Doveis, Shahin, Amir, Shahriar, Fètr; locations 14–20; Table 1), most deposits are platy and composed of one or several horizons, up to 40 m thick, of disseminated ore. They may be traced along strike for several 100 m to several km and dip shallowly to the NW or NE. In the southern unit, chromite deposits occur as steeply dipping to vertical lenses and arrays of parallel lenses carrying disseminated, nodular and massive ore (Reza Mine, Loc. 21, Table 1); the lenses are probably connected by isoclinal folds.

The extensive mining areas of Doveis and of Bahar Sang are located close to the Rudan fault in the stratigraphically upper parts of the banded dunitic unit that either represents a transition zone or a cumulate zone dunite. Nine to eleven subhorizontal to 10° NE dipping chromite horizons containing disseminated to banded ore, 0.5–3 m thick, have been extensively mined by open pits and short adits. At present, the low grade (40–45% Cr_2O_3) renders mining uneconomic. A sequence of chromitite deformed into open folds at Doveis may attest to slumping processes in a magma chamber at the base of the crust. A sulphide-mineralized (pentlandite, pyrrhotite) dunite horizon, 1.5 m thick, is present in the immediate hanging wall of a prominent chromitite horizon of 2 m thickness.

The Fètr Tunnel 6 mine (Loc. 17, Table 1) is presently active and contains reserves of 3 million tonnes. It is located in the same stratigraphic level as the deposits of Nemat, Amir and Shahriar, which are separated from each other by faults. Approximately 5 horizons of disseminated to massive, often cataclastic chromitite are mined in this level along the foot of a cone-shaped mountain that has been eroded on all sides (Hillebrand, 1983). Veinlets of pegmatoidal clinopyroxenite are fairly abundant in the chromitite. The 24 m thick main ore body at the Shahriar Mine (Loc. 20, Table 1) is overlain by massive pyroxenite, wehrlite and olivine websterite that carry disseminated chromite and sulphide mineralization (Fig. 3F). The chromite mineralization is believed to belong to the mantle–crust transition zone of the Sorkhband ophiolite complex. Deformation textures within the chromitites, such as boudins, attest to high-temperature mantle deformation.

5. Geochemistry of the chromite ores

5.1. Major and trace elements

In chromite ore, Cr_2O_3 concentrations range from 15 to 60 wt.%, SiO_2 from 0.5 to 25 wt.%, and MgO from 14 to 34 wt.%, respectively (Appendix 1). This indicates that the samples represent mixtures of chromite and Mg-rich silicates in variable proportions. Cr–Al ratios (expressed as $100*Cr_2O_3/(Cr_2O_3+Al_2O_3)$ in wt.%) correlate well with Cr numbers (molar $100*Cr/(Cr+Al)$) calculated from electron microprobe analyses of individual chromite grain cores (see Section 6.1). Thus, the Cr–Al ratio is governed by chromite alone. In contrast, the Mg–Fe ratios (expressed as $100*MgO/(MgO+Fe_2O_3)$ in wt.%) display no correlation with Mg numbers in spinel (molar $100*Mg/(Mg+Fe^{2+})$) but correlate well with SiO_2, indicating that silicate phases have a variable influence on the whole-rock Mg–Fe ratio. The samples from the Neyriz ophiolite have slightly lower Cr–Al (81–83), whereas those from Abdasht, Sikhuran and Faryab overlap to a large degree at Cr–Al of 83–88. Overall, chromitites from Faryab are characterised by the highest Cr–Al ratios.

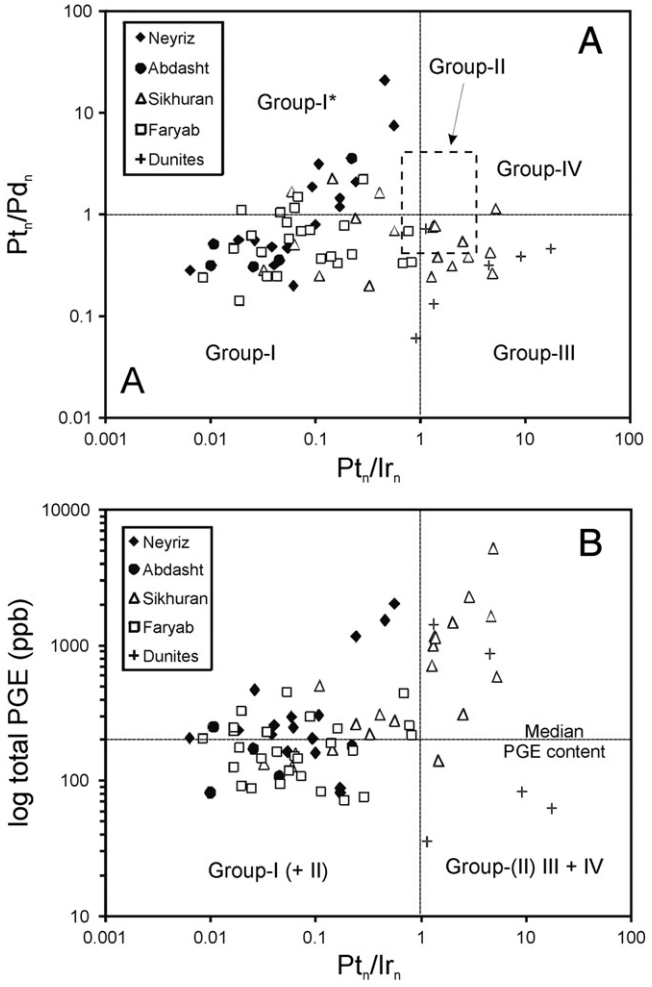

Fig. 6. A) Mantle-normalised ratios of Pt/Ir versus Pt/Pd for chromitites and some dunites (locations of dunites from Sikhuran and Faryab are not distinguished in the diagram). Group definition according to Burgath et al. (2002); B) Normalised Pt/Ir versus total PGE concentration. Both diagrams also include PGE analyses from Iranian chromitite taken from the literature (cited in the text).

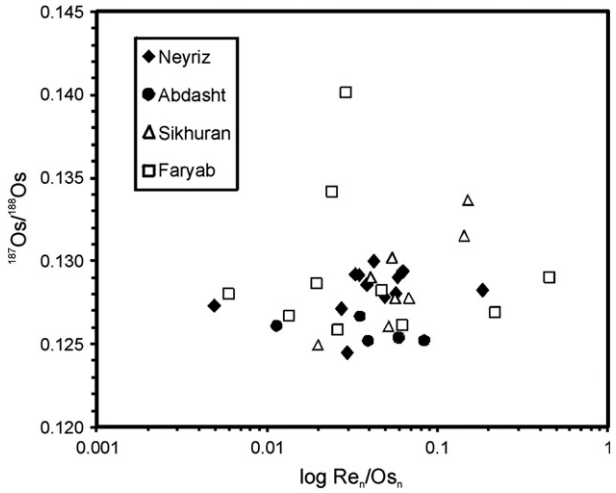

Fig. 7. Re/Os ratio normalised to primitive upper mantle versus $^{187}Os/^{188}Os$ ratios in chromitites.

A consistent level of 1000 ppm Ni in the Cr-rich samples points to substitution of considerable amounts of Ni in the chromite structure. Sulphide-bearing chromitites from Sikhuran have higher Ni concentrations (5000–8500 ppm), along with Cu (1550–4600 ppm) indicating that Ni and Cu are controlled by sulphides. Elevated Cu was also observed in one sample each from Abdasht (168 ppm) and Faryab (494 ppm). In the remaining chromitites, Cu is below the detection limit of 10 ppm. Some chromites from Abdasht and Sikhuran also carry elevated contents of As (25–263 ppm).

Harzburgite and dunite hosting chromitite are moderately to highly serpentinized in all complexes investigated; loss on ignition ranges from 6.2 to 16.4 wt.%. Their refractory chemical compositions are reflected by low Al_2O_3 (0.25–1.1 wt.%) and CaO (<1.2 wt.%) concentrations, as well as high Mg–Fe ratios (77–89), Ni (1800–3100 ppm) and Cr concentrations (1700–16000 ppm). Pyroxenites are characterised by low Al_2O_3 (0.8–2.5 wt.%), high Mg-Fe ratios (75–84), variable CaO (1.5 wt.% in orthopyroxenite to 20 wt.% in clinopyroxenite), high Cr (2600–5000 ppm) and moderate Ni concentrations (280–900 ppm).

5.2. PGE and Os isotope geochemistry

PGE concentrations in the majority of the Iranian chromitites range from 100 to 500 ppb; the median value for the total PGE content (6 PGE) of 52 analyses is 208 ppb (Table 2). PUM (Primitive Upper Mantle; Becker et al., 2006)-normalised PGE patterns are characterised by negative slopes from the IPGE to the PPGE (Fig. 5). The IPGE and Rh have almost equal normalised abundances displaying values ranging from 5 to 100 times PUM, whereas Pt, Pd, Au and Re often display a minimum ranging from 0.1 to 10 times the respective PUM values.

Most PGE patterns of chromitites from the Neyriz ophiolite have similar shapes characterised by negative Pt anomalies (normalised $Pt_n/Pd_n<1$) and low Pd, Au and Re concentrations (Fig. 5A). Only two samples collected from chromite pods at Tange Hana have elevated PGE concentrations and $Pt_n/Pd_n>1$. With the exception of samples from Razouki/Sikhuran, chromitites are also highly depleted in Pt and Pd in the Abdasht and lower Sikhuran complexes, Esfandagheh area (Fig. 5B). At the Sikhuran mine, two types of PGE patterns are observed (Fig. 5C): (1) most chromitites have low to moderate PGE concentrations, negative Pt anomalies and Pt_n/Pd_n close to 1; (2) a group of sulphide-bearing chromitites and chromite-rich dunites, however, is characterised by higher PGE totals, by PPGE > IPGE, by $Pt_n/Pd_n<1$ and also by elevated Au and Re concentrations (Fig. 5C). PGE patterns published by Alinia and Facherabadi (2005) from chromitites of the Sikhuran mine reveal somehow flatter curves, but also display $Pt_n/Ir_n>1$ and $Pt_n/Pd_n>1$. Chromitites of the Faryab complex have negatively shaped normalised patterns with IPGE > PPGE, but reveal more variation in their Pt and Pd concentrations (Fig. 5D). Ten PGE patterns of chromitites published by Najafzadeh et al. (2008) and five published by Rajabzadeh (1998) are similar to those presented in this paper; one analysis, however, was slightly enriched in Pt (84 ppb), Pd (126 ppb) and Au (17 ppb) (Najafzadeh et al., 2008).

Burgath et al. (2002) developed a classification for ophiolitic chromitites that is primarily based on Pt/Ir and Pt/Pd ratios. Group-I, termed the "normal ophiolite type" is characterised by negative slopes in normalised diagrams from Os to Pt and by $Pt_n/Ir_n<0.9$; the total PGE content is <200 ppb but individual samples with unusual high contents up to 7.7 ppm have been found. Group-II, the "diverging ophiolite type", has higher proportions of base metal sulphides and may carry up to 11 ppm PGE. The Pt_n/Ir_n ratio varies from 0.9 to 4.6, and the PGE pattern is generally flat with PPGE/IPGE ~1. Group-III is dominated by Pd and abundant base metal sulphides, by $Pt_n/Ir_n>1$ and Pt_n/Pd_n mostly <1. Three subgroups are distinguished based on the abundance of PGM (low in IIIa, high in IIIb) and the host rock of mineralization (chromitite in IIIa and IIIb, dunite in IIIc). Up to 23 ppm PGE contents were recorded. Group-IV, the "Pt-dominated sulphide-poor ophiolite type" is restricted to late-stage chromitites in ultramafic cumulates close to the crust–mantle transition zone. The Pt_n/Ir_n and Pt_n/Pd_n ratios are >1, and PGE contents may reach up to 25 ppm.

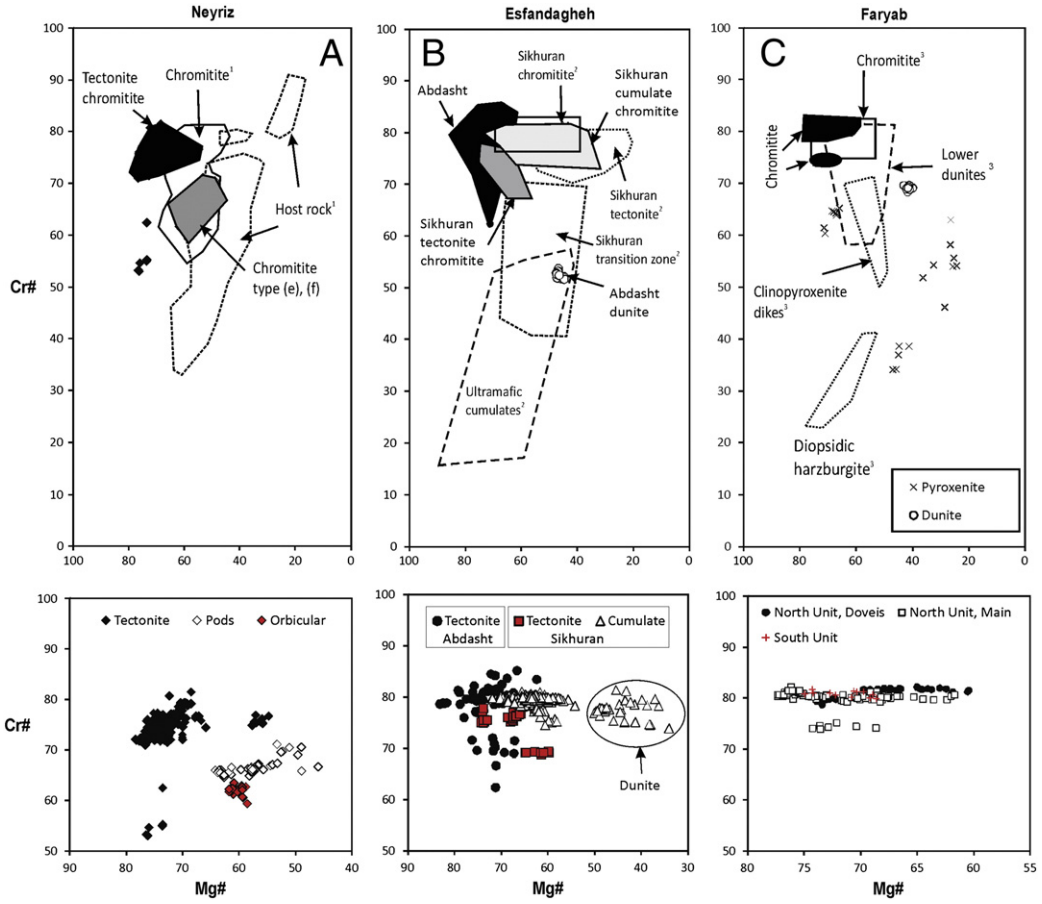

Fig. 8. Variation of Mg# and Cr# in chromites from chromitites of ultramafic complexes in southern Iran. Upper diagrams illustrate the spinel compositional field; lower diagrams outline details in the high-Cr area. A) Chromite from the Neyriz complex, including samples from tectonite-hosted chromitite (black diamonds), orbicular clinopyroxenite-hosted chromitite (red) and small podiform chromitite pods in dunite (open diamonds); [1]fields for chromitite and host rock chromites from Jannessary (2003). B) Chromite from the Esfandagheh area, including tectonite-hosted chromitite from Abdasht (black circles), accessory chromite in dunite from Abdasht (open circles), tectonite-hosted chromitite from Sikhuran (red squares), cumulate-hosted chromitite from Sikhuran (open triangles); [2]fields for chromite from chromitite, mantle tectonite, transition zone and ultramafic cumulates from Sikhuran are from Ghasemi et al. (2002). C) Chromite from the Faryab area, including the Doveis mine (black circles), the main ore body in the northern unit (□), the Reza mine in the southern part of the complex (+) and discordant clinopyroxenite veins (x); [3]fields outlining chromite compositions from chromitite, the lower dunites (northern Faryab complex), diopsidic harzburgites (southern Faryab complex) and clinopyroxenite dikes according to Najafzadeh et al. (2008).

According to this concept, most (n = 18) of the chromitites investigated during this study have group-I PGE patterns characterised by $Pt_n/Ir_n < 0.9$ and $Pt_n/Pd_n < 1$, representing the "normal ophiolite type". Another 16 samples have $Pt_n/Pd_n > 1$ (up to 20) and PGE totals up to 1.5 ppm and are classified here as group-I* (Fig. 6a). Examples representing the group-II have not been clearly encountered in this study.

Although most chromitites have low total PGE concentrations (<500 ppb) and low Pt/Ir ratios (Fig. 6b), two exceptions are encountered, namely sulphide-bearing chromitite from Sikhuran with high Pd + Pt, and pods of sulphide-poor chromitite from Neyriz. At Sikhuran, total PGE may reach 5 ppm (Fig. 6b), while Pd_n/Ir_n ranges from 4 to 15 and Pt_n/Ir_n from 1 to 5, respectively. At Tange Hana in the Neyriz ophiolite, small pods of sulphide-poor chromitite have total PGE of 1.5 to 2 ppm, and Pt_n/Ir_n of 0.5. At Faryab, most chromitites have low Pt + Pd; one sample from the Doveis ore body has normalised Pt and Pd concentrations similar to those from associated sulphide-bearing dunites. These patterns represent group-III of Burgath et al. (2002), namely the "Pd-dominated sulphide-enriched ophiolite type". One sample (Razouki/Sikhuran) straddles the boundary to the group-IV field. The scarcity of discrete Pd- and Pt mineral phases in these samples (see later) suggests group-IIIa rather than-IIIb that has frequent PGM.

In most of the chromitites, $^{187}Os/^{188}Os$ ratios vary from 0.125 to 0.130, and Re/Os is low (<0.1) (Table 2; Fig. 7). Chromites from Abdasht show the most "primitive" (least radiogenic), and least variable Os isotopic composition (average 0.1257). In contrast, $^{187}Os/^{188}Os$ in chromitites from Neyriz average to 0.1282 (range 0.1245–0.1300), whereas those from Sikhuran scatter more widely (0.125–0.134) and average to 0.1289. Chromitites from Sikhuran form a well-defined positive trend towards more radiogenic Os with increasing Re/Os ratio and increasing Os concentration (Fig. 7). Chromitites from Faryab range from 0.126 to 0.140 and average to 0.1294, and thus are similar to Sikhuran. Sulphide-bearing dunites from Faryab (not shown in Fig. 7) have higher Re/Os (>1) and rather radiogenic $^{187}Os/^{188}Os$ compositions (>0.16). In contrast, sulphide-poor dunites from Abdasht have primitive compositions with low Re/Os (0.013) and chondritic $^{187}Os/^{188}Os$ (0.1275).

6. Mineralogy and mineral chemistry of chromitite, dunite and platinum-group minerals

6.1. Chromite and olivine in chromitite and dunite

The chemical composition of chromite and olivine from chromitite and a few ultramafic host rocks is illustrated in Figs. 8 to 10; a summary of the data can be found in Appendix 2. Only homogeneous core compositions of chromite are considered. In general, southern Iranian chromites are Cr- and Mg-rich, and are all classified as high-Cr magnesiochromites. Aluminium-rich chromites are restricted to

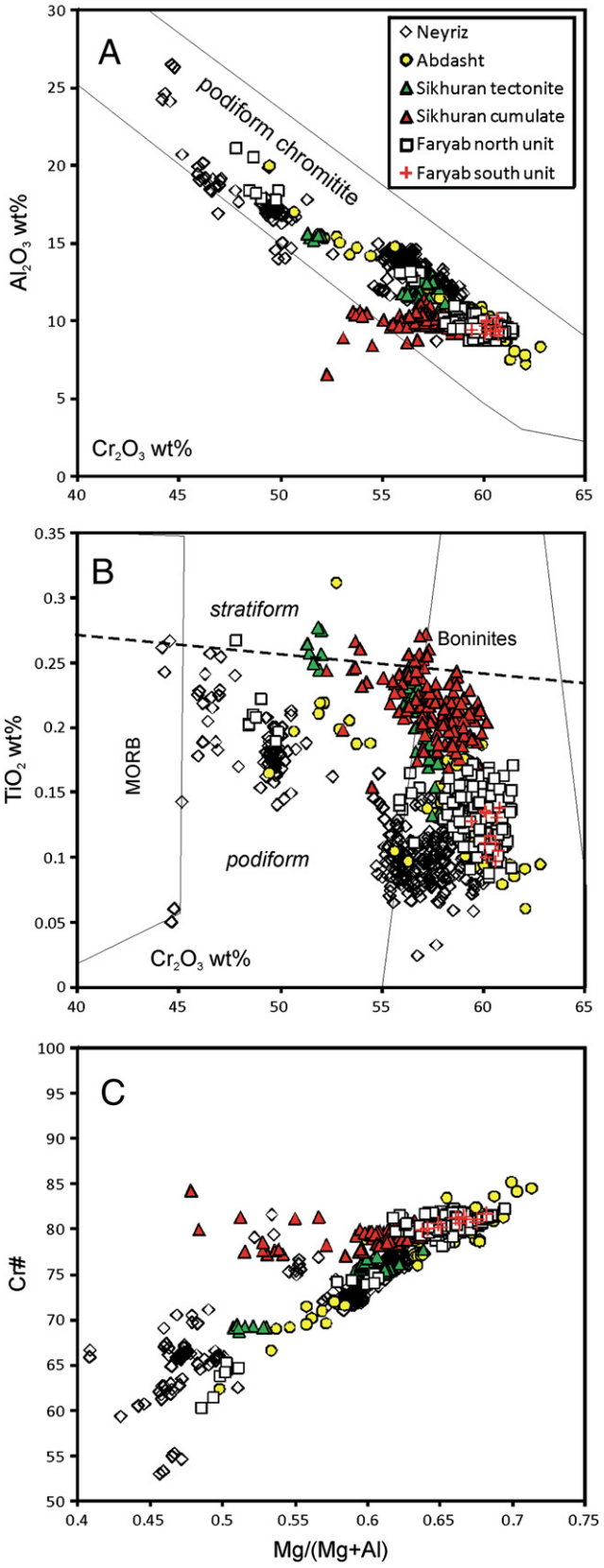

Fig. 9. Compositions of chromite from chromitite of southern Iran. A) Variation of Cr_2O_3 and Al_2O_3 (wt.%). Compositional field of podiform chromitite after Bonavia et al. (1993). B) Variation of Cr_2O_3 and TiO_2 (wt.%). Fields of MORB and boninite are from Dick and Bullen (1984) and Arai (1992). C) Variation of Mg/(Mg + Al) versus Cr# (after Stowe, 1994). Same legend for all diagrams.

some ultramafic host rocks and some pyroxenites (Figs. 8, 9a). Titanium concentrations are generally below 0.3 wt.% (Fig. 9b).

Olivine in dunite-hosted chromitite and chromite-bearing dunite from all massifs is highly magnesian (Mg# 90–98). The concentration of NiO in olivine varies from 0.1 to 1 wt.% (Fig. 10a). Within-sample standard deviations of Mg# in olivine are low, except in dunites from Sikhuran where olivine close to chromite grains has higher Mg# than olivine at some distance to chromite; such differences typically reach 3.5 mol% forsterite component (Appendix 2).

Chemical parameters such as Mg# and Ni concentrations correlate between chromite and olivine, indicating equilibration between them (Fig. 10b). Overall, the spinel and olivine compositions point to derivation from highly depleted, refractory upper mantle. The most primitive (e.g. Mg-rich) compositions are encountered in the Abdasht complex and in basal parts of the Sikhuran complex (Razouki). In the Faryab complex, two distinct populations are observed, a more primitive (Mg# in olivine 95, Cr# in spinel 60–80) in dunitic host rocks, and a more differentiated in websterites and pyroxenites (Mg# in olivine 82–90, Cr# in spinel 30–65).

6.1.1. Neyriz

The mantle tectonite-hosted chromitites from the two larger ore bodies (Cheshmesh Bid, Khajeh Jamali) reveal Cr# of 73–80 and Mg# from 50 to 80, with the bulk at 60–80 (Fig. 8a). The compositions of chromite grains analysed from three concentrate samples of different grain sizes taken at the Khajeh Jamali plant are Mg- and Cr-rich (Cr#, 70–80; Mg#, 65–78), with only a few more Al-rich compositions (Cr#, 52–63). Chromite in small pods of massive chromitite, and clinopyroxenite-hosted chromite at Tange Hana have lower Cr# (60–70) and Mg# (50–60), but higher Ti, V, Mn and Zn. The V concentrations are highest in the most-Fe-rich sample from the tectonite-hosted Cheshmesh Bid mine. Chromite from chromitite at Neyriz analysed by Jannessary (2003) had more variable Cr# (50–85) and overall lower Mg# (45–70). Olivine associated with chromitite (mainly inclusions in chromite) has high Mg# (ca. 95) and NiO, whereas Mg# of matrix olivine from harzburgite and dunite shows typical ranges of residual mantle rocks (Mg#, 90–92).

6.1.2. Abdasht

Chromites from three chromitite levels vary little in Cr# (77–81) and Mg# (65–85) (Fig. 8b), but individual samples plot into distinct fields. The minor element levels are low (<0.2 wt.% TiO_2). NiO correlates with Mg# in chromite throughout the complex, with level Abdasht 1 being considerably lower in Ni and Mg, but higher in Cr# compared to the levels Abdasht 2 and 3. Accessory chromite in dunite in the hanging-wall of level 1 chromitite has Cr# of 52 and Mg# of 45, very different from the chromite ore. A concentrate collected at the Abdasht plant reveals a more variable composition, with Cr# = 60–85 and Mg# = 65–75; however, this plant is also fed by ores mined at the Soghan complex further to the east. According to Ahmadipour et al. (2003), Cr# in massive chromitites at Soghan ranges from 78 to 83, and Mg# from 48 to 65. At Abdasht, olivine associated with chromite is highly magnesian (Mg#, 96–97) and Ni-rich; olivine in dunite in the hanging-wall of level 1 chromite has Mg# 89–90 and NiO concentrations of 0.3–0.4 wt.% (Fig. 10a).

6.1.3. Sikhuran

Most of the chromite analysed from chromitite has high Cr# (75–82), irrespective of the textural and structural positions (Fig. 8b). Only one sample (from Sorkh Jallab) has lower Cr# of 70 at Mg# = 60. From its structural position, it is attributed to the tectonite unit. Other chromitites in the tectonite unit have Cr# ranging up to 78. Chromite from the chromitite ore body at the Sikhuran mine in the cumulate zone has higher Cr# (75–81) and intermediate Mg# (45–65), whereas chromite in associated dunite has similar Cr# (74–80), but is more Fe-rich (Mg#, 29–50). Both, dunite and chromitite are often associated with sulphides.

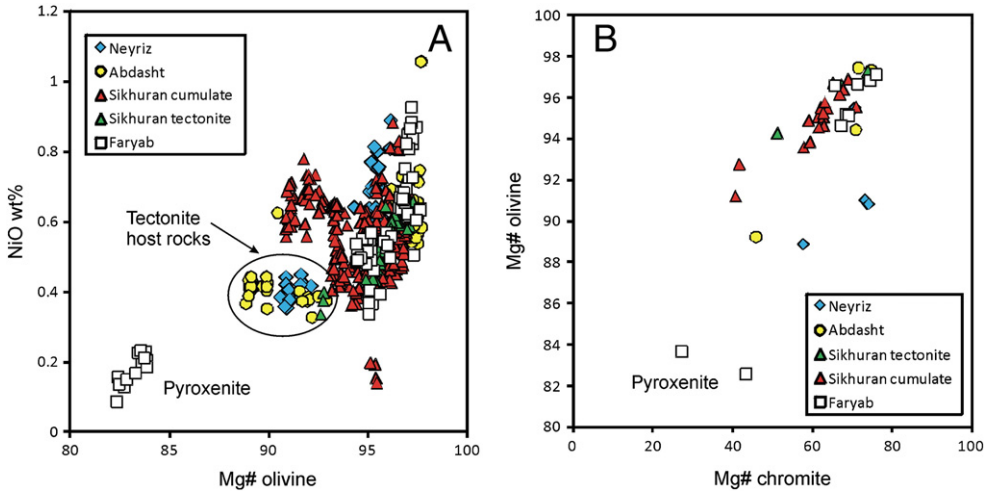

Fig. 10. A) Composition of olivine in chromitite and ultramafic rocks of southern Iran. B) Average Mg numbers of chromian spinel and olivine from different complexes.

Minor element concentrations are low and rather similar between tectonite and cumulate chromite; despite diverse textures and slightly different Cr#, there is no clear chemical distinction between them.

Olivine associated with chromite is Mg- and Ni-rich (Mg#>95). In sulphide-rich chromitite and in dunite, Mg# ranges from 90 to 95 (Fig. 10a). In these rocks, primary olivine may be transformed into a Mg-rich (Mg# 95) and Ni-poor (0.2 wt.% NiO) olivine, especially along contacts with Ni-rich sulphides.

6.1.4. Faryab

Chromites from ore bodies in the lower unit (Reza) and the upper unit (Main ore horizon and Dovais) have very similar chemical compositions in terms of Cr# (75–82) and Mg# (60–80) (Fig. 8c).

Accessory chromite associated with sulphides in pyroxenite veins has different compositions (Fig. 8c). Their Cr# (30–65) and Mg# (20–70) are correlated, and the trend plots off the ophiolitic chromite trend to higher Fe^{2+}. Pyroxenitic chromite also carries higher TiO_2 (up to 0.65 wt.%), V_2O_3 (up to 0.9 wt.%), ZnO (up to 0.5 wt.%), slightly higher MnO (up to 0.5 wt.%), CoO (up to 0.08 wt.%), and lower NiO (<0.15 wt.%) than dunite and harzburgite-hosted chromite. Ti, V, Mn and Ni correlate with Fe^{2+}, whereas Zn correlates with Mg (different to dunite-hosted chromite, where Zn correlates with Fe). This may indicate sulphide control of Ni and Zn.

In the Faryab complex, olivine associated with chromite is Mg- and Ni-rich (Mg#>95, >0.3 wt.% NiO), except for pyroxenite dikes that have low Mg# (82–83) and NiO (0.1–0.3 wt.%) (Fig. 10a).

6.2. Platinum-group minerals

Eighty-two polished sections of chromitite and associated dunite were investigated by reflected light microscopy to characterise the carriers of PGE mineralization. 160 grains or aggregates carrying at least one platinum-group mineral (PGM) and ranging in size up to 40 μm were identified. Their parageneses and distributions within the different complexes are summarised in Table 3. Representative analyses are given in Tables 4 and 5, and examples of PGM are presented in Figs. 11 and 12. Three types of PGE mineralization were distinguished in the samples: (1) mono- or polyphase inclusions of PGM in chromite. They occur without or with base metal sulphide (usually Ni and/or Cu sulphides, mainly pentlandite, millerite and bornite) and/or silicate (usually calcic amphibole, clinopyroxene and chlorite); (2) mono- or polyphase PGM in silicate matrix between chromite grains, without base metal sulphides (BMS); and (3) PGM associated with base metal sulphides (usually pentlandite, millerite) interstitial to chromite, or within dunite.

6.2.1. Laurite–erlichmanite

Laurite is the most abundant PGM and is present in all ultramafic complexes studied. It usually forms euhedral crystals from less than 1 to 20 μm in size, and is commonly intergrown with other PGM, BMS, and/or silicates (Fig. 11A–C) occurring in chromite, but rarely in silicate matrix. Along cracks and in alteration halos of chromite, laurite is replaced by Ru-rich alloys and Ru-rich oxides (Fig. 11E). Erlichmanite was observed in all ophiolites as well, but is particularly abundant in samples from the Faryab complex (Fètr 6 and Nemat mines).

Altogether, 114 grains of laurite and erlichmanite were documented, and 95 microprobe analyses were carried out. Ninety-five percent of the laurites are hosted by chromite, 2% by ferritchromite, 2% by silicates, and 2 grains occur at the chromite/silicate grain boundary. Eighty-five percent form euhedral inclusions (either hexagonal or cubic shapes), 10% are subhedral and only 5% are classified as anhedral. Thirty-eight percent of the laurite inclusions are associated with a silicate phase in polished sections; calcic amphibole appears to be most abundant, but clinopyroxene, phlogopite, olivine, chlorite, uvarovite and serpentine have been observed as well. Excluding silicates, 55% of the laurite-bearing inclusions appear monophase, 33% are two-phase (laurite + PGM or laurite + BMS; e.g. Fig. 11A, B), and 12% are three- and four-phase inclusions (Fig. 11C). Due to the small grain size (average diameter of the inclusions is 5.8 μm) and the two-dimensional arbitrary cut we assume that far more than the observed 45% of the inclusions consist of more than one phase.

Among coexisting PGM, BM-PGE-sulphides are most abundant (26% of the polyphase inclusions with laurite–erlichmanite), followed by Os–Ir–Ru alloy (7%) and irarsite (5%). Other partners are rare; no Pd phases have been observed and Pt phases are subordinate. Among coexisting BMS, Cu-bearing sulphides such as bornite are most common (33% of the polyphase inclusions with laurite–erlichmanite), followed by Ni-rich sulphides such as pentlandite (15%).

The chemical composition of laurite is dominated by the Ru–Os substitution (Table 4, Fig. 13a), with minor Ir, Rh, Fe, Ni, Cu, Co and As. A similar Ru–Os trend has been already documented for the Neyriz and Assemion (Faryab) complexes (Rajabzadeh et al., 1998). The maximum Os concentrations correspond to XOs [Os/(Ru + Os + Ir + Rh)] of 0.83, those of XIr to 0.26 and XRh to 0.05. The homogeneity of laurite compositions was evaluated in samples

Table 3
Summary of PGM and BMS mineralogy and of PGE concentrations in chromitites of southern Iran.

			Platinum-group minerals (PGM)	Base metal sulphides (BMS)	Textural position of PGM and BMS	Number of samples investigated for PGM	Number of PGM in all samples	% of samples PGM-bearing	Total PGE (6 PGE)	
Complex	Mine/ prospect	Chromitite and chromite type	Minerals	Minerals		N	N		range (ppb)	Pt_n/Ir_n
Neyriz	Tange Hana	e; Massive, tectonized	Laurite, (Cu,Ni,Ir)S, Ru–Ir–Os, Ru–Fe, irarsite, PtFe, RhNiAs, Ru–oxide	Pentlandite (pn)	Abundant PGM (+BMS+sil) inclusions in chromite	2	46	100	1161–2018	0.24–0.55
Neyriz	Tange Hana	f; Massive, disseminated, orbicular in cpxite	–	Ni–S, Co–Ni–Fe–S	Few interstitial BMS	1	0	0	82	0.17
Neyriz	Khajeh Jamali	c; Folded schlieren-type	–	Ni–S	Rare BMS inclusions in chromite	1	0	0	57–208	0.17
Neyriz	Cheshmesh Bid	b; Platy	Laurite, Ru–oxide, RhNiAs	Ni–S, Cu–Co–Ni–S	Rare PGM (+BMS+sil) incl	4	9	75	160–258	<0.1
Abdasht	Abdasht level 1	c; Folded schlieren-type, nodular	Laurite, cuproiridsite, Ir–Ru	pn, bn, Ni–S, Cu–S, NiAsS, NiSbS	Abundant BMS inclusions in chromite and silicate	2	2	50	81–249	0.01
Abdasht	Abdasht level 2	a; Folded platy	Laurite, Ru–Os–Ni–Ir, IrAsS, RhAsS, Rh–Sb–Cu	Ni–S, Cu–S, pn	PGM inclusions common, abundant BMS in chromite and silicate	2	6	50	100*	0.05
Abdasht	Abdasht level 3	a; Massive, nodular, disseminated	Laurite, (Ni,Ir)S	Ni–S, Ni–As	Anhedral BMS in chromite	2	2	50	36–172	0.03
Sikhuran	Razouki	c; Disseminated, massive, banded	Laurite, cuproiridsite, (Ni,Ir,Rh)S, osmium	pn, bn, Ni–S, chalcopentlandite, Cu–S	Abundant subhedral to anhedral BMS in chromite	2	4	50	158–581	0.06–5.2
Sikhuran	Sorkh Jallab	c; Disseminated folded schlieren-type	Laurite, Os–Ir	pn, bn, cp, Ni–S, Cu–S	Abundant BMS in ferritchromite rims	3	2	66	97	0.03
Sikhuran	Sobhan	b; Banded	Laurite	pn, cp, Ni–S, Cu–S	Interstitial BMS and abundant BMS in ferritchromite rims	3	3	66	134	<0.1
Sikhuran	Sikhuran mine	a; Banded, massive and nodular types; cumulate textures	Laurite, (Ni,Ir)S, Os–Ir–Ru, Ru–oxide, tolovkite	pn, Ni–S, bn, cp, Cu–S	Interstitial BMS and BMS in ferritchromite rims and chromite	17	27	71	110–1415	0.06–0.56
Sikhuran	Sikhuran mine	a; Sulphide-bearing, nodular and disseminated ore	Laurite, irarsite, Pd–Sb, Pt–oxide, gold	pn, Ni–S, cp, cub, bn, Cu–S, aspy, viol	Interstitial BMS, and in olivine and chromite	8	8	57	704–5183	1.3–4.8
Faryab	Doveis	a; Disseminated, banded; open folds	Laurite, Ru–oxide	bn, pn, Ni–S, Cu–S	Interstitial BMS and abundant BMS in ferritchromite rims	8	5	38	83–298	0.05–0.77
Faryab	Sohrab–Kamali	a; Banded, disseminated	Laurite, Os–Ir–Ru, Ru–oxide	awaruite	PGM (+BMS+silicate) inclusions	2	11	100	452	0.05
Faryab	Shahin	a; Disseminated	Laurite, Ru–oxide	awaruite, Ni–S	PGM (+BMS+silicate) inclusions	1	3	100	235	0.02
Faryab	Fètr Tunnel 6	a; Disseminated, massive and cataclastic	Cuproiridsite, (Ni,Ir)S>Laurite, Os–Ir–Ru, Ru–oxide	Ni–S, Cu–S	PGM (+BMS+silicate) inclusions, interstitial BMS	5	17	100	105–326	<0.02
Faryab	Amir	a; Banded, disseminated, schlieren-type	Laurite, (Ni,Ir)S	Ni–S, Cu–S, Ni–Co–Cu–Fe–S	PGM (+BMS+silicate) inclusions	3	8	100	152	0.06
Faryab	Nemat	a; Densely disseminated to massive	Cuproiridsite>Laurite, (Ni,Cu,Ir)S	Cu–S	PGM (+BMS+silicate) inclusions	1	4	100	n.a.	
Faryab	Shahriar	a; Banded, disseminated	Laurite, cuproiridsite, Ir–Ru	po, pn, cp, Cu–S	BMS interstitial	2	7	50	146	0.03
Faryab	Reza	e; Disseminated, nodular	–	Awaruite	BMS interstitial	1	0	0	108	0.07
Total						70	164			

Chromitite type: (a) layered/massive to disseminated, (b) tabular/disseminated to massive, (c) schlieren (-folded)/disseminated, (e) podiform s.str./massive, and (f) orbicular/disseminated chromitite.
BMS: aspy, arsenopyrite; bn, bornite; cp, chalcopyrite; cub, cubanite; pn, pentlandite; viol, violarite.
* Only one less PGM-rich sample was analysed.

where more than 5 grains had been quantitatively characterised; in most samples, the typical within-sample variation of XRu is expressed by standard deviations of 0.03–0.1; within massifs, the standard deviation is close to 0.2 (e.g., in sample 7462 from Neyriz,

Table 4
Representative electron microprobe analyses of PGE sulphides and sulpharsenides in chromitite of southern Iran.

Phase	Laurite	Laurite	Laurite	Laurite	Laurite	Erlichmanite	Erlichmanite	Erlichmanite	Cuproiridsite	Cuproiridsite	(Cu,Ni,Ir)S	(Ni,Cu,Ir)S	Hollingworthite	Irarsite	Irarsite
Section	7499	7559	7569b	7533a	7567	7575b	7524	7572	7575b	7562	7464	7562	7504b	7462	7464
Analysis no.	1	1	4	1	3	5	2	4	2	1	4	7	16	5	14
Complex	Abdasht	Faryab	Faryab	Sikhuran	Faryab	Faryab	Sikhuran	Faryab	Faryab	Faryab	Neyriz	Faryab	Abdasht	Neyriz	Neyriz
Host phase	Chromite	Chromite	Chromite	Chromite	Chromite	Chromite	Chromite	Chromite	Chromite	Chromite	Chromite	Chromite	Chromite/ chlorite	Silicate	Chlorite
Texture	Euhedral laurite + silicate	Euhedral 2-phase laurite + Os–Ir alloy	Euhedral monophase	Euhedral monophase, zoned grain	Euhedral monophase	Euhedral monophase	Euhedral 2-phase laurite + Ni–Ir–S	Euhedral 3-phase PGM + BMS	Euhedral monophase	Euhedral polyphase	Euhedral 3-phase laurite + (Cu,Ni,Ir)S + bornite + amphibole	Euhedral 3-phase with amphibole	Euhedral 2-phase with millerite	Anhedral polyphase with Pt phase	Anhedral crystals in chlorite matrix
Size (μm)	7.5	5	7	3	4	4	7	5	6	5.5	9	9	3.5	5	5
wt.%															
S	34.82	32.09	34.98	33.11	34.24	26.31	27.79	26.00	25.06	24.01	25.88	24.48	14.01	13.30	11.53
Fe	0.43	0.56	0.76	1.03	0.78	0.87	1.01	0.96	1.35	0.96	7.92	6.90	0.51	0.56	1.13
Co	bdl	bdl	bdl	bdl	bdl	bdl	bdl	bdl	bdl	bdl	0.13	0.11	bdl	bdl	bdl
Ni	0.25	bdl	0.10	0.10	bdl	bdl	0.29	bdl	0.27	0.13	6.75	13.81	0.38	0.11	bdl
Cu	bdl	bdl	bdl	0.17	bdl	bdl	bdl	1.63	10.59	10.21	17.35	6.27	bdl	bdl	bdl
As	bdl	bdl	bdl	bdl	bdl	bdl	0.26	0.60	bdl	bdl	bdl	bdl	28.91	23.56	29.46
Ru	43.22	30.98	42.87	37.85	40.05	5.38	12.24	3.94	bdl	1.06	7.99	bdl	bdl	4.75	1.19
Rh	0.44	bdl	0.85	bdl	1.79	bdl	bdl	bdl	12.40	6.77	2.51	0.65	36.87	9.99	15.28
Pd	bdl	bdl	bdl	bdl	bdl	bdl	bdl	bdl	bdl	bdl	bdl	bdl	bdl	bdl	bdl
Ag	bdl	bdl	bdl	bdl	bdl	bdl	bdl	bdl	bdl	bdl	bdl	bdl	bdl	bdl	bdl
Sb	bdl	bdl	bdl	bdl	bdl	bdl	bdl	bdl	bdl	bdl	bdl	bdl	2.28	bdl	0.10
Te	bdl	bdl	bdl	bdl	bdl	bdl	bdl	bdl	bdl	bdl	bdl	bdl	bdl	bdl	bdl
Os	15.14	22.63	12.21	22.88	12.68	59.65	42.86	50.58	bdl	1.28	5.98	bdl	bdl	1.27	0.22
Ir	2.92	12.79	7.32	2.74	7.47	7.16	14.30	13.74	47.88	52.53	20.90	44.08	14.26	44.45	33.69
Pt	bdl	bdl	bdl	bdl	bdl	bdl	bdl	bdl	1.08	bdl	0.41	bdl	bdl	bdl	5.20
Bi	bdl	bdl	bdl	bdl	bdl	bdl	bdl	bdl	bdl	bdl	bdl	bdl	bdl	bdl	bdl
Cr	1.43	2.13	2.21	2.89	2.70	2.67	2.36	3.13	2.62	2.89	3.79	3.05	1.84	0.75	1.61
Si	bdl	bdl	bdl	bdl	bdl	bdl	bdl	bdl	bdl	0.10	bdl	0.33	bdl	0.32	bdl
Total	98.66	101.16	101.28	100.77	99.71	102.04	101.12	100.59	101.25	99.95	99.63	99.68	99.06	99.07	99.41
at.%															
S	66.85	66.60	66.50	66.01	66.71	66.16	65.96	65.49	57.81	58.27	50.93	52.35	33.88	36.93	31.63
Fe	0.48	0.66	0.82	1.18	0.87	1.26	1.38	1.39	1.78	1.34	8.95	8.47	0.70	0.89	1.78
Co	–	–	–	–	–	–	–	–	–	–	0.13	0.12	–	–	–
Ni	0.26	–	0.10	0.11	–	–	0.37	–	0.34	0.18	7.25	16.13	0.50	0.17	–
Cu	–	–	–	0.17	–	–	–	2.07	12.33	12.49	17.23	6.77	–	–	–
As	–	–	–	–	–	–	0.26	0.65	–	–	–	–	29.92	28.00	34.57
Ru	26.32	20.39	25.84	23.93	24.75	4.29	9.21	3.15	–	0.82	4.99	–	–	4.19	1.03
Rh	0.27	–	0.50	–	1.09	–	–	–	8.91	5.12	1.54	0.43	27.78	8.64	13.06
Sb	–	–	–	–	–	–	–	–	–	–	–	–	1.46	–	0.07
Os	4.90	7.92	3.91	7.69	4.16	25.29	17.15	21.47	–	0.52	1.98	–	–	0.60	0.10
Ir	0.94	4.43	2.32	0.91	2.43	3.01	5.66	5.77	18.42	21.26	6.86	15.73	5.75	20.59	15.41
Pt	–	–	–	–	–	–	–	–	0.41	–	0.13	–	–	–	2.34
apfu															
S	2.01	2.00	1.99	1.98	2.00	1.98	1.98	1.96	1.73	1.75	1.02	1.05	1.02	1.11	0.95
Fe	0.01	0.02	0.02	0.04	0.03	0.04	0.04	0.04	0.05	0.04	0.18	0.17	0.02	0.03	0.05
Co	–	–	–	–	–	–	–	–	–	–	0.00	0.00	–	–	–
Ni	0.01	–	0.00	0.00	–	–	0.01	–	0.01	0.01	0.15	0.32	0.01	0.01	–
Cu	–	–	–	0.01	–	–	–	0.06	0.37	0.37	0.34	0.14	–	–	–
As	–	–	–	–	–	–	0.01	0.02	–	–	–	–	0.90	0.84	1.04
Ru	0.79	0.61	0.78	0.72	0.74	0.13	0.28	0.09	–	0.02	0.10	–	–	0.13	0.03
Rh	0.01	–	0.02		0.03	–	–	–	0.27	0.15	0.03	0.01	0.83	0.26	0.39
Sb	–	–	–	–	–	–	–	–	–	–	–	–	0.04	–	0.00
Os	0.15	0.24	0.12	0.23	0.12	0.76	0.51	0.64	–	0.02	0.04	–	–	0.02	0.00
Ir	0.03	0.13	0.07	0.03	0.07	0.09	0.17	0.17	0.55	0.64	0.14	0.31	0.17	0.62	0.46
Pt	–	–	–	–	–	–	–	–	0.01		0.00	–	–		0.07
Z	3	3	3	3	3	3	3	3	3	3	2	2	3	3	3

Table 5
Representative electron microprobe analyses of PGM and secondary PGE-bearing minerals in chromitite of southern Iran.

Phase	Ruthenium	Ru–Ir	Ir–Os	Garutiite?	Tolovkite	Pd_5Sb_2	Rh_2SbCu	RhNiAs	Pt–Fe	Os–Ir–Fe ox	Ru–Os–Ni ox	Ru–Os ox	Fe–Ru ox	Fe–Ru carb?	Pt oxide
Section	7464	7464	7507b	7499	7523b	7539	7504b	7489	7462	7559	7504b	7462	7561	7523b	7541
Analysis no.	17	18	1	4	1	5	14	2	29	3	12	13	1	3	61
Complex	Neyriz	Neyriz	Abdasht	Abdasht	Sikhuran	Sikhuran	Abdasht	Neyriz	Neyriz	Faryab	Abdasht	Neyriz	Faryab	Sikhuran	Sikhuran
Host phase	Chlorite	Chlorite	Chromite	Chromite	Serpentine	Pentlandite/ silicate	Chlorite	Chromite/ serpentine	Silicate	Chromite	Chlorite	Ferritchromite/ chlorite	Chromite	Serpentine	Ferritchromite/ serpentine
Texture	Anhedral blebs in Fe-hydroxide	Anhedral blebs in Fe-hydroxide	Euhedral 2-phase rimmed by $CuIr_2S_4$	Euhedral 3-phase laurite, Ni–Ir–S, Ir–Ni	Subhedral in Fe–Ru carbonate(?)	Attached to interstitial pentlandite	Round phase, with Os–Ir–Ru oxides	Subhedral 2-phase RhNiAs + Cu–Co–Ni–S	Subhedral with irarisite + RuIrOs	Anhedral in serpentine-filled crack in chromite	Euhedral monophase	Euhedral monophase	Euhedral monophase	Anhedral polyphase with pentlandite and tolovkite	Anhedral soft PGM
Size (μm)	2	2	5	1	7	25	2.5	3.5	5	7	10	25	3.5	25	33
wt.%															
S	bdl	bdl	bdl	3.82	9.67	bdl	bdl	bdl	bdl	0.08	0.08	bdl	0.80	0.26	0.08
Fe	1.67	4.23	0.72	6.44	1.46	0.54	1.66	0.66	10.83	11.77	1.81	8.89	43.33	24.65	1.41
Co	bdl	0.07	bdl	bdl	bdl	bdl	bdl	bdl	bdl	0.43	0.08	0.10	1.07	5.55	bdl
Ni	0.80	3.42	bdl	6.50	0.44	0.46	1.27	23.79	7.22	2.33	7.88	0.60	0.96	11.77	5.95
Cu	bdl	bdl	bdl	0.22	bdl	1.26	13.53	bdl	3.88	bdl	0.17	bdl	bdl	bdl	2.75
As	bdl	0.23	bdl	bdl	0.28	bdl	bdl	29.75	bdl	bdl	bdl	bdl	bdl	bdl	bdl
Ru	93.41	55.12	0.81	0.85	bdl	bdl	bdl	1.29	bdl	4.26	52.87	36.10	29.74	14.17	bdl
Rh	0.38	bdl	bdl	bdl	2.64	bdl	46.24	39.53	bdl	bdl	0.62	0.26	bdl	0.10	bdl
Pd	bdl	bdl	bdl	bdl	bdl	68.60	bdl	1.22	bdl	bdl	bdl	bdl	bdl	bdl	bdl
Ag	bdl	bdl	bdl	bdl	bdl	bdl	bdl	bdl	bdl	bdl	bdl	bdl	bdl	bdl	0.82
Sb	bdl	bdl	bdl	bdl	36.60	28.93	28.65	bdl	bdl	bdl	0.38	bdl	bdl	bdl	1.39
Te	bdl	bdl	bdl	bdl	bdl	bdl	bdl	bdl	bdl	bdl	bdl	bdl	bdl	bdl	1.20
Os	bdl	0.49	48.03	2.02	bdl	bdl	bdl	bdl	bdl	55.05	17.21	21.40	16.06	bdl	bdl
Ir	3.65	38.28	49.14	52.36	49.73	bdl	0.38	bdl	0.99	12.27	10.37	8.34	4.45	bdl	bdl
Pt	bdl	bdl	bdl	bdl	bdl	bdl	bdl	bdl	73.70	bdl	bdl	bdl	bdl	bdl	77.30
Bi	bdl	bdl	bdl	bdl	bdl	bdl	bdl	bdl	bdl	bdl	bdl	bdl	bdl	bdl	0.49
Cr	0.47	0.59	1.94	7.45	0.33	bdl	1.52	2.17	0.74	3.50	1.09	1.30	4.17	0.53	1.27
Si	bdl	bdl	bdl	0.33	0.19	bdl	0.41	0.47	bdl	bdl	bdl	2.29	bdl	0.28	bdl
O	na	na	na	na	na	na	na	na	na	na	na	16.87	na	36.51	6.64
Total	100.39	102.43	100.64	79.99	101.35	99.79	93.65	98.88	97.37	89.69	92.55	96.15	100.58	93.81	99.29
at.%															
S	–	–	–	–	32.65	–	–	–	–	0.40	0.28	–	2.01	0.07	0.24
Fe	3.03	8.55	2.44	22.15	2.84	1.06	3.12	0.97	25.49	32.16	3.82	9.14	62.74	14.40	2.49
Co	–	0.13	–	–	–	–	–	–	–	1.08	0.16	0.09	1.44	3.00	–
Ni	1.38	6.59	–	21.26	0.81	0.85	2.28	33.15	16.17	6.04	15.80	0.59	1.32	6.54	10.00
Cu	–	–	–	0.66	–	2.16	22.39		8.02	–	0.31	–	–	–	4.27
As	–	0.35	–	–	0.41	–	–	32.48	–	–	–	–	–	–	–
Ru	93.30	61.59	1.51	1.61	–	–	–	1.04	–	6.42	61.55	20.51	23.79	4.57	–
Rh	0.37	–	–	–	2.77		47.26	31.42	–	–	0.71	0.14	–	–	–
Pd	–	–	–	–	–	70.09	–	0.93	–	–	–	–	–	–	–
Ag	–	–	–	–	–	–	–	–	–	–	–	–	–	–	0.74
Sb	–	–	–	–	32.53	25.84	24.75	–	–	–	0.36	–	–	–	1.13
Te	–	–	–	–	–	–	–	–	–	–		–	–	–	0.93
Os	–	0.29	47.73	2.04	–	–	–	–	–	44.15	10.65	6.46	6.83	–	–
Ir	1.92	22.50	48.32	52.29	27.99	–	0.21	–	0.68	9.74	6.35	2.49	1.87	–	–
Pt	–	–	–	–	–	–	–	–	49.65	–	–	–	–	–	39.06
Bi	–	–	–	–	–	–	–	–	–	–	–	–	–	–	0.23
O	–	–	–	–	–	–	–	–	–	–	–	60.56	–	70.73	40.91

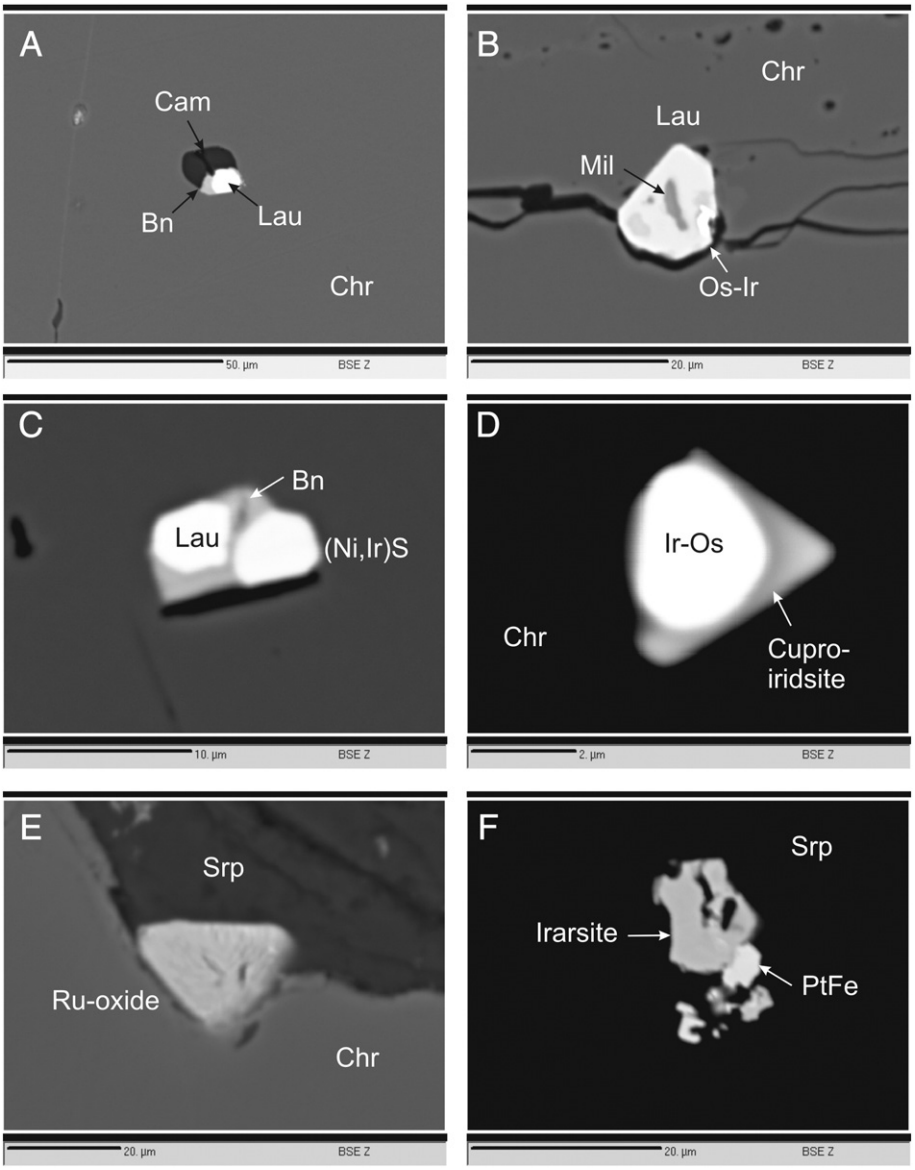

Fig. 11. Back-scatter electron images of platinum-group mineral inclusions in chromitites. A) Polyphase inclusion in chromite, polished section 7462, Neyriz ophiolite; B) polyphase inclusion in chromite, polished section 7517, Sorkh Jalla mine, Sikhuran complex; C) polyphase inclusion in chromite, polished section 7511, Razouki, Sikhuran complex; D) two-phase inclusion in chromite, polished section 7507b, level 1, Abdasht mine; E) Ru–(Os,Fe,Ir,Ni) oxide at margin of chromite towards serpentine, polished section 7462, Neyriz ophiolite; F) aggregate of irarsite and tetraferroplatinum (PtFe) in serpentine, polished section 7462, Neyriz ophiolite. Abbreviations: Bn, bornite; Cam, calcic amphibole; Chr, chromite; Lau, laurite; Mil, millerite; Srp, serpentine; Os–Ir and Ir–Os, alloys.

$XRu = 0.70 \pm 0.06$; in all samples from the Sikhuran massif, $XRu = 0.74 \pm 0.19$).

6.2.2. BM-PGE sulphides

Small amounts of BM-PGE-sulphides were observed in all complexes, and are most abundant at Faryab. Minerals of the thiospinel-type solution series cuproiridsite [$CuIr_2S_4$]–cuprorhodsite [$CuRh_2S_4$]–malanite [$CuPt_2S_4$] form euhedral to subhedral inclusions in chromite (Table 4). Most analyses plot into the cuproiridsite field with XIr (Ir/(Ir + Rh + Pt)) ranging from 0.64 to 0.97, XRh ranging from 0 to 0.32 and XPt ranging from 0 to 0.23. One analysis yielding $XPt = 0.5$ and $XIr = 0.3$ is classified as malanite. BM-PGE-thiospinel grains often are present in polyphase associations with laurite and erlichmanite, complex Ni–Fe–Cu–Ir–Rh–Ru–Os–Pt sulphides, Ni–Cu sulphides, and in one case cuproiridsite rims an Ir–Os alloy phase (Fig. 11D).

Complex Ni–Fe–Cu–Ir–Rh–Ru–Os–Pt sulphides of variable stoichiometry are encountered as part of polyphase assemblages with laurite, bornite and silicates (commonly calcic amphibole) in chromite (Fig. 11C). Most are very small, but quantitative analyses of the larger grains indicate a "monosulphide" stoichiometry with metal/sulphur ratios close to unity. When calculated to 2 atoms per formula unit, the base metals account for 0.6–0.8 apfu, and the PGE to 0.2–0.4 apfu. Base metals are Ni, Cu, Fe and traces of Co in variable proportions. PGE is mainly Ir and Rh, with some Ru, Os, Pt and even Pd present. The minerals are "BM-PGE-monosulphides" sensu Melcher (2000a), and fit to the Ni–Ir ("iridian millerite") and Cu–Ir (xingzhongite?) subgroups.

6.2.3. Os–Ir–Ru alloy phases

In the chromitite samples investigated, primary Os–Ir–Ru-rich alloy phases are rare. Most Os–Ir-rich phases form very small grains (<5 µm) intergrown with laurite, and thus are difficult to analyse by microprobe (Fig. 11B, D). However, the analyses demonstrate the presence of ruthenium, osmium, and iridium (Fig. 13b, Table 4).

Six laurites (4 from Faryab, 2 from Sikhuran) included in chromite investigated in this study are associated with minute Os–Ir-rich alloy phases. Recalculation of microprobe analyses (by subtraction of

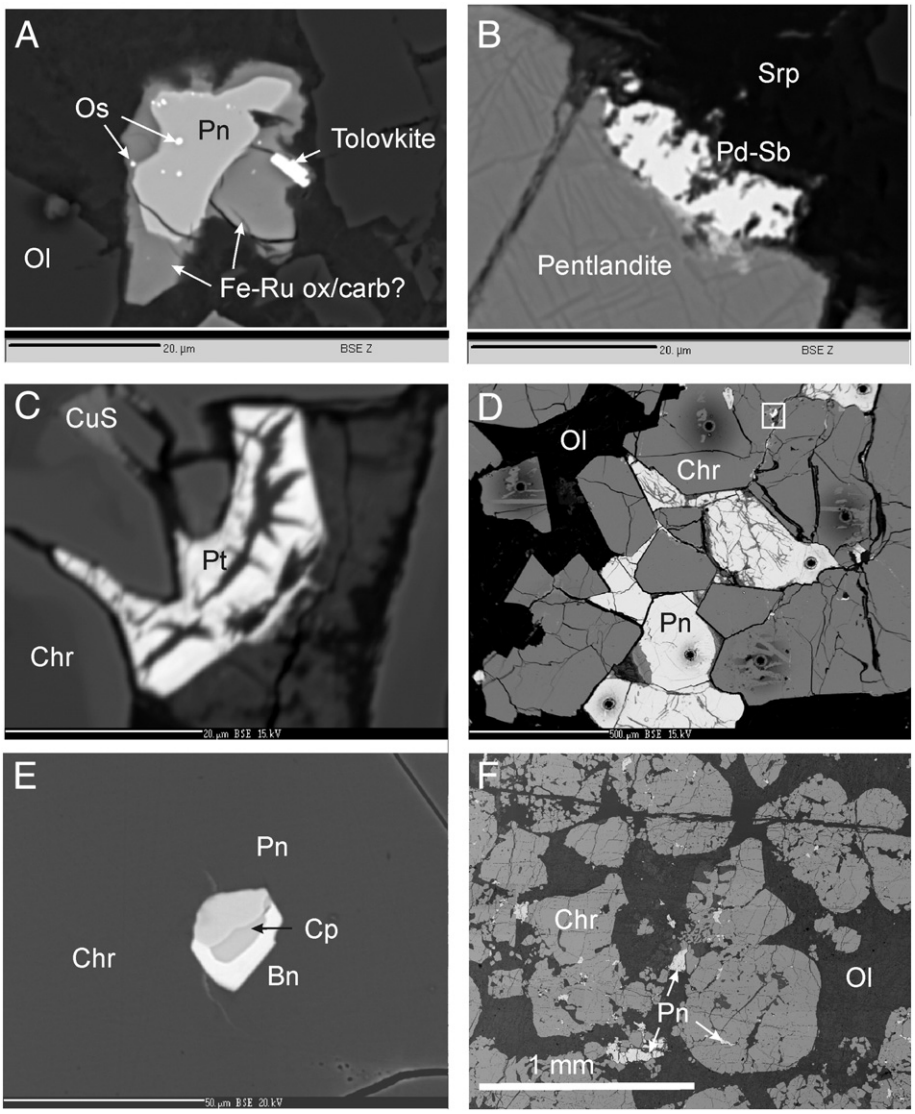

Fig. 12. Back-scatter electron images of base metal sulphides and platinum-group minerals in chromitites from the Sikhuran Mine, Esfandagheh district. A) Polyphase inclusion of pentlandite (Pn) with blebs of native osmium (Os) surrounded by Fe–Ru oxide or carbonate with included crystal of tolovkite (IrSbS) in serpentinized olivine (Ol) matrix, polished section 7523b; B) stibiopalladinite (Pd–Sb) attached to pentlandite in sulphide-rich chromitite, polished section 7539. Brighter area at margin of stibiopalladinite to pentlandite corresponds to Pd-enriched pentlandite. C) Probable platinum oxide (Pt) in fracture of chromite, polished section 7541, sulphide-bearing chromitite; CuS = copper sulphide; exact location is given as a quadrangle in Fig. 12D; D) laser spots in chromite (Chr), pentlandite (Pn) and olivine (Ol) from sulphidebearing chromitite, polished section 7541. Small Pt phase (quadrangle) is enlarged in Fig. 12C. E) Polyphase sulphide inclusion (Pn: pentlandite, Cp: chalcopyrite, Bn: bornite) in chromite, polished section 7544, sulphide-bearing chromitite; F) backscatter mosaic image of section 7544 showing relative proportions of chromite (light grey), weakly serpentinized olivine (dark grey) and pentlandite (bright).

appropriate proportions of laurite) indicates that they are Os–Ir and Ir–Os alloys with minor contributions of Ru, Rh, Pt and Ni; tie lines for coexisting laurite-alloy pairs are presented in Fig. 13d. Just one example from Abdasht was found with a primary $Os_{49}Ir_{48}Ru_3$ alloy phase without associated laurite (7530; Fig. 13d); in this case, the alloy is rimmed by cuproiridsite (Fig. 11D). Analyses of a small laurite grain (3.5 µm) included in olivine from Abdasht indicate the presence of laurite (XRu = 86) intergrown with irarsite and an alloy of $Ir_{69}Ru_{14}Os_9Rh_8$ composition (7504b; Fig. 13d).

In PGE-rich chromitite from Neyriz, three different alloy phases were identified forming drop-like inclusions (ca. 2 µm in size) included in an Fe-hydroxide aggregate in chlorite matrix: (1) Ru alloy ($Ru_{93}Ir_2Fe_3Ni_2$); (2) Ru–Ir alloy ($Ru_{62}Ir_{22}Fe_9Ni_7$); and (3) Ru–Os alloy ($Ru_{42}Os_{41}Fe_{12}Ir_3Ni_2$) (Fig. 13b). The minor concentrations of Fe and Ni are partly attributed to fluorescence from the Fe-hydroxide host phase. In a further sample from the same chromitite, several cluster of subhedral PGM in serpentine matrix include a Ru–Ir–Os alloy phase, 5 µm in size, of $Ru_{43}Ir_{28}Os_{13}Fe_8Ni_5Cu_1Pt_1$ composition, besides irarsite (11 µm) and several grains of PtFe (2–5 µm) (Fig. 11F).

Several examples reveal PGE alloys (mainly Os–Ru-dominated) as minute drop-like inclusions in base metal sulphides. In a complex aggregate hosted by serpentine in a chromitite sample from Sikhuran mine, numerous small (<1 µm) drop-shaped inclusions of an Os-rich phase are included in Co–Ru-bearing pentlandite; the pentlandite is rimmed by an Fe–Ni–Ru–Co oxide or carbonate phase that hosts a euhedral tolovkite [IrSbS] crystal (Fig. 12A). The small size of the inclusions excludes an accurate quantitative analysis; however, after proper consideration of the pentlandite matrix, the phase is $Os_{84}Ru_{13}Ir_3$ in composition. In a second example (AS7511, Razouki), an Os–Ru–Cu-rich phase is included in millerite.

In a polyphase inclusion with laurite and iridian millerite (AS7499, Abdasht), a phase of approximate composition $Ir_{50}Ni_{25}Fe_{25}$ was identified

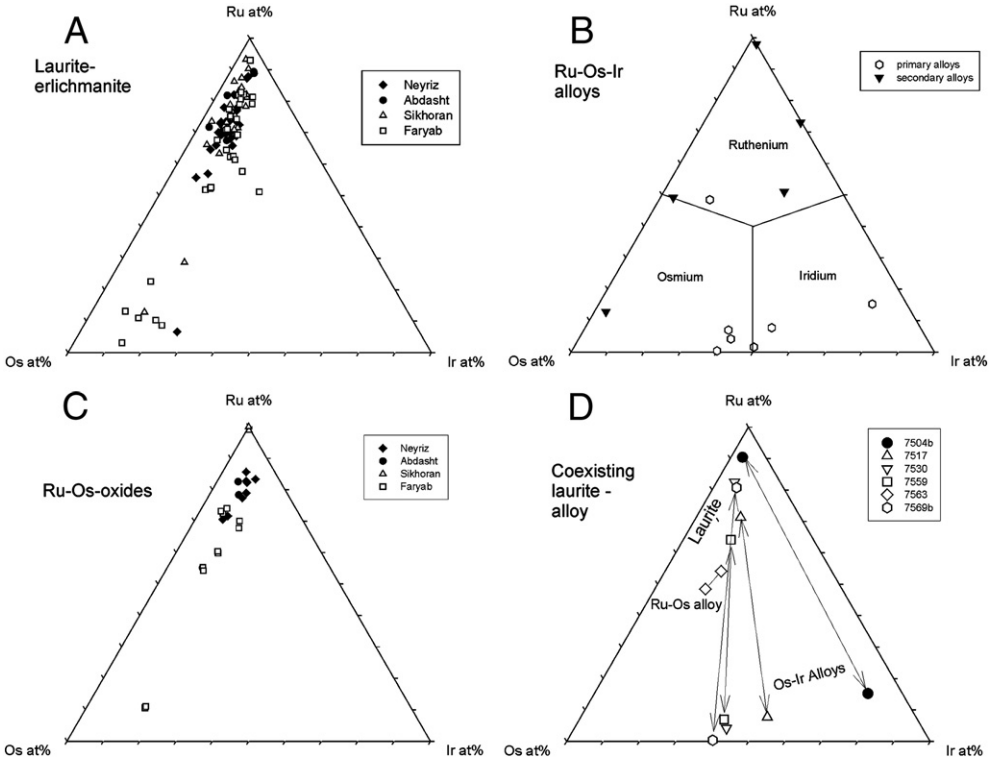

Fig. 13. Ru–Os–Ir ternary diagrams showing compositions of PGM associated with chromite. A) Laurite–erlichmanite; B) primary and secondary Ru–Os–Ir alloys; C) Ru–Os–"oxides"; D) coexisting laurite-alloy grains.

(Table 5) – probably an intermetallic phase of the garutiite (Ni,Ir,Fe) – hexaferrum (Fe,Os,Ru,Ir) solid solution series (McDonald et al., 2010).

Textural arguments, i.e. anhedral aggregates and crystals enclosed by secondary silicates (Fig. 11F), reveal that all of the alloy phases described above are of "secondary" origin, i.e. not primary magmatic. Compared to the primary alloys coexisting with laurite, they are devoid of Ir and enriched in Ru and Os (Fig. 13b). They might have formed from exsolution (e.g. Os in pentlandite), desulfurization of laurite (Ru-rich alloy phases; see e.g. El Ghorfi et al., 2008), or from fluid-induced transformation/recrystallisation processes (e.g. irarsite – Ru–Os–Ir alloy – PtFe assemblage).

6.2.4. Pt-rich alloy phases and probable Pt-rich oxides

Pt–Fe alloy phases are rare, and were mainly encountered in chromitite from Neyriz. They form small grains (<1 to 5 μm) either associated with laurite and/or BMS (Fe–Ni–Cu–S) and amphibole forming euhedral inclusions in chromite, or anhedral grains as part of polyphase PGM (with irarsite, Ru–Ir–Os alloy) in silicate matrix (chlorite, serpentine). The composition of the largest phase corresponds to tetraferroplatinum, Pt(Fe,Ni,Cu) (Fig. 11F, Table 5).

In sulphide-bearing chromitite samples from the Sikhuran mine, Pt-rich phases are associated with chromite, pentlandite, Cu sulphide, and laurite. Pt-rich phases of 20 to 40 μm size are present both along cracks (Fig. 12C) in chromite and in alteration rims of pentlandite. The anhedral grains have shrinkage cracks and high concentration of Pt (77–85 wt.%), along with minor Ni (4–6 wt.%), Cu (1–3 wt.%), Fe (1–2 wt.%), Ag (0.8–1.8 wt.%), Sb (0.4–1.4 wt.%), Te (0.2–1.0 wt.%), and Bi (<0.5 wt.%). About 7 to 9.5 wt.% oxygen was measured in several spots, suggesting the presence of a Pt-rich oxide mineral close to PtO stoichiometry (Table 5). The detection of small quantities of Sb, Te, Bi and Ag is noteworthy, because PGE-bearing phases carrying these (semi-)metals are hardly encountered in the sections studied. Rare submicroscopic Pt-rich phases found in alteration halos surrounding interstitial pentlandite carry Pt, Pd, Cu Fe and Ni in variable proportions (e.g. Cu(Pd,Pt,Ni,Fe), $Pt(Cu,Ni,Fe,Pd,Ag)_2$), but could not be unequivocally identified.

6.2.5. Ru-rich secondary phases

Microprobe analyses of many euhedral to subhedral PGM of mostly cubic shapes revealed the presence of Ru, Os, minor Ir, and variable Fe, Ni and Cu. These grains are almost devoid of sulphur and have, without measuring oxygen, low analytical totals (80–90 wt.%). The concentration of oxygen in the largest grain (Fig. 11E) is about 16–17 wt.%, suggesting the presence of an Ru–Os–Ir rich oxide phase of approximate RuO_2 stoichiometry (Table 5). In a Ru–Os–Ir ternary diagram, the compositions mimic the distribution of laurite–erlichmanite solid solution minerals (Fig. 13c). It is thus concluded, that most of them formed

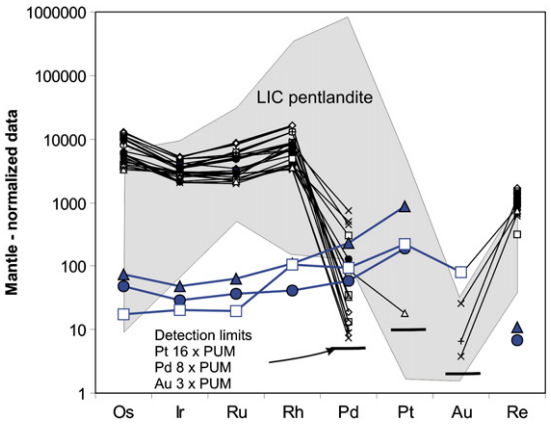

Fig. 14. PGE, Au and Re concentrations in pentlandite from two chromitite samples (7541, 7543) of Sikhuran normalised to PUM (Primitive Upper Mantle) values (Becker et al., 2006). Range for LA–ICP-MS analyses of pentlandite from PGE reefs in layered igneous complexes (LIC) using data of Barnes et al. (2008) and Godel and Barnes (2008). Whole-rock concentrations of sulphide-bearing chromitite from Sikhuran are given as blue lines (see Table 2).

Table 6
Analyses of pentlandite by EPMA and LA–ICP-MS.

Section	Mineral	Number	Number	S	Fe	Co	Ni	Cu	As	Total	Os	Ir	Ru[a]	Rh	Pt	Pd	Au	Re
		LA–ICP-MS	EPMA	wt.%	wt.%	wt.%	wt.%	wt.%	wt.%	wt.%	ppm	ppm	ppm	ppm	ppm	ppm	ppm	ppm
7541	Pentlandite	1	64	33.08	32.78	0.55	33.67	<0.042	<0.026	100.09	22.1	13.6	15.6	5.02	<0.051	<0.053	<0.026	0.292
7541	Pentlandite	2	70	33.07	32.53	0.52	33.79	<0.042	<0.026	99.90	37.5	15.9	23.8	5.99	<0.051	<0.053	<0.026	0.302
7541	Pentlandite	3	68	33.27	32.91	0.54	33.99	<0.042	<0.026	100.71	37.3	15.9	25.6	6.30	<0.062	<0.059	<0.032	0.279
7541	Pentlandite	5	78	33.15	33.11	0.52	33.48	<0.042	<0.026	100.26	14.8	9.77	13.3	7.04[b]	<0.099	4.88[b]	0.484	0.265
7541	Pentlandite	6	77	33.20	32.98	0.52	33.58	<0.042	<0.026	100.29	18.0	6.60	9.86	3.53	<0.071	0.542	<0.032	0.195
7541	Pentlandite	7	75	33.17	33.09	0.53	33.69	<0.042	<0.026	100.48	20.0	6.79	10.8	3.78	<0.062	0.861	<0.029	0.369
7541	Pentlandite	8	74	33.14	33.12	0.52	33.67	<0.042	<0.026	100.45	19.7	6.70	9.75	3.52	<0.051	<0.052	<0.026	0.245
7541	Pentlandite	9	72	33.15	33.09	0.53	33.67	<0.042	<0.026	100.44	15.7	6.48	8.98	3.53	<0.058	3.38	0.167	0.217
7541	Pentlandite	10	80	33.05	32.78	0.48	33.66	<0.042	<0.026	99.97	19.3	9.36	12.8	3.17	<0.036	0.048	<0.021	0.214
7541	Pentlandite	11	79	32.97	33.06	0.47	33.65	<0.042	<0.026	100.15	16.7	8.58	12.6	3.12	<0.041	0.060	0.025	0.213
7541	Pentlandite	12	82	33.03	32.90	0.48	33.57	<0.042	<0.026	99.98	12.2	8.67	10.3	4.49[b]	<0.040	2.02[b]	<0.020	0.100
7541	Pentlandite	13	83	33.09	32.33	0.47	32.89	1.40	<0.026	100.18	11.4	9.23	9.62	3.38	0.060	0.571	<0.024	0.242
7543	Pentlandite	1		na	na	na	na	na	na		29.1	10.6	29.0	11.9	<0.053	<0.046	<0.031	0.408
7543	Pentlandite	2		na	na	na	na	na	na		27.6	11.6	28.4	11.9	<0.047	<0.052	<0.026	0.439
7543	Pentlandite	3		na	na	na	na	na	na		28.4	11.6	27.3	12.1	<0.057	0.063	0.044	0.386
7543	Pentlandite	4		na	na	na	na	na	na		41.8	17.1	37.4	14.5	<0.059	<0.054	<0.035	0.392
7543	Pentlandite	5		na	na	na	na	na	na		44.0	16.3	39.3	15.5	<0.056	0.085	<0.028	0.428
7543	Pentlandite	6		na	na	na	na	na	na		41.8	17.1	38.9	15.4	<0.051	0.123	<0.025	0.538
7543	Pentlandite	9		na	na	na	na	na	na		13.8	9.29	14.6	6.47	<0.046	0.087	<0.029	0.356
7543	Pentlandite	10		na	na	na	na	na	na		13.3	8.08	12.7	6.57	<0.063	0.211	<0.034	0.352
7543	Pentlandite	11		na	na	na	na	na	na		15.1	9.08	11.2	8.42[b]	<0.057	2.95[b]	<0.025	0.415
7543	Pentlandite	13	13	33.15	33.18	0.37	33.88	<0.042	<0.026	100.57	33.6	11.2	22.9	7.64	<0.038	<0.038	<0.023	0.471
7543	Pentlandite	14	11	33.17	33.29	0.40	34.03	<0.042	<0.026	100.89	34.0	11.0	22.3	7.51	<0.049	<0.035	<0.023	0.429
7543	Pentlandite	15		na	na	na	na	na	na		34.1	10.9	21.6	7.75	<0.042	<0.033	<0.020	0.394
7543	Pentlandite	16	10	32.89	32.80	0.42	33.33	1.01	<0.026	100.45	35.2	11.3	22.1	8.03	<0.075	0.358	<0.030	0.372
7543	Pentlandite	19	7, 8, 9	33.21	33.43	0.37	33.91	<0.04	<0.026	100.92	37.8	12.8	25.4	8.30	<0.050	0.236	<0.025	0.491

na, not analysed.
[a] Possible NiAr interference on ^{101}Ru (<1 ppm total).
[b] Possible CuAr interference on ^{103}Rh and ^{105}Pd due to high signals for Cu in LA–ICP-MS analyses.

from desulphurization of laurite–erlichmanite, and uptake of base metals from hydrothermal or weathering solutions. This is supported by textural arguments that reveal in all cases direct contact relationships with hydrous silicates (Fig. 11E) or ferritchromite, and occasionally with unaltered laurite. In most of the analyses, PGE/BM ratios range from 1.0 to 4.4.

Some, however, have low PGE/BM ratios (0.25); the largest of these grains has about 25 wt.% Fe, 10 wt.% Ni, 5 wt.% Co and 15 wt.% Ru and rims pentlandite with exsolved osmium. It includes a tolovkite crystal (Fig. 12A). The oxygen concentration in this particular Fe–Ru–rich grain, determined by EPMA, is 36 wt.% (Table 5). This value is too high to account for an oxide or hydroxide phase. Thus, it may represent a Ru-bearing carbonate phase of approximate $(Fe_{0.5}Ni_{0.2}Co_{0.1}Ru_{0.2})CO_3$ composition.

6.2.6. PGE sulpharsenides

Irarsite [IrAsS] and hollingworthite [RhAsS] are invariably included in silicates (chlorite, serpentine) or associated with chromite/ferritchromite–silicate contacts, and are most frequent in samples from the Neyriz ophiolite (Fig. 11F). Only one laurite included in fresh chromite was found associated with irarsite in a sample from Abdasht. The sulpharsenides commonly form clusters of anhedral bleb-like inclusions, <1 to 10 μm in size. Associated are Pt-rich phases, Ru–Ir–Os alloy, and Ni- and Cu-sulphides. The composition of irarsite is characterised by XIr [Ir/(Ir + Rh + Ru + Os)] = 0.48–0.80, with Rh as the major PGE substituting for Ir. One grain of hollingworthite has XRh = 0.83 and XIr = 0.17. The maximum concentrations of Ru, Os and Pt in the PGE-sulpharsenides are 4.7, 1.3 and 5.2 wt.%, respectively (Table 4).

6.2.7. Rare PGM

Stibiopalladinite was observed in pentlandite-bearing chromiferous dunite at Sikhuran mine forming grains up to 25 μm in size at the margin of pentlandite towards serpentine (Fig. 12B). The average of two analyses gives a formula of $[Pd_{4.9}(Cu,Ni,Fe)_{0.2}Sb_{1.8}]$ (Table 5). The adjacent pentlandite appears brighter in the BSE image than ordinary pentlandite (Fig. 12B) and carries high Pd concentrations (22–50 wt.%), but no Sb. Calculated formulae still retain the M_9S_8 pentlandite stoichiometry, e.g. $[(Ni,Pd)_{5.5–6.5}Fe_{2.5–3.5}S_8]$.

Two small (3–4 μm) grains of unnamed RhNiAs were identified in chromitite from Neyriz. One is part of an anhedral polyphase inclusion in chlorite + Cr–Fe garnet matrix close to ferritchromite, the second forms part of a subhedral two-phase PGM + BMS (Cu–Co–Ni-sulphide) inclusion at the rim of a round serpentine inclusion in chromite. Both RhNiAs grains carry low concentrations of further PGE (Table 5). Phases of RhNiAs composition, probably belonging to the stibiopalladinite–palladoarsenide group, are listed as unnamed phases 0387 and 1625 in the MINERAL Database of Nickel & Nichols (www.materialsdata.com). They most probably represent Rh-analogues to majakite [PdNiAs]. RhNiAs has been reported, among other occurrences, in association with the new mineral garutiite (Ni,Fe,Ir) from the Loma Peguera chromitite, Dominican Republic (McDonald et al., 2010; Proenza et al., 2007; Zaccarini et al., 2009). An anhedral (4 μm size) polyphase Ir–Ru–Fe–Ni–As phase is associated with the above mentioned RhNiAs mineral. The recalculation of two analyses suggests a phase of $[(Ir_{2.3}Ru_{1.0}Rh_{0.7})_4(Ni_{1.1}Fe_{1.3})_{2.4}As_{0.6}]$ composition.

Two grains of tolovkite [IrSbS] were detected in samples from the Sikhuran mine forming subhedral to euhedral grains <10 μm in size associated with altered chromite. In one case, an euhedral tolovkite grain is enclosed in a homogeneous Fe–Ni–Ru–Co oxide or carbonate phase; this phase also includes Co-bearing pentlandite that by itself carries numerous blebs of osmium (Fig. 12A). The compositions of both tolovkite grains are similar, including some Fe, Ni, Co and As, as well as 2.6–3.0 wt.% Rh and up to 1.2 wt.% Ru (Table 5). Tolovkite is a cubic or pseudocubic mineral of the gersdorffite group and was first described by Razin et al. (1981) from placer deposits in Siberia. Ir–Rh sulphantimonide corresponding to IrSbS was also found in ophiolitic chromitites at Harold's Grove, Shetland (Prichard and Tarkian, 1988), and at Osthammeren, Norway (Nilsson, 1990) —in a complex association with laurite, erlichmanite, Ir–Os alloys, Ir–Rh sulpharsenides and $[(Ir,Pt,Pb)S_2]$.

One small round grain (2.5 μm in size) of a Rh–Sb–Cu mineral was found enclosed by chlorite close to a ferritchromite rim, and associated with Os–Ir–Ru oxides. Its composition corresponds to [$(Rh,Ir)_2$(Cu, Ni,Fe)Sb], with Ir (0.4 wt.%), Ni (1.3 wt.%) and Fe (1.6 wt.%) present in minor quantities; Fe and Ni may also be derived from the host chlorite (Table 5). The formula resembles that of the phase UN 0389, [Rh_2-SnCu] (Corrivaux and Laflamme, 1990), an unnamed mineral of the niggliite group. An unnamed phase of [Pd_2CuSb] composition (presumably of the atheneite–vincentite group) was repeatedly reported from the Driekop pipe in the Bushveld complex, South Africa (Melcher and Lodziak, 2007; Stumpfl, 1961), and from placer deposits in Burma (Hagen et al., 1990), and probably is the Pd-analogue of the phase described here.

6.3. Base metal sulphides

Pentlandite is the major constituent of base metal sulphide mineralization in chromitite and dunite of the ultramafic massifs studied, forming (larger) aggregates interstitial to chromite and olivine (mainly in Sikhuran and Faryab; Fig. 12B, D, F), or (smaller) inclusions within chromite (Fig. 12E) and occasionally in olivine. In some chromitites, pentlandite forms euhedral grains interstitial to both, unaltered chromite and olivine. In such samples, sulphides account for 0.3 to 1.2% of the sample volume (Fig. 12D, F). Pentlandite is frequently intergrown with a Cu-rich sulphide phase, either with chalcopyrite, cubanite or chalcocite in interstitial aggregates, or with bornite and chalcopyrite in inclusions (Fig. 12E). Pentlandite aggregates are commonly veined by millerite, rarely by violarite, and are further oxidised to complex mixtures of Fe–Ni–Co–Cu minerals (hydroxides, carbonates). In inclusions within chromite, monophase Ni sulphide inclusions often consist of millerite instead of pentlandite, but heazlewoodite, pentlandite and Co-rich sulphides were also identified. Pyrrhotite is a very rare phase in the samples studied and was chiefly identified in sulphide-mineralized and chromite-bearing pyroxenite samples from Faryab. Accessory phases associated with BMS mineralization include rare PGM (see Section 6.2), arsenopyrite, awaruite, native silver, valleriite, mcguinessite, cuprite, and further secondary minerals.

The composition of pentlandite from Sikhuran measured by microprobe varies within the following ranges (mean in brackets, $n = 90$, in atomic %): S 45.7–48.6 (46.8)%, Fe 20.2–28.1 (26.5)%, Ni 24.2–32.0 (26.1)%, Co 0.27–1.52 (0.45)%, Cu < 1%. Fe and Ni are closely correlated, and Fe/Ni ratios are close to unity (mean 1.02, range 0.63–1.13). One grain carrying 20 at.% Co occurs as a monophase BMS in silicate rimmed by a Co-rich alteration phase in a PGE-rich massive chromitite sample from the Neyriz ophiolite. Co- and Ru-bearing pentlandite (4 at.% Co, 3.8 at.% Ru) was identified in an aggregate enclosed by serpentine close to olivine and chromite grains; the pentlandite carries minute blebs of osmium, and is surrounded by an Fe–Ni–Ru–Co oxide or carbonate phase with an included euhedral tolovkite crystal (sample AS7523b, Sikhuran, Fig. 12A).

Despite using optimised analytical conditions (i.e., detection limits of 50 ppm for Pd), Pd, Rh and Pt were not detected in pentlandite by electron microprobe analysis, except in areas close to PGM. In addition, LA–ICP-MS analyses indicate that interstitial pentlandite is not a host of submicroscopic Pd, Pt and Au, but carries on average 25 ppm Os, 11 ppm Ir and 8 ppm Rh (Fig. 14). Concentrations of Ru in pentlandite are difficult to quantify due to interfering Ni argide, but are probably in a similar range as Os and Ir. Palladium concentrations of 0.5–5 ppm correlate with counts for Cu, and are interpreted to partly reflect interfering Cu argides (Table 6). Microprobe analyses carried out on areas of heterogeneous pentlandite reveal Cu concentrations up to 18 at.%. Cu-rich analyses tend to have higher S concentrations as well, suggesting mixtures of pentlandite and a phase with a BM/S ratio higher than in pentlandite, e.g. chalcopyrite or cubanite. In such grains, Ni is negatively correlated with Cu, whereas Fe and Cu are not correlated. This points to the original presence of a Cu-bearing monosulphide solution phase that underwent exsolution into intimately intergrown Ni- and Cu-rich phases.

Pentlandite from PGE-reefs in layered igneous complexes, such as the Bushveld (Merensky Reef), Stillwater (JM Reef) and Great Dyke (MSZ), is commonly enriched in Pd and Rh, and has positive slopes in (mantle-) normalised PGE diagrams (Barnes et al., 2008; Godel et al., 2007). However, typical concentrations of Os, Ir and Ru are below 10 ppm for most analyses published; thus, the pentlandites from sulphide-bearing chromitite of Sikhuran have higher-than-average IPGE, but lower-than-average PPGE (except Pt) concentrations.

7. Discussion

7.1. Geodynamic setting of the chromitites based on chromite and olivine chemistry

In southern Iran, chromitites are related to ultramafic rocks, such as dunite, harzburgite, pyroxenite and occur in a diversity of textural types. Despite their diverse palaeostratigraphic positions with respect to the Moho (Fig. 4), the chromites have a rather restricted chemical variation, especially in their Cr# number [$100 * Cr/(Cr + Al)$]. Two groups are distinguished, one at Cr# around 74 to 81, and a more variable group at lower Cr# ranging from 60 to 70 (Fig. 8A–C). Most samples that are petrographically classified either as mantle tectonite or as cumulate (see chapter 4) plot in the high-Cr# group. A few samples from Neyriz (small chromite pods in the mantle), Faryab (accessory chromite in pyroxenite and dunite) and Sikhuran (e.g., tectonite-hosted chromitite at Sorkh Jallab) make up the lower-Cr# group. No Al-rich chromites (Cr# < 60) are encountered in chromitite of any of the complexes investigated. Lower Cr# numbers (30–60) are only found in accessory chromites associated with pyroxenite and websterite from Faryab, and their relation to the bulk ores is presently unknown.

The Mg# numbers [$100 * Mg/(Mg + Fe^{2+})$] of chromite from southern Iranian chromitites span a wide range from 50 to 90. Some chromites from sulphide-bearing chromitites tend to have lower Mg# than those from ordinary mantle tectonites and sulphur-poor cumulate chromites. Within-sample heterogeneities of Cr# and Mg# are small, but may vary significantly within single ore bodies, and the within-sample range in Mg# is much larger than in Cr# (Appendix 2). All chromitites have a podiform character, indicated by a prominent Cr–Al trend and low TiO_2 concentrations (Fig. 9A, B). In the Cr_2O_3 vs. TiO_2 classification diagram (Fig. 9B), they plot into the field of fore-arc boninites or are transitional to MORB. The transitional character is best expressed in podiform lenses associated with dunite and clinopyroxenite in the Neyriz ophiolite.

In many cumulate chromites documented from ophiolites, Cr# numbers are lower than in mantle-hosted podiform chromite (Stowe, 1994). In New Caledonia, cumulate ores have low Cr# (50–63) compared to podiform ore (Cr#, 62–76). In the Semail ophiolite, Cr# in cumulate zone chromitite ranges from 42 to 52 compared to 52 to 77 in the tectonites (Augé, 1987). Both the Cr# and Mg# numbers commonly decrease upward in the cumulate chromite, corresponding to a fractional crystallisation trend. However, the Cr# number does not distinguish between layered chromitites from Sikhuran that are interpreted as cumulate chromitites and mantle tectonite chromitites in the same complex (Fig. 8B). Stowe (1994) used $Mg/(Mg + Al)$ ratios to discriminate ophiolitic cumulate chromitite from mantle-hosted podiform ores. Our data show different trends for tectonite (correlation of Cr# and $Mg/(Mg + Al)$) and presumed cumulate chromites that display a large variation in $Mg/(Mg + Al)$ at constant Cr# numbers (Fig. 9C).

Minor element concentrations vary little in the chromites investigated. Titanium, V, Mn, Co and Zn correlate with Fe; TiO_2 concentrations range up to 0.3 wt.% (Fig. 9B). Chromites in ultramafic

cumulate rocks of Sikhuran have higher Ti than in the layered chromitites at Faryab and in most tectonite-hosted chromitites. However, some mantle chromites (Sorkh Jallab, Tange Hana) also have slightly elevated Ti concentrations. This probably reflects interaction of mantle rocks with percolating melts (see below). Most chromites carry 0.05 to 0.15 wt.% V_2O_3; some from Neyriz have higher (0.2–0.4 wt.%) concentrations. Manganese (0.15–0.4 wt.% MnO) correlates with Fe^{2+} and does not show significant differences between the complexes studied. Nickel (0.02–0.2 wt.% NiO) correlates with Mg. Analyses from individual samples always display a range of trace element concentrations at more or less constant Cr# and Mg# numbers.

The chemistry of spinel reflects the composition of their parental melts and the geodynamic setting in which they crystallised (Dick and Bullen, 1984). Subsolidus exchange reactions between spinel and associated silicate or sulphide may significantly change the mineral compositions, which then are not useful for such calculations. Massive unaltered chromitites with little interstitial Mg–Fe or Al silicates, however, represent prime candidates for this approach. Al_2O_3 and TiO_2 concentrations of the melts from which chromite crystallised may be recovered from experimental data (e.g., Maurel and Maurel, 1982, 1983), or from empirical data on coexisting chromite and melt inclusions (Kamenetsky et al., 2001). Rollinson (2008) developed a set of best fit regression lines using the data of Kamenetsky et al. (2001) and Roeder and Reynolds (1991) for MORB and arc magmas, and calculated the composition of parental melts for chromites from the Oman ophiolite. Zaccarini et al. (2011) developed similar regression lines for chromites from the Santa Elena ophiolite, Costa Rica. The good correlation of Cr, Al and Ti contents in chromites from southern Iran permits the use of the equations for Al and Ti in melts coexisting with chromite as formulated for arc magmas (Rollinson, 2008); these data are summarised in Table 7. The FeO/MgO ratio of the melts are estimated using an equation developed by Maurel (1984, cited by Augé, 1987); however, due to re-equilibration between chromite and olivine the Mg number in chromite might have been modified and the numbers given in Table 7 are regarded as less reliable. There are slight differences in the Al_2O_3 values obtained by the two approaches. Nevertheless, melts in equilibrium with mantle tectonites and ultramafic cumulates in the Neyriz, Abdasht, Sikhuran and Faryab complexes must have been low in Al_2O_3 (11–13 wt.%), TiO_2 (0.2–0.3 wt.%) and had a range of FeO/MgO (0.5–1.2), but mostly MgO > FeO. Such compositions are not attributable to melts producing primitive MORB and arc basalts (13–17 wt.% Al_2O_3, 0.7–1.2 wt.% TiO_2, 0.7 < FeO/MgO < 1.2), but point to more silica-rich high-Mg and boninitic melts produced in a supra-subduction zone setting (10.6–14.4 wt.% Al_2O_3, 0.25 wt.% TiO_2, 0.7 < FeO/MgO < 1.4; e.g., Crawford et al., 1989; GERM Reservoir database, http://earthref.org/GERM/). The extreme Cr# numbers of chromite in all complexes, but especially at Abdasht, Sikhuran and Faryab support a low-Ca boninite parental magma (Crawford et al., 1989). Minor occurrences of more Al-rich chromites, such as in dunite pods and clinopyroxenite at Tange Hana, Neyriz, may indicate either fluxing of mantle tectonite by more Al- and Fe-rich melts (ca. 13–14 wt.% Al_2O_3, FeO/MgO ca. 1.5), differentiation of a more primitive melt, or may result from interaction of a primitive MORB-type melt with abyssal harzburgite (e.g., Rollinson, 2008). Pyroxenites at Faryab would have crystallised from Fe-rich basaltic melts having 15 wt.% Al_2O_3 and more than 0.5 wt.% TiO_2.

In many ophiolite complexes (e.g. Oman, Cpyrus, Albania, Turkey), chromite compositions in chromitite range from low Cr# to high Cr# numbers. This is explained by mixing of different parental melts, e.g. melts of MORB mantle and melts of depleted mantle of different depths, and reaction with the host harzburgites on their way upward (Rollinson, 2008). Therefore, the constantly high Cr# and Mg# numbers of chromites in all complexes investigated in southern Iran are unusual. Some variation is only evident in the Neyriz ophiolite (e.g., Jannessary, 2003), whereas Abdasht, Sikhoran and Faryab essentially host high-Cr# (>75), high-Mg# (>60) chromites. Such chromites must have been derived from high-Mg boninitic mantle melts generated in a suprasubduction zone setting.

7.2. PGE concentrations in Iranian chromitites

Previous studies on PGE concentrations in chromitites from Iranian ophiolites did not reveal encouraging results concerning their PGE potential. In addition to the 38 partial (Page et al., 1979; Weber-Diefenbach and Davouadzadeh, 1998) and complete data sets (Alinia and Facherabadi, 2005; Najafzadeh et al., 2008; Rajabzadeh, 1998; Rajabzadeh et al., 1998) of PGE distributions in Iranian chromitites, the 58 new analyses of the present study add to a more complete picture (Table 2). The characteristic features of PGE mineralization associated with chromitites in south-eastern Iranian ultramafic complexes are summarised in Tables 3 and 8. Chromitites in most complexes are characterised by low to moderate PGE concentrations that hardly exceed totals of 500 ppb (Σ6 PGE), and by low Pt and Pd concentrations. The median total PGE concentrations of chromitite in the four areas studied are as follows: 209 ppb (Neyriz), 172 ppb (Abdasht), 269 ppb (Sikhuran), and 201 ppb (Faryab). This is within

Table 7
Composition of melts in equilibrium with chromite.

Complex	Chromite type[1]; setting (location)	Al_2O_3 liquid[2]	Al_2O_3 liquid[3]	TiO_2 liquid[3]	FeO/MgO liquid[4]
Neyriz	e; Pods in dunite (Tange Hana)	12.8	13.5	0.28	1.5
	f; Clinopyroxenite dike (Tange Hana)	13.5	13.8	0.29	1.3
	b, c; Mantle tectonite	11.7	12.3 ± 0.8	0.18 ± 0.04	0.7 ± 0.1
Abdasht	a, b, c; Mantle tectonite	10–10.8	11.3 ± 1.0	0.24 ± 0.05	0.7 ± 0.1
Sikhuran	c, b; Tectonite (Razouki)	11.3	12.1	0.27	0.7
	c; Tectonite (Sorkh Jalla)	11.0–12.4	12.2 ± 0.6	0.35	0.95
	b; Transition zone (Sobhan)	10.8	11.5	0.33	1.0
	a; Cumulate (Sikhuran mine)	10.3–11.0	11.0 ± 0.3	0.33 ± 0.05	1.1 ± 0.4
Faryab	a; Northern unit (Doveis)	10–12	11.2 ± 1.0	0.27 ± 0.05	1.2 ± 0.8
	a; Northern unit (main ore bodies)	10	10.9 ± 0.4	0.22 ± 0.03	0.7 ± 0.1
	c; Transition to southern unit (Reza)	10	10.7	0.21	0.7
	Cr-clinopyroxenite (veins)	13.5	11.6 ± 1.3	0.23 ± 0.05	0.7–1.0
	Pyroxenite, websterite	13–16	15.1 ± 1.6	0.48 ± 0.18	4.8 ± 1.5

[1] Modified from Burgath et al. (2002): (a) layered/massive to disseminated, (b) tabular/disseminated to massive, (c) schlieren (-folded)/disseminated, (e) podiform s.str./massive, and (f) orbicular/disseminated chromitite.
[2] Maurel and Maurel (1982, 1983).
[3] Rollinson (2008) for arc settings.
[4] Maurel (1984, cited in Augé, 1987).

Table 8
Summary of characteristic features in chromitites of south-eastern Iran.

	Type[1]	Cr#	Mg#	PGE (ppm)	Pt_n/Ir_n	$^{187}Os/^{188}Os$	PGM, BMS
Neyriz	e, f	65–70	50–60	1–2	<0.55	0.127–0.128	Laurite, Os–Ir alloys, RhNiAs, irarsite, Pt–Fe; rare Ni–Co–S
	b, c	70–80	55–75	<0.2	<0.2	0.125	Laurite, RhNiAs; rare Ni–S
Abdasht	a, b, c	77–81	71–82	<0.25	<0.2	0.125	Laurite, cuproiridsite, Ir-Rh-sulpharsenides; locally abundant Ni–S
Sikhuran	c, b	69–79	51–74	0.1–0.6	<0.1–5.2	0.126–0.129	Laurite-erlichmanite, cuproiridsite, (Ni,Ir,Rh)S, Os–Ir alloys; locally abundant interstitial and included Ni–(Fe–Cu)–S
	a	75–80	41–71	0.1–5.2	<0.1–4.8	0.125–0.134	Laurite, Os–Ir–Ru alloy, Ni–Ir sulphide, tolovkite, irarsite, Pd–Sb, Pt, Au–Ag; locally abundant interstitial pentlandite
Faryab	c	81	71	0.1	<0.1	0.126	Rare Ni–S and Ni–Fe
	a	74–82	61–76	<0.1–0.45	<0.1–0.8	0.126–0.14	Laurite-erlichmanite, cuproiridsite, (Ni,Ir)S; locally abundant Ni–Co–Cu–Fe sulphides

[1] Modified from Burgath et al. (2002): (a) layered/massive to disseminated, (b) tabular/disseminated to massive, (c) schlieren (-folded)/disseminated, (e) podiform s.str./massive, and (f) orbicular/disseminated chromitite.

the range typically observed in Alpine-type ophiolitic chromitites, e.g. within the Neo-Tethys ocean (e.g., Ahmed and Arai, 2002; Economou-Eliopoulos, 1996; Kocks et al., 2007; Melcher, 2000b; Ucurum et al., 2006; Uysal et al., 2010). Most of the investigated chromitites are characterised by low ratios of Pt_n/Ir_n and $PPGE_n/IPGE_n$ (Figs. 5 and 6). Furthermore, they have negative Ir anomalies (expressed by both Os/Ir and Ru/Ir usually >1, averaging 1.24 and 1.95, respectively) and generally high Rh/Pt values (average 20). Only the sulphide-bearing chromitites of Sikhuran display PPGE/IPGE ratios >1.

The average $^{187}Os/^{188}Os$ ratios are indistinguishable in the four complexes, ranging from 0.1245 to 0.14 (median ca. 0.128) (Fig. 7). Walker et al. (2002) have demonstrated that ophiolitic chromites (both from MOR and SSZ settings) are robust indicators of the initial Os isotopic composition of the mantle, and representative of the convecting upper mantle. Their data suggest that the present isotopic upper mantle composition is on average 1.2% less radiogenic than estimates of the primitive upper mantle (Meisel et al., 2001a). Assuming an evolution in the convecting upper mantle and using the regression equation of Walker et al. (2002), the median $^{187}Os/^{188}Os$ ratios for the Neyriz, Sikhuran and Faryab chromitites would point to a young age (indistinguishable from modern convecting mantle with $^{187}Os/^{188}Os = 0.12808 \pm 0.00085$), whereas the slightly lower median for the Abdasht chromites (0.125) would indicate a higher model age.

A Cretaceous age (ca. 100 Ma) is attributed to the Neyriz ophiolite based on ^{40}Ar–^{39}Ar data (Babaie et al., 2006; Haynes and Reynolds, 1980; Jannessary, 2003). For this time, γOs(t) values (the deviation in permil from a chondritic evolution; e.g. Walker et al., 2002) in

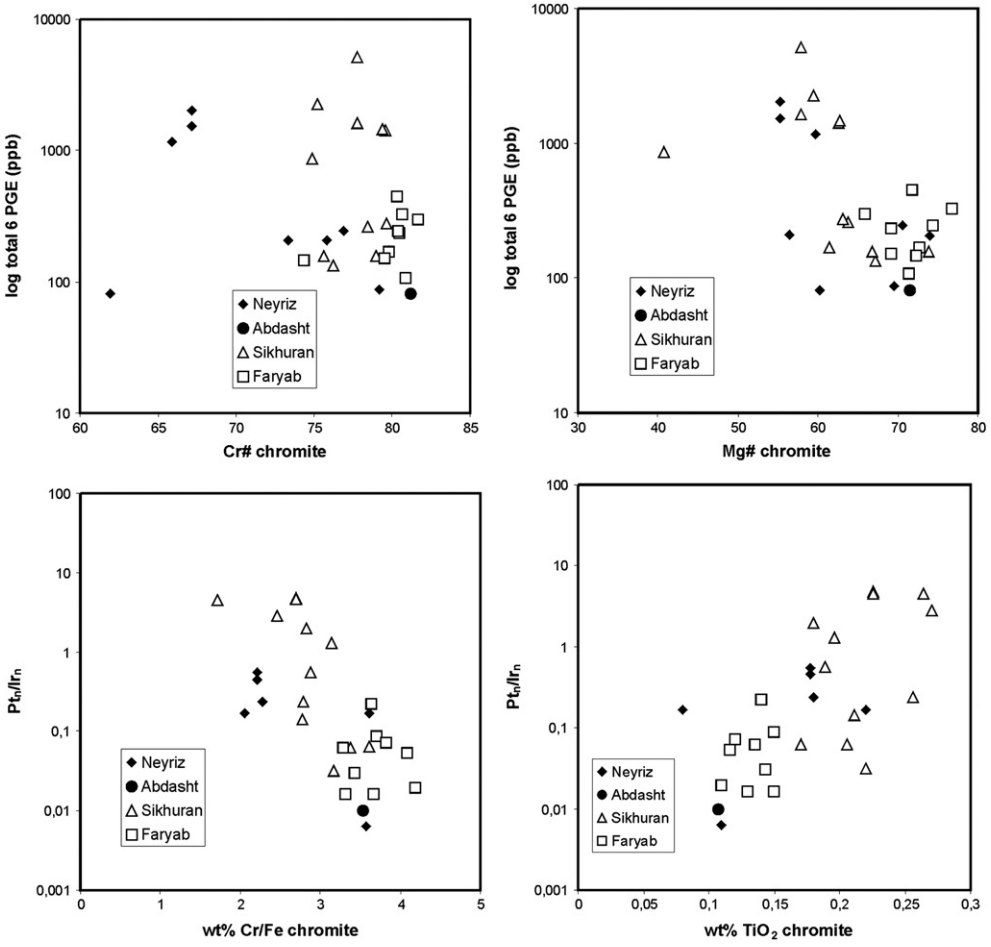

Fig. 15. Relationships between PGE concentrations, PGE ratios and mineral chemical parameters of chromite.

chromitites indicate slightly suprachondritic (more radiogenic than the chondritic evolution) Os isotopic signatures for the Neyriz chromitites (mean +1.5; range −1.5 to +2.9). The lower Os isotope values of the Abdasht chromitites translate into γOs(t) values of −0.25 (−0.9 to +0.9) for t = 100 Ma. However, the history of ultramafic rocks in the Esfandagheh area is disputed; Ghasemi et al. (2002) report Permian intrusion ages (250–280 Ma) of gabbro-pegmatite dykes cutting the ultramafic–mafic cumulates at Sikhuran. The sulphide-poor Faryab chromitites have suprachondritic γOs(t) values, irrespective of their presumed age.

The high γOs(t) values calculated for sulphide-bearing chromitite from Sikhuran (+3 to +5.8 for t = 100 Ma) and sulphide-bearing chromitite and dunite from Faryab (>+6 for t = 100 Ma) are partly due to low Os concentrations and partly to elevated Re–Os ratios (>0.1), that make these samples more susceptible to Re-enriched sources. Sulphides are often made responsible for the disturbation of the Re–Os system. The Re/Os ratios of pentlandite in sulphide-bearing chromitite are below 0.3 (average 0.15), and Os concentrations average to 26 ppm (Table 6). Thus, the contribution of pentlandite to the bulk rock Os content is high and pentlandite appears as the phase controlling the Os budget.

The suprachondritic initial $^{187}Os/^{188}Os$ isotopic ratios measured in most chromitites that are coupled with low $^{187}Re/^{188}Os$ indicate a contribution of radiogenic Os rather than Re during petrogenesis. This seems a rather common feature of many ophiolitic chromitites and it has been proposed that fluids or melts derived from the dehydrating slab in subduction zone settings may transfer radiogenic Os into the overlying peridotite and thus elevate its Os isotopic composition (Ahmed et al., 2006; Büchl et al., 2004). Kocks et al. (2007) showed that transition zone chromitites in the Shebeniku massif, Albania, have rather heterogeneous Os isotopic signatures (e.g., γOs(t) = −3 to +8). This is confirmed by the present study as the most radiogenic chromitites are from ultramafic cumulates (Sikhuran) and probable transition zones (Faryab).

PGE concentrations in the investigated chromitites reveal vague correlations with chemical compositions of the host phases, e.g. negative correlations of the total PGE (Σ6 PGE), Pt/Ir and Pd/Ir ratios with Mg# in both chromite and olivine, and positive correlations with TiO_2 in chromite (Fig. 15). $^{187}Os/^{188}Os$ increases with decreasing Mg# in olivine. This indicates that higher PGE concentrations, and especially higher values of Pt and Pd, can be expected in more Fe- and Ti-rich chromitites hosted by olivine of lower Mg# (<95). Such chromitites are produced either by fractional crystallisation in cumulate zones (e.g., Sikhuran), by mixing of primitive melts with more evolved melts, or by reaction of small portions of melt with residual mantle (e.g. Neyriz).

7.3. Distribution of PGM in Iranian chromitites

Low PPGE/IPGE ratios in all except some sulphide-bearing chromitites attest to the presence of laurite–erlichmanite as the major PGM. Laurite–erlichmanite forms a complete solid solution series from RuS_2 to OsS_2 with only limited miscibility to IrS_2 in natural occurrences. In contrast, primary alloys of Ru–Os–Ir–(Rh–Pt) are commonly Ru-poor and Ir-rich. Thus, negative Ir anomalies in normalised PGE patterns (Fig. 5) indicate the predominance of IPGE sulphide versus alloys, and therefore are indicative of the relative sulphur fugacity and thus the oxidation state of the system (e.g. Garuti et al., 1999; González-Jiménez et al., 2009b; Nakagawa and Franco, 1997). Most podiform chromitites in ophiolite complexes are dominated by IPGE sulphides, whereas PGE alloy-dominated systems are rare, e.g. in the Massif du Sud, New Caledonia (Augé and Johan, 1988; Augé and Maurizot, 1995; Augé et al., 1998) and at Luobusa, Tibet (Bai et al., 2000). Iridium may be present within sulpharsenides and sulphides with thiospinel structure (cuproiridsite).

The elevated concentrations of Rh in many Iranian chromitites may be explained either by substitution of Rh into laurite-erlichmanite, by the presence of PGE sulpharsenides of the hollingworthite–irarsite–platarsite group (RhAsS–IrAsS–PtAsS), or by other Rh-bearing phases (e.g. RhNiAs, Rh_2CuSb) which have been detected in some samples. Sulpharsenides and BM-PGE sulphides of the cuproiridsite–cuprorhodsite–malanite solid solution series also account for slightly elevated Pt concentrations in some chromitites; very rarely, Pt–Fe alloy phases were identified. Palladium does neither form sulpharsenides nor does it substitute into laurite–erlichmanite. It is also not present to any significant amount in pentlandite or other BMS. However, pentlandite is a major carrier of Os, Ir and Rh (probably also of Ru) in PGE- and sulphide-bearing chromitites from Sikhuran. Rare Pd phases such as stibiopalladinite are associated with interstitial pentlandite. However, the small number of Pd minerals identified in the present study necessitates a different mineralogical sink for Pd. The same is true for Pt that is also enriched in sulphide-bearing chromitites. No discrete primary Pt-bearing minerals were identified; however, secondary Pt-rich phases (with Au, Ag, Cu, Ni, Pd) are present (Melcher, 2005), and are associated with Ni-rich alteration products in serpentine. The precursor phases of platinum remain unknown.

The PGM assemblage identified in sulphide-poor chromitite in this study matches typical podiform chromitites elsewhere (González-Jiménez et al., 2009a). In unaltered chromite, laurite–erlichmanite makes up 78% of the PGM detected, followed by Os–Ir–Ru alloys (12%), irarsite (4%) and up to 1% each of phases such as cuproiridsite, hollingworthite, sperrylite and kashinite. Altered chromite and silicate matrix, however, is in many cases rich in Pt–Pd–Rh phases occurring as Pt–Pd–Rh–(BM) alloys, sperrylite, stibiopalladinite and others. González-Jiménez et al. (2009a) also observed higher amounts of Pt–Pd phases in concentrates from samples prepared by electric-pulse disaggregation and hydroseparation techniques, when compared to observations made in polished sections in situ. This largely reflects the higher proportion of PGM liberated from altered phases and silicate matrix in concentrates.

7.4. Formation and PGE potential of sulphide-poor chromitite in southern Iran

The chromitites carrying PGE mineralization in southern Iran are either sulphide-poor or sulphide-bearing, with sulphide-poor types prevailing. In sulphide-poor chromitite, total PGE concentrations may reach 2 ppm in small pods, but are generally an order of magnitude lower, i.e. 200 ppb, and always dominated by the IPGE (Pt/Ir<1). Chromite compositions are quite homogeneous within all chromitites hosted by dunite and harzburgite, being Cr-rich (Cr# = 60–80), Mg-rich (Mg# = 50–83) and low in Ti (<0.3 wt.% TiO_2).

In the sulphur-poor chromitites, PGM are dominated by early crystallised laurite accompanied by rare Os–Ir alloy and Ir–Rh sulpharsenide, occasionally by BM-PGE sulphides (cuproiridsite) and by Ni-rich BMS. The possible mechanisms of IPGE enrichment in chromitites lacking sulphide are still a matter of debate; this cannot be explained by sulphide segregation processes. Recent in-situ micro-analytical work has shown that the chromite lattice does not accommodate enough PGE to account for measured whole-rock concentrations; less than 25% of the whole-rock PGE budget can be explained by mantle chromite (Locmelis et al., 2011; Pagé et al., 2012). Instead, the PGE budget is clearly governed by discrete PGM included in chromite, or subordinate, in silicate. Some PGM, including laurite–erlichmanite, Pt alloy, and probably also cuproiridsite–cuprorhodsite–malanite s.s. and Ni–Ir–Rh sulphides may crystallise directly from a sulphide-undersaturated silicate magma (Andrews and Brenan, 2002; Bockrath et al., 2004; Brenan and Andrews, 2001). PGM may precipitate with chromite during local reduction around chromite grains caused by uptake of Fe^{3+} and Cr^{3+} by crystallising chromite (Finnigan et al., 2008).

PGMs intragranular to chromite tend to survive metamorphic, hydrothermal or supergene processes. However, if attacked by fluids along grain boundaries or cracks, high-temperature PGMs will change compositions depending on their solubility in the respective fluids. This leads to destruction of the less stable PGM, to partial replacement by low-temperature phases, and also to neoformation of minerals (Prichard et al., 1994). All these stages have been documented in the chromitite samples from Iran, including the formation of secondary Ru-rich alloy phases and Ru-rich oxides. This topic is extensively discussed (e.g., Ahmed and Arai, 2003; El Ghorfi et al., 2008; Garuti and Zaccarini, 1997; Garuti et al., 1997; Melcher et al., 2005; Moreno et al., 1999; Prichard et al., 1986, 2008a, 2008b; Stockman and Hlava, 1984; Uysal et al., 2009; and references therein).

PGE are released from sulphide and/or Ir–Os–Ru alloy precursor phases within the mantle by partial melting processes. The type of melting regime and the stages of destruction of PGE carrier phases will govern the composition of the basaltic or more Mg-rich boninitic melt, and of residual PGE phases in the mantle (e.g. Prichard et al., 2008b). Approximately 20 to 25% melting is required to enter the critical melting interval for PGE extraction from fertile mantle peridotite (O'Hara et al., 2001; Prichard et al., 2008b). Higher degrees of melting will dilute the concentrations of PGE in the melt. If sulphide saturation is achieved during crystallisation of the PGE-rich melt, the PGE will concentrate in the cumulate sequence. Otherwise, the PGE will be retained in the lavas. Small batches of melt produced in the critical melting interval will have higher PGE concentrations than melts formed by large increments of melting that extensively reacted and mixed along their way upwards in the mantle (O'Hara et al., 2001). This would explain why small pods of chromite, such as those found at location (1) in the Neyriz ophiolite (Tables 1, 3), have up to ten times higher PGE tenors (2 ppm) than larger ore bodies, such as those at locations (3) and (4) in the same ophiolite and similar host rocks (200 ppb).

The south Iranian chromitites have Cr# exceeding 60, and commonly range from 70 to 80; more than 30%, and up to 45% of partial melting are required to precipitate these minerals in equilibrium with Mg-rich olivine (e.g., Pagé and Barnes, 2009). This is perfectly in line with an origin in a suprasubduction zone environment where high-Mg boninitic melts have been produced from second-stage melting of already depleted mantle (e.g., Melcher et al., 1997, 1999; Pagé and Barnes, 2009). First melts are PGE-poor, but second-stage melts have the potential to produce PGE-enriched magma pulses (Hamlyn and Keays, 1986). Such melts may reach sulphur saturation easier than tholeiitic melts because their SCSS (sulphur content at sulphur saturation; Shima and Naldrett, 1975) will be lower (Li and Ripley, 2009).

7.5. Formation and PGE potential of sulphide-bearing chromitite in southern Iran

Sulphide-bearing dunite and chromite ores carrying 0.1 to 1.2% Ni–-Fe–(Cu) sulphides have been encountered at Sikhuran and Faryab. However, PGE enrichment is only evident at the Sikhuran mine. Mg# numbers of chromite associated with sulphides are more variable than of sulphide-poor chromites, but Cr# numbers are similarly high. The chromites have rare inclusions of primary PGM, mainly of laurite. BMS not only are present interstitial to chromite and Mg-rich olivine (Fig. 12D, F), but also occur included in chromite and olivine (Fig. 12E). Sulphide-bearing chromitites from Sikhuran are enriched in Pt and particularly in Pd relative to the IPGE, corresponding to group IIIa chromitites of Burgath et al. (2002), and to the PGE-rich chromitite group defined by Prichard et al. (2008a,b) in the Al'Ays ophiolite, Saudi Arabia. Os, Ir, Ru and Rh concentrations in pentlandite from Sikhuran are high, whereas Pd and Pt are low. This is in contrast to pentlandites found in stratiform intrusions that tend to be rich in Rh and Pd (Fig. 14; Barnes et al., 2008; Godel and Barnes, 2008; Godel et al., 2007; Oberthür et al., 2003). In some samples, pentlandites contain exsolution blebs of Os–Ru-rich alloy (Fig. 12A) indicating local saturation of these elements. Platinum and Pd have not been found to be hosted in pentlandite, but instead form rare, but comparatively large grains of Pt- and Pd phases such as stibiopalladinite and Pt oxide associated with the pentlandite, and often occur in alteration rims around the BMS. The PGE patterns of pentlandite from Iranian ophiolitic chromitites are similar to those expected in monosulphide solid solution (MSS) coexisting with sulphide liquids: Ni-rich MSS prefers IPGE and Rh, whereas the Cu-rich sulphide liquid prefers Pt, Pd and Au (Li et al., 1996). Thus, the base metal phase may have formed when sulphur-rich melts passed through mantle rocks, transporting PGE and precipitating sulphides under favourable conditions. The dominance of Ni versus Cu in the BMS assemblage attests to a Ni–Fe-rich MSS crystallising from this melt, leaving behind only a small portion of Cu-rich liquid that was enriched in Pt, Pd and Au. This liquid may have crystallised small amounts of intermediate solid solution (ISS) that later exsolved chalcopyrite and some cubanite, as well as discrete Pd- and Pt-rich PGM. Due to intense alteration, neither significant amounts of Cu-rich sulphides nor high-temperature PGM are preserved in the specimens. If not protected by chromite crystals, these PGM are partly dissolved and the contained elements are dispersed within the alteration haloes (e.g., up to 4 wt.% Pt in Fe–Ni carbonate rimming pentlandite from Sikhuran).

Most ophiolitic chromitites have very low sulphur concentrations, and PGE sulphides such as laurite–erlichmanite are the only primary magmatic sulphide phases. However, round globules of polyphase sulphide droplets with exsolved Ni-, Cu- and Fe-rich phases are reported from ophiolithic chromitites (e.g. González-Jiménez et al., 2010). Such droplets are occasionally associated with small PGM and gold grains (e.g., Kozlu-Erdal and Melcher, 2006). Droplets of sulphides, mainly containing bornite, chalcopyrite, pentlandite and millerite were also observed in some of the sulphide-poor chromitites investigated in this study (Fig. 12E), elucidating that the ore-forming systems locally reached sulphur saturation already during chromite crystallisation. This phase preceded a second phase of sulphur saturation resulting in interstitial pentlandite-dominated BMS mineralization that is partly concomitant with, and partly postdates chromite crystallisation. Thus, evidences for multiple phases of sulphur saturation are documented in some of the ophiolitic chromitites of Iran. The highest PGE potential is in transition zone or cumulate dunites characterised by elevated Fe and Ti concentrations in chromite and interstitial primary sulphides. The cumulate zone chromitites have undergone limited fractional crystallisation, evidenced by variable Mg# numbers and slightly increasing concentrations of Ti.

8. Conclusions

The chromitites investigated in this study, originating from different provinces in the complex south Iranian tectonic assembly, are quite homogeneous in terms of textures, mineral chemistry, PGE mineralogy and PGE geochemistry (Table 8). Their derivation and origin from oceanic mantle are disputed in some cases (e.g. Sikhuran), as are their formation ages (Sikhuran, Faryab). However, refractory chromites (high Cr# numbers) and olivine (high Mg# numbers), moderate to low PGE concentrations of the group-I type (Burgath et al., 2002), and a dominance of laurite over other PGM (mainly sulphides) are features common to all chromitites investigated. In addition, variable amounts of Ni–Fe–Cu sulphides are present. Most chromitites do not show evidence of early sulphide separation concomitant with precipitation of PGM from melt.

Pd and Pt enrichment is restricted to chromitites with abundant (0.3–1.2%) interstitial Ni–Fe–(Cu) sulphides in the ultramafic cumulate zone of Sikhuran. PGE patterns and ratios indicate that they are representative of group-IIIa. The PGM enclosed by these chromites do not differ from normal type-I chromitite, e.g. dominated by laurite. However, Pt and Pd are associated with the interstitial sulphide phase, and probably

originate from local sulphur saturation of melts, crystallising a PGE-enriched high-temperature sulphide phase that later exsolved to the presently observed pentlandite + chalcopyrite + cubanite + millerite + PGM assemblage. Earlier sulphur saturation is indicated by polyphase BMS inclusions in some chromitites, notably from Sikhuran.

In summary, potential Pt-/Pd-rich ores in Iranian ultramafic complexes should be expected to occur in sulphide-bearing chromitites and associated dunites. The best targets are in the cumulate dunite zone of the Sikhuran complex. Elevated Fe and Ti concentrations in chromite may guide to PPGE-rich chromitite. In addition, small pods of chromite resulting from melt-rock interaction in the mantle may carry elevated PGE, but will mostly have low Pt/Ir ratios (e.g., at Neyriz).

Acknowledgements

We gratefully acknowledge the support provided by the GSI through its General Director, Mr. Korehie. The following colleagues are thanked for help during field work: Dr. K.-P. Burgath (BGR), A. Karimi, F. Baniadam and B. Shamsi (GSI). The mining companies generously provided access to all facilities and samples. K.-P. Burgath, S. Sturm, G. Ehlers and A. Scheibner (BGR) carried out heavy mineral separation experiments. XRF data were provided by F. Korte (BGR). M. Frey (Köln), P. Rendschmidt and D. Henry (BGR) prepared the polished sections. Laser ablation analyses were provided by Dr. H. Brätz (University of Erlangen-Nürnberg, Germany). Analysis of PGE in whole-rock samples using ID-ICP-MS was carried out at MU Leoben; the team led by Dr. T. Meisel is gratefully acknowledged. M.R. Jannessary acknowledges support through a DAAD postdoctoral research fellowship. The project was undertaken under a Memorandum of Understanding between the BGR and GSI. T. Oberthür is acknowledged for a thorough first review of the manuscript. The valuable comments by Hazel Prichard, Federica Zaccarini and Maryse Ohnenstetter are highly appreciated.

Appendix A. Supplementary data

Supplementary data to this article can be found online at http://dx.doi.org/10.1016/j.oregeorev.2012.05.001.

References

Ahmadipour, H., Sabzehei, M., Whitechurch, H., Rastad, E., Emami, M.H., 2003. Soghan complex as an evidence for paleospreading center and mantle diapirism in Sanadaj–Sirjan zone (south-east Iran). J. Islam. Repub. Iran. 14, 157–172.

Ahmed, A.H., Arai, S., 2002. Unexpectedly high-PGE chromitite from the deeper mantle section of the northern Oman ophiolites and its tectonic implications. Contrib. Mineralog. Petrol. 143, 263–278.

Ahmed, A.H., Arai, S., 2003. Platinum-group minerals in podiform chromitites of the Oman ophiolites. Can. Mineralog. 41, 597–616.

Ahmed, A.H., Hanghøj, K., Kelemen, P.B., Hart, S.R., Arai, S., 2006. Osmium isotope systematics of the Proterozoic and Phanerozoic ophiolitic chromitites: in situ ion probe analysis of primary Os-rich PGM. Earth Planet. Sci. Lett. 245, 777–791.

Alavi-Tehrani, N., 1977. Geology and Petrography in the Ophiolitic Range of Sabzevar (Khorasan, Iran). Geological Survey of Iran. Report 43.

Alinia, F., Facherabadi, A., 2005. Geochemical exploration and economic geological investigation for Ni, Co, PGE in sulphide mineralization in chromitite and pyroxenite of Sikhuran, Esfandagheh area, Kerman, Iran. Abstracts to 20th World Mining Congress 2005, pp. 453–455.

Andrews, D.R.S., Brenan, J.M., 2002. Phase-equilibrium constraints on the magmatic origin of laurite + Ru + Os–Ir alloy. Can. Mineralog. 40, 1705–1716.

Arai, S., 1992. Chemistry of chromian spinel in volcanic rocks as a potential guide to mamga chemistry. Mineralog. Mag. 56, 173–184.

Arvin, M., 1987. Petrology and geochemistry of ophiolites and associated rocks from the Zagros suture, Neyriz, Iran. Proceedings of the International Ophiolite Symposium Cyprus, Nicosia, pp. 351–365.

Arvin, M., Robinson, P.T., 1994. The petrogenesis and tectonic setting of lavas from the Baft ophiolitic mélange, southwest of Kerman, Iran. Can. J. Earth Sci. 31, 824–834.

Augé, T., 1987. Chromite deposits in the northern Oman ophiolite: mineralogical constraints. Miner. Deposita 22, 1–10.

Augé, T., Johan, Z., 1988. Comparative study of chromite deposits from Troodos, Vourinos, North Oman and New Caledonia ophiolites. In: Boissonnas, J., Omenetto, P. (Eds.), Mineral Deposits within the European Community: Society for Geology Applied to Mineral Deposits Special Publication, 6. Springer-Verlag, pp. 267–288.

Augé, T., Maurizot, P., 1995. Stratiform and alluvial platinum mineralization in the New Caledonia ophiolite complex. Can. Mineralog. 33, 1023–1045.

Augé, T., Legendre, O., Maurizot, P., 1998. The distribution of Pt and Ru–Os–Ir minerals in the New Caledonia ophiolite. In: Laverov, N.P., Distler, V.V. (Eds.), International Platinum. Theophrastos Publications, St.-Petersburg-Athens, pp. 141–154.

Babaie, H.A., Ghazi, A.M., Babaie, A., La Tour, T.E., Hassanipak, A.A., 2001. Geochemistry of arc volcanic rocks of the Zagros Crush Zone, Neyriz, Iran. J. Asian Earth Sci. 19, 61–76.

Babaie, H.A., Babaie, A., Ghazi, A.M., Arvin, M., 2005. Tectonic evolution of the Neyriz ophiolite, Iran: an accretionary prism model. Ofioliti 30, 65–74.

Babaie, H.A., Babaie, A., Ghazi, A.M., Arvin, M., 2006. Geochemical, $^{40}Ar/^{39}Ar$ age, and isotopic data for crustal rocks of the Neyriz ophiolite, Iran. Can. J. Earth Sci. 43, 57–70.

Bai, W., Robinson, P.T., Fang, Q., Yang, J., Yan, B., Zhang, Z., Hu, X.F., Zhou, M.F., Malpas, J., 2000. The PGE and base-metal alloys in the podiform chromitites of the Luobusa ophiolite, southern Tibet. Can. Mineralog. 38, 585–598.

Barnes, S.-J., Prichard, H.M., Cox, R.A., Fisher, P.C., Godel, B., 2008. The location of the chalcophile and siderophile elements in platinum-group element ore deposits (a textural, microbeam and whole rock geochemical study): implications for the formation of the deposits. Chem. Geol. 248, 295–317.

Becker, H., Horan, M.F., Walker, R.J., Gao, S., Lorand, J.P., Rudnick, R.L., 2006. Highly siderophile element composition of the Earth's primitive upper mantle: constraints from new data on peridotite massifs and xenoliths. Geochim. Cosmochim. Acta 70, 4528.

Bockrath, C., Ballhaus, C., Holzheid, A., 2004. Stabilities of laurite RuS_2 and monosulphide liquid solution at magmatic temperature. Chem. Geol. 208, 265–271.

Bonavia, F.F., Diella, V., Ferrario, A., 1993. Precambrian podiform chromitites from Kenticha Hill, southern Ethiopia. Econ. Geol. 88, 198–202.

Braud, J., 1970. Les formations du Zagros dans la région de Kermanshah (Iran) et leurs rapports structuraux. C. R. Acad. Sci. 271, 1241–1244.

Brenan, J.M., Andrews, D.R.A., 2001. High-temperature stability of laurite and Ru–Ir–Os alloy and their role on PGE fractionation in mafic magmas. Can. Mineralog. 39, 341–360.

Büchl, A., Brüggmann, G., Batanova, V.G., Hofman, A.W., 2004. Os mobilization during melt percolation. The evolution of Os isotope heterogeneities in the mantle sequence of the Troodos complex, Cyprus. Geochim. Cosmochim. Acta 68, 3397–3404.

Burgath, K.-P., Krauss, U., Mohr, M., 2002. Chromium ores and platinum-group-element occurrences in Europe and Turkey: inventory, evaluation and possibilities. Chronique de la recherche minière, N° hors série, pp. 55–75.

Cassard, D., Nicolas, A., Rabinovitch, M., Moutte, J., Leblanc, M., Prinzhofer, A., 1981. Structural classification of chromite pods in southern New Caledonia. Econ. Geol. 76, 805–831.

Cawthorn, R.G., Barnes, S.J., Ballhaus, C., Malitch, K.N., 2005. Platinum group element, chromium, and vanadium deposits in mafic and ultramafic rocks. Econ. Geol. 215–249 (100th Anniversary Volume).

Corrivaux, L., Laflamme, J.H.G., 1990. Minéralogie des éléments du groupe du platine dans les chromitites de l'ophiolite de Thetford Mines, Québec. Can. Mineralog. 28, 579–595.

Crawford, A.J., Falloon, T.J., Green, D.H., 1989. Classification, petrogenesis and tectonic setting of boninites. In: Crawford, A.J. (Ed.), Boninites and Related Rocks. Unwin Hyman, London, pp. 1–49.

Davoudzadeh, M., 1972. Geology and Petrography of the Area North of Nain, Central Iran. Geological Survey of Iran. Report 14.

Delaloye, M., Desmons, J., 1980. Ophiolites and mélange terranes in Iran: a geochronological study and its paleotectonic implication. Tectonophysics 68, 83–111.

Desmons, J., Beccaluva, L., 1983. Mid-ocean ridge and island-arc affinities in ophiolites from Iran: palaeographic implications. Chem. Geol. 39, 39–63.

Dick, H.J.B., Bullen, T., 1984. Chromian spinel as a petrogenetic indicator in abyssal and Alpine-type peridotites and spatially associated lavas. Contrib. Mineralog. Petrol. 86, 54–76.

Economou-Eliopoulos, M., 1996. Platinum-group element distribution in chromite ores from ophiolite complexes: implications for their exploration. Ore Geol. Rev. 11, 363–381.

El Ghorfi, M., Melcher, F., Oberthür, T., El Boukhari, A., Maacha, L., Maddi, A., Mhaili, M., 2008. Platinum group minerals in podiform chromitites of the Bou Azzer ophiolite, Anti Atlas, Central Morocco. Mineralog. Petrol. 92, 59–80.

Finnigan, C.S., Brenan, J.M., Mungall, J.E., McDonough, W.F., 2008. Experiments and models bearing on the role of chromite as a collector of platinum group minerals by local reduction. J. Petrol. 49, 1647–1665.

Gansser, A., 1960. Ausseralpine Ophiolithprobleme. Eclogae Geol. Helv. 52 (2), 659–680.

Garuti, G., Zaccarini, F., 1997. In situ alteration of platinum-group minerals at low temperature: evidence from serpentinized and weathered chromitites of the Vourinos complex, Greece. Can. Mineralog. 35, 611–626.

Garuti, G., Zaccarini, F., Cabella, R., Fershtater, G.B., 1997. Occurrence of unknown Ru–Os–Ir–Fe oxides in the chromitites of the Nurali ultramafic complex, southern Urals, Russia. Can. Mineralog. 35, 1431–1439.

Garuti, G., Zaccarini, F., Moloshag, V., Alimov, V., 1999. Platinum-group elements as indicators of sulphur fugacity in ophiolithic upper mantle: an example from chromitites of the Ray-Iz ultramafic complex, Polar Urals, Russia. Can. Mineralog. 37, 1099–1115.

Ghasemi, A., Talbot, C.J., 2006. A new tectonic scenario for the Sanandaj–Sirjan Zone (Iran). J. Asian Earth Sci. 26, 683–693.

Ghasemi, H., Juteau, T., Bellon, H., Sabzehei, M., Whitechurch, H., Ricou, L.-E., 2002. The mafic–ultramafic complex of Sikhuran (central Iran): a polygenetic ophiolite suite. C.R. Geosci. 334, 431–438.

Godel, B., Barnes, S.-J., 2008. Platinum-group elements in sulfide minerals and the whole rocks of the J-M Reef (Stillwater Complex): Implication for the formation of the reef. Chem. Geol. 248, 272–294.

Godel, B., Barnes, S.-J., Maier, W.D., 2007. Platinum-group elements in sulphide minerals, platinum-group minerals, and whole-rocks of the Merensky Reef (Bushveld Complex, South Africa): implications for the Formation of the Reef. J. Petrol. 48, 1569–1604.

González-Jiménez, J.M., Gervilla, F., Proenza, J.A., Augé, T., Kerestedjian, T., 2009a. Distribution of platinum-group minerals in ophiolithic chromitites. Trans. Inst. Min. Metall. (Appl. Earth Sci.) B118, 101–110.

González-Jiménez, J.M., Gervilla, F., Proenza, J.A., Kerestedjian, T., Augé, T., Bailly, L., 2009b. Zoning of laurite (RuS_2)-erlichmanite (OsS_2): implications for the origin of PGM in ophiolite chromitites. Eur. J. Mineral. 21, 419–432.

González-Jiménez, J.M., Gervilla, F., Proenza, J.A., Augé, T., Griffin, W.L., O'Reilly, S.Y., 2010. Contemporaneous segregation of PGE- and BM-rich sulphide melts and chromite crystallization: the Caridad chromite deposit, Mayarí–Baracoa ophiolitic belt (Eastern Cuba). Ontario Geological Survey, Miscellanous Release-Data 269, 11th International Platinum Symposium, June 21–24, 2010.

Hagen, D., Weiser, Th., Htay, T., 1990. Platinum-group minerals in Quaternary gold placers in the Upper Chindwin area of Burma. Mineralog. Petrol. 42, 265–286.

Hall, R., 1980. Contact metamorphism by an ophiolite peridotite from Neyriz, Iran. Science 208, 1259–1262.

Hamlyn, P.R., Keays, R.R., 1986. Sulfur saturation and second stage melts: application to the Bushveld Pt metal deposits. Econ. Geol. 81, 1431–1445.

Haynes, S.J., Reynolds, P.H., 1980. Early development of Tethys and Jurassic ophiolites displacement. Nature 283, 1534–1542.

Hillebrand, J., 1983. Chromite deposits in the province of Kerman, Iran. Ind. Miner. 35–43 (May 1983).

Jannessary, M.R., 2003. Les ophiolites de Neyriz (sud de l'Iran): naissance d'une dorsale en pied de marge continentale (étude des structures internes, de la fabrique du manteau, et de l'évolution pétro-géochimique des magmas); Ph.D. thesis. Université Louis Pasteur, Strasbourg, France, 384pp.

Kamenetsky, V.S., Crawford, A.J., Meffre, S., 2001. Factors controlling chemistry of magmatic spinel: an empirical study of associated olivine, Cr-spinel and melt inclusions from primitive rocks. J. Petrol. 42, 655–671.

Kananian, A., Juteau, T., Bellon, H., Darvishzadeh, A., Sabzehi, M., Whitechurch, H., Ricou, L.-E., 2001. The ophiolite massif of Kahnuj (western Makran, southern Iran): new geological and geochronological data. C.R. Acad. Sci. Paris, Sci. Terre Planets 332, 543–552.

Kocks, H., Melcher, F., Meisel, T., Burgath, H.-P., 2007. Diverse contributing sources to chromitite petrogenesis in the Shebenik Ophiolitic Complex, Albania: evidence from new PGE- and Os-isotope data. Mineralog. Petrol. 91, 139–170.

Kozlu-Erdal, H., Melcher, F., 2006. First results on unusual platinum group element and mineral enrichments in the chromitites from the Berit Metaophiolite (Maras), southeastern of Turkey. Understanding the Genesis of Ore Deposits to Meet the Demands of the 21st Century, 12th. Quadrennial IAGOD Symposium, Moscow, Russia, p. 35. Abstract.

Lensch, G., Davoudzadeh, M., 1982. Ophiolites in Iran. Neues Jb. Geol. Paläontol. Monatsh. 5, 306–320.

Lensch, G., Mihm, A., Alavi-Tehrani, N., 1977. Petrography and geology of the ophiolite belt of Sabzevar, Khorassan (Iran). Neues Jb. Mineralog. Abh. 131, 156–178.

Li, C., Ripley, E.M., 2009. Sulfur contents at sulfide-liquid or anhydrite saturation in silicate melts: empirical equations and example applications. Econ. Geol. 104, 405–412.

Li, C., Barnes, S.-J., Makovicky, E., Rose-Hansen, J., Makovicky, M., 1996. Partitioning of nickel, copper, iridium, rhenium, platinum, and palladium between monosulfide solid solution and sulfide liquid: effects of composition and temperature. Geochim. Cosmochim. Acta 60, 1231–1238.

Locmelis, M., Pearson, N.J., Barnes, S.J., Fiorentini, M., 2011. Ruthenium in komatiitic chromite. Geochim. Cosmochim. Acta 75, 3645–3661.

Lotfi, M., Sadeghi, M.M.M., Omrani, S.J., 1993. Mineral distribution map of Iran, 1:1,000.000. Treatise on the Geology of Iran, Geological Survey of Iran.

Maurel, C., 1984. Etude expérimentale de l´équilibre spinelle chromifère liquide silicaté basique. SFMC Meeting "Les spinelles", Lille (oral communication).

Maurel, C., Maurel, P., 1982. Étude expérimentale de la distribution de l'aluminium entre bain silicaté basique et spinelle chromifère. Implications pétrogénétiques: teneur en chrome des spinelles. Bull. Minér. 105, 197–202.

Maurel, C., Maurel, P., 1983. Influence du fer ferrique sur la distribution de l'aluminium entre bain silicaté basique et spinelle chromifère. Bull. Minér. 106, 623–624.

McCall, G.J.H., 1985. Explanatory text of Minab quadrangle map, J 13. Geological Survey of Iran, 530 pp.

McCall, G.J.H., 1997. The geotectonic history of the Makran and adjacent areas of southern Iran. J. Asian Earth Sci. 15, 517–531.

McDonald, A.M., Proenza, J.A., Zaccarini, F., Rudashevsky, N.S., Cabri, L.J., Stanley, C.J., Rudashevsky, V.N., Melgarejo, J.C., Lewis, J.F., Longo, F., Bakker, R.J., 2010. Garutiite, (Fe,Ni,Ir), a new hexagonal polymorph of native Ni from Loma Peguera, Dominican Republic. Eur. J. Mineral. 22, 293–304.

Meisel, T., Moser, J., 2004. Reference materials for geochemical PGE analysis: new analytical data for Ru, Rh, Pd, Os, Ir, Pt and Re by isotope dilution ICP-MS in 11 geological reference materials. Chem. Geol. 208, 319–338.

Meisel, T., Walker, R.J., Irving, A.J., Lorand, J.-P., 2001a. Osmium isotopic compositions of mantle xenoliths: a global perspective. Geochim. Cosmochim. Acta 65, 1311–1323.

Meisel, T., Moser, J., Fellner, N., Wegscheider, W., Schoenberg, R., 2001b. Simplified method for the determination of Ru, Pd, Re, Os, Ir and Pt in chromitites and other geological materials by isotope dilution ICPMS and acid digestion. Analyst 126, 322–328.

Meisel, T., Fellner, N., Moser, J., 2003a. A simple procedure for the determination of platinum group elements and rhenium using ID-ICP-MS with an inexpensive on-line matrix separation on geological and environmental materials. J. Anal. At. Spectrom. 18, 720–726.

Meisel, T., Reisberg, L., Moser, J., Carignan, J., Melcher, F., Brügmann, G., 2003b. Re–Os systematics of UB-N, a serpentinized peridotite reference material. Chem. Geol. 201, 161–179.

Melcher, F., 2000a. Base metal–platinum group element sulfides from the Urals and the Eastern Alps: characterization and significance for mineral systematics. Mineralog. Petrol. 68, 177–211.

Melcher, F., 2000b. Chromite and platinum-group elements as indicator of mantle petrogenesis—a review of geochemical and petrological work on chromitite in different geotectonic settings. Habilitation thesis, University of Leoben.

Melcher, F., 2005. Mineralogy and chemistry of chromite, sulphides and platinum-group minerals from Esfandagheh, SE Iran—a reconnaissance study. Unpublished Report, Bundesanstalt fuer Geowissenschaften und Rohstoffe, Diary number 11327/05.

Melcher, F., Lodziak, J., 2007. Platinum-group minerals of concentrates from the Driekop platinum pipe, Eastern Bushveld Complex—tribute to Eugen F. Stumpfl. Neues Jb. Mineralog. 183, 173–195.

Melcher, F., Grum, W., Simon, G., Stumpfl, E.F., Thalhammer, T.V., 1997. The giant ophiolitic chromite deposits of Kempirsai, Kazakhstan: a study of solid and fluid inclusions in chromite. J. Petrol. 38, 1419–1458.

Melcher, F., Grum, W., Thalhammer, T.V., Thalhammer, O.A.R., 1999. The giant chromite deposits at Kempirsai, Urals: constraints from trace element (PGE, REE) and isotope data. Miner. Deposita 34, 250–272.

Melcher, F., Oberthür, T., Lodziak, J., 2005. Modification and alteration of detrital platinum-group minerals from the Eastern Bushveld Complex, South Africa. Can. Mineralog. 43, 1711–1734.

Mobbs, P.M., 2010. The mineral industry of Iran. USGS. 2008 Minerals Yearbook (advance release). http://minerals.usgs.gov/minerals/pubs/country/2008/myb3-2008-ir.pdf.

Moore, F., Rajabzadeh, M.A., 1993. First report on platinum-group minerals in chromitites from northwestern Neyriz ophiolite, Iran. J. Sci., Islam. Repub. Iran 4, 47–54.

Moreno, T., Prichard, H.M., Lunar, R., Monterrubio, S., Fisher, P., 1999. Formation of a secondary platinum-group mineral assemblage in chromitites from the Herbeira ultramafic massif in Cabo Ortegal, NW Spain. Eur. J. Mineral. 11, 363–378.

Najafzadeh, A.R., Arvin, M., Pan, Y., Ahmadipour, H., 2008. Podiform chromitites in the Sorkhband Ultramafic Complex, southern Iran. Evidence for ophiolithic chromitite. J. Sci., Islam. Repub. Iran 19, 49–65.

Nakagawa, M., Franco, H.E.A., 1997. Placer Os–Ir–Ru alloys and sulfides: indicators of sulfur fugacity in an ophiolite? Can. Mineralog. 35, 1441–1452.

Naldrett, A.J., von Gruenewaldt, G., 1989. Association of platinum-group elements with chromitite in layered intrusions and ophiolite complexes. Econ. Geol. 84, 180–187.

Nilsson, L.P., 1990. Platinum-group mineral inclusions in chromitite from the Osthammeren ultramafic tectonite body, south central Norway. Mineralog. Petrol. 42, 249–263.

O'Hara, M.J., Fry, N., Prichard, H.M., 2001. Minor phases as carriers of trace elements in non-modal crystal-liquid separation processes II: illustrations and bearing on behaviour of REE, U, Th and PGE in igneous processes. J. Petrol. 42, 1887–1910.

Oberthür, T., Weiser, T.W., Gast, L., 2003. Geochemistry and mineralogy of platinum-group elements at Hartley Platinum Mine, Zimbabwe. I. Primary distribution patterns in pristine ores of the Main Sulfide Zone of the Great Dyke. Miner. Deposita 38, 327–343.

Ohnenstetter, M., Karaj, N., Neziraj, A., Johan, Z., Cina, A., 1991. Le potentiel platinifère des ophiolites: minéralisations en éléments du groupe de platine (PGE) dans les massifs de Tropoja et Bulqiza, Albanie. C. R. Acad. Sci. Paris 313 (Série II), 201–208.

Orberger, B., Friedrich, G., Wörmann, E., 1988. Platinum-group element mineralization in the ultramafic sequence of the Acoje block, Zambales, Philippines. In: Prichard, H.M., Potts, P.J., Bowles, J.F.W., Cribb, S.J. (Eds.), Geo-Platinum 87 Symposium Volume. Elsevier, London and New York, pp. 361–380.

Page, N.J., Engin, T., Haffty, J., 1979. Palladium, platinum, and rhodium concentrations in mafic and ultramafic rocks from the Kizildag and Guleman areas, Turkey, and the Faryab and Esfandagheh–Abdasht areas, Iran. U.S. Geological Survey Open File Report 79–840.

Pagé, P., Barnes, S.-J., 2009. Using trace elements in chromites to constrain the origin of podiform chromitites in the Thetford Mines ophiolite, Québec, Canada. Econ. Geol. 104, 997–1018.

Pagé, P., Barnes, S.-J., Bédard, J.H., Zientek, M.L., 2012. In situ determination of Os, Ir, and Ru in chromites formed from komatiite, tholeiite and boninite magmas: implications for chromite control of Os, Ir and Ru during partial melting and crystal fractionation. Chem. Geol. 302–303, 3–15.

Paliulionyte, V., Meisel, T., Ramminger, P., Kettisch, P., 2006. High pressure asher digestion and an isotope dilution-ICP-MS method for the determination of platinum group elements in chromitite reference materials CHR-Bkg, GAN-Pt-1 and HHH. Geostand. Geoanal. Res. 30, 87–96.

Papp, J., 2004. Chromium. USGS Minerals Yearbook 2004. .

Pedersen, R.B., Johannesen, G.M., Boyd, R., 1993. Stratiform PGE mineralization in the ultramafic cumulates of the Leka ophiolites complex, central Norway. Econ. Geol. 88, 782–803.

Prichard, H.M., Tarkian, M., 1988. Platinum and palladium minerals from two PGE-rich localitites in the Shetland ophiolites complex. Can. Mineralog. 26, 979–990.

Prichard, H.M., Neary, C.R., Potts, P.J., 1986. Platinum-group minerals in the Shetland ophiolite. In: Gallagher, M.J., Ixer, R.A., Neary, C.R., Prichard, H.M. (Eds.), Metallogeny of Basic and Ultrabasic Rocks. Institution of Mining and Metallurgy, London, pp. 395–414.

Prichard, H.M., Ixer, R.A., Lord, R.A., Maynard, J., Williams, N., 1994. Assemblages of platinum-group minerals and sulphides in silicate lithologies and chromite-rich rocks within the Shetland ophiolite. Can. Mineralog. 32, 271–294.

Prichard, H.M., Economou-Eliopoulos, M., Fisher, P.C., 2008a. Contrasting platinum-group mineral assemblages from two different podiform chromitite localities in the Pindos ophiolites complex, Greece. Can. Mineralog. 46, 329–341.

Prichard, H.M., Neary, C.R., Fisher, P.C., O'Hara, M.J., 2008b. PGE-rich podiform chromitites in the Al'Ays ophiolites complex, Saudi Arabia: an example of critical mantle melting to extract and concentrate PGE. Econ. Geol. 103, 1507–1529.

Proenza, J.A., Zaccarini, F., Lewis, J.F., Longo, F., Garuti, G., 2007. Chromian spinel composition and the platinum group minerals of the PGE-rich Loma Peguera chromitites, Loma Caribe peridotite, Dominican Republic. Can. Mineralog. 45, 631–648.

Rajabzadeh, M.A., 1998. Minéralisation en chrome et éléments du groupe du platine dans les ophiolites d'Assemion et de Neyriz, ceinture de Zagros, Iran; Ph.D. thesis. Institute Polytechnique de Lorraine, Nancy, 335pp.

Rajabzadeh, M.A., Ohnenstetter, R.M., Ohnenstetter, D., Reisberg, L., 1998. Chrome and platinum-group element (PGE) mineralization in chromitites from the Assemion and Neyriz ophiolites, Zagros Belt, Iran. 8th International Platinum Symposium abstracts, The Geological Society of South Africa and The South African Institute of Mining and Metallurgy Symposium Series S18, pp. 343–345.

Razin, L.V., Rudashevsky, N.S., Sidorenko, G.A., 1981. Tolovkite, IrSbS, a new sulfoantimonide of iridium from northeastern USSR. Int. Geol. Rev. 24, 849–854.

Ricou, L.-E., 1971a. Le métamorphisme au contact des péridotites de Neyriz (Zagros interne, Iran): développement de skarn à pyroxène. Bull. Soc. Geol. Fr. 7 (XIII), 146–155 (no 1–2).

Ricou, L.-E., 1971b. Le croissant ophiolitique péri-arabe, une ceinture de nappes mise en place au crétacé supérieur. Rev. Géogr. Phys. Géol. Dynam. 18 (f. 4), 327–350.

Ricou, L.-E., 1976. Evolution structurale des Zagrides. La région clef de Neyriz (Zagros Iranien). Mem. Soc. Geol. Fr. 125 (140 pp. (Thése Orsay, 1974)).

Roeder, P.L., Reynolds, I., 1991. Crystallisation of chromite and chromium solibility in basaltic melts. J. Petrol. 32, 909–934.

Rollinson, H., 2008. The geochemistry of mantle chromitites from the northern part of the Oman ophiolite: inferred parental melt composition. Contrib. Mineralog. Petrol. 156, 273–288.

Sabzehei, M., 1974. Les mélange ophiolitiques de la région d'Esfandagheh (Iran méridional). Etude pétrologique et structurale. Interprétation dans le cadre Iranien. Thèse d'Etat, Université de Grenoble, France, 306 pp.

Sabzehei, M., 1998. Upper Protrozoic–Lower Paleozoic ultramafic–mafic association of southeast Iran, Product of an ophiolitic magma of Komatiitic affinity. International Ophiolite Symposium, Finland, Abstracts, p. 201.

Sarkarinejad, K., 2003. Structural and microstructural analysis of a palaeo-transform fault zone in the Neyriz ophiolite, Iran. In: Dilek, Y., Robinson, P.T. (Eds.), Ophiolites in Earth History: Geological Society of London, Special Publication, 218, pp. 129–145.

Schmidt, H.L., 1974. Iran. Rohstoffwirtschaftliche Länderberichte, Teil V. Bundesanstalt für Bodenforschung. . 89 pp.

Schürenberg, H., 1959. Untersuchungen an iranischen Chromerzlagerstätten. Tech. Mitt. Krupp 17, 37–43.

Sengör, A.M.C., 1979. Mid-Mesozoic closure of Permo-Triassic Tethys and its implications. Nature 279, 590–593.

Shima, H., Naldrett, A.J., 1975. Solubility of sulphur in an ultramafic melt and the relevance of the system Fe–S–O. Econ. Geol. 70, 960–967.

Stöcklin, J., 1977. Structural correlation of the Alpine range between Iran and Central Asia. Mémoire Hors-Série No.8 de la Société Géologique de la France, 8, pp. 333–353.

Stockman, H.W., Hlava, P.F., 1984. Platinum-group minerals in Alpine chromitites from southwestern Oregon. Econ. Geol. 79, 491–508.

Stowe, C.W., 1994. Compositions and tectonic settings of chromite deposits through time. Econ. Geol. 89, 528–546.

Stumpfl, E.F., 1961. Some new platinoid-rich minerals, identified with the electron microanalyser. Mineralog. Mag. 32, 833–847.

Ucurum, A., Koptagel, O., Lechler, P., 2006. Main-component geochemistry and platinum-group-element potential of Turkish chromite deposits, with emphasis on the Mugla area. Int. Geol. Rev. 48, 241–254.

Uysal, I., Zaccarini, F., Sadiklar, M.B., Bernhardt, H.-J., Bigi, S., Garuti, G., 2009. Occurrence of rare Ru–Fe–Os–Ir–oxide and associated platinum-group minerals (PGM) in the chromitite of Muğla ophiolite, SW-Turkey. Neues Jb. Mineralog. Abh. 185 (3), 323–333.

Uysal, I., Sadiklar, M.B., Zaccarini, F., Garuti, G., Tarkian, M., Meisel, T., 2010. Cr-PGE mineralization in the Turkish ophiolites: the state of the art. Ontario Geological Survey, Miscellanous Release-Data 269, 11th International Platinum Symposium, June 21–24, 2010.

Walker, R.J., Prichard, H.M., Ishiwatari, A., Pimentel, M., 2002. The osmium isotopic composition of convecting upper mantle deduced from ophiolite chromites. Geochim. Cosmochim. Acta 66, 329–345.

Weber-Diefenbach, K., Davouadzadeh, M., 1998. Geology and geochemistry of the chromite deposits of Iran. Münchner Geologische Hefte, A23, pp. 89–100.

Weber-Diefenbach, K., Davoudzadeh, M., Alavi-Tehrani, N., Linsch, G., 1986. Paleozoic ophiolites in Iran, geology and geochemistry, and geodynamic implication. Ofioliti 11, 305–338.

Wensink, H., Varekamp, J.C., 1980. Paleo-magnetism of basalts from Alborz: Iran part of Asia in the Cretaceous. Tectonophysics 68, 113–129.

Wohlgemuth-Ueberwasser, C.C., Ballhaus, C., Berndt, J., Stotter nee Paliulionyte, V., Meisel, T., 2007. Synthesis of PGE sulfide standards for laser ablation inductively coupled plasma mass spectrometry (LA–ICP-MS). Contrib. Mineralog. Petrol. 154, 607–617.

Yaghubpur, A., 2005. Mineral deposits of Iran: a brief review. In: Roonwal, G.S., Shahriar, K., Ranjbar, H. (Eds.), Mineral Resources and Development. Daya Publishing House, Delhi-110 035, pp. 191–202.

Yaghubpur, A., Hassannejad, A.A., 2006. The spatial distribution of some chromite deposits in Iran, using Fry Analysis. J. Sci., Islam. Repub. Iran 17, 147–152.

Zaccarini, F., Proenza, J.A., Rudashevsky, N.S., Cabri, L.J., Garuti, G., Rudashevsky, V.N., Melgarejo, J.C., Lewis, J.F., Longo, F., Bakker, R.J., Stanley, C.J., 2009. The Loma Peguera ophiolitic chromitite (Central Dominican Republic): a source of new platinum group minerals (PGM) species. Neues Jb. Mineralog. Abh. 185, 335–349.

Zaccarini, F., Garuti, G., Proenza, J.A., Campos, L., Thalhammer, O.A.R., Aiglsperger, T., Lewis, J.F., 2011. Chromite and platinum group elements mineralization in the Santa Elena ultramafic nappe (Costa Rica): geodynamic implications. Geol. Acta 9, 407–423.